Inaugural dissertation

for

obtaining the doctoral degree

of the

Combined Faculty of Mathematics, Engineering and Natural Sciences

of the

Ruprecht - Karls - University

Heidelberg

Presented by

M. Sc. Sung Min Eu

Born in: Ulsan, South Korea

Oral examination: 28.06.2022

Functional and morphological analysis of hepatitis C virus assembly

Referees: Prof. Dr. R. Bartenschlager

Prof. Dr. O. Fackler

Declaration

The applicant, Sung Min Eu, declares that he is the sole author of the submitted dissertation and no other sources for help apart from those specifically referred to have been used. Additionally, the applicant declares that he has not applied for permission to enter examination procedure at another institution and that this dissertation has not been presented to another faculty and has not been used in its current or any other form in another examination.

Date Signature

Acknowledgement

This study was conducted under the supervision of **Prof. Dr. Ralf Bartenschlager** at the Molecular Virology Unit, Department of Infectious Diseases at the University Hospital of Heidelberg. The work was funded by the **Sonderforschungsbereich/ Transregio (Collaborative Research Centre) 83**.

First of all, I would like to thank **Ralf** for his support during my PhD. I have appreciated your open-minded attitude towards my ideas and your constructive input. Thank you for being a supportive, patient and fair supervisor.

I also want to thank **Prof. Dr. Oliver Fackler** for being my second supervisor and for the constructive discussion and input during my TAC meetings.

Next, I would like to thank **Prof. Dr. Britta Brügger** and her (former) PhD students **Markus, Daniela** and **Laura** for providing experimental knowledge and materials.

Another thanks go to **Dr. Doris Höglinger** and **Prof. Dr. Sebastian Schuck**, who agreed to be part of my PhD Defense Committee.

Then, I would like to thank **Dr. Vibor Laketa** for his technical assistance and **Dr. Berati Cerikan** for his proofreading of my dissertation as well as **Minh Tu Pham** for constructive critiques and discussion.

Additionally, I want to say thanks to **Ji-Young**, who kindly introduced me into the laboratory practice and who was a supportive supervisor in the beginning of my PhD.

I further want to thank **members of AGB** and **all in Molecular Virology**. I really appreciated the mutually supportive environment in our department.

Looking back, my PhD was a long journey full of joy, sadness, success and disappointment, where I have not only learned science, but also things important for life. During this time, I met new friends and had to say goodbye to some of them, who have become important to me. Without these people, there would not have been this valuable time. Especially, I want to thank **Antoine, Sun Hye, David, Cornelius, Jayson, Simon** and **Matthew** for enriching my life by doing sport, visiting concerts, having nice weekend as well as having discussion and for supporting me during my PhD.

Last but not least, I want to say to my family that I really am appreciating their presence. I thank my brother **Sung Jun** for being there as my flat mate and especially for overcoming the corona situation together. I also would like to thank **my parents** whom I can always count on.

Abstract

Hepatitis C Virus (HCV) induces liver inflammation, which can develop to liver cirrhosis and hepatocellular carcinoma. In 2021, approximately 58 million people are chronically infected with HCV and in 2019, 290,000 people died as consequence of HCV-induced liver failure, representing HCV as a major global health burden. With the development of direct acting antiviral drugs, the cure rate of treated patients has increased drastically. However, the low access to diagnosis and treatment due to high costs as well as emergence of drug resistant mutants pronounce the importance of further research on HCV in terms of generating a prophylactic vaccine and making antiviral drugs widely available to achieve global elimination of chronic hepatitis C.

Two aspects that have not been elucidated yet in sufficient depth are the role of cholesterol in the HCV replication cycle and how lipid droplets (LDs) might contribute to the assembly of infectious virus particles. Therefore, my thesis addressed two complementary aspects. The first one dealt with the mechanism how cholesterol contributes to HCV replication and virus production. To address this question, I screened HCV proteins for direct interaction with cholesterol. To this end photoactivatable and clickable (PAC) cholesterol was applied for crosslinking proteins in proximity. I found that nonstructural protein 2 (NS2) was most efficiently crosslinked to PAC cholesterol. Subsequent screening of 20 NS2 mutants for PAC cholesterol crosslinking and 3D modeling of the NS2 transmembrane domain identified a cholesterol recognition amino acid consensus (CRAC) motif in the third transmembrane segment of NS2 (amino acid reside 87-94) mediating PAC cholesterol crosslinking, with a major contribution of amino acid residue Tyr 91 to cholesterol binding. Virological analysis of NS2 CRAC mutants revealed the importance of NS2 cholesterol interaction for infectious virus production. Further characterization of NS2 CRAC mutants by using immunofluorescence (IF) and co-immunoprecipitation assays provided evidence that NS2 - cholesterol interaction might be necessary for NS2 - envelope protein E2 interaction, which most likely is required to recruit E2 to the site of HCV virion assembly. In addition, I obtained evidence that NS2 - cholesterol interaction might be involved in modulating late endosome motility and subcellular cholesterol distribution.

The second aspect of my thesis dealt with the role of LDs for the assembly of infectious HCV particles. The viral core protein, forming the capsid, and NS5A, a component of

the viral replicase, directly localize on LDs. Notably, in the late phase of the viral replication cycle, the viral envelope proteins are recruited to NS5A-decorated LDs and these E2-/NS5A double-positive LDs are tightly surrounded by ER membranes. Since this trapping of LDs by the ER depends on virus assembly, we assumed that these LDs correspond to virion assembly sites, allowing lipid transfer from LDs to the ER, thus promoting formation of lipidated HCV particles. For establishing ER-LD contacts, Ras-related small GTPase Rab18 has been considered as an important host factor. Rab18 not only is responsible for bringing ER membranes in close contact with LDs, but also supports the HCV replication cycle. To study the possible contribution of Rab18 to HCV virion production, I generated Rab18 knockout (KO) cell lines and characterized them in detail. As expected, I could confirm the importance of Rab18 in establishing ER - LD contacts. However due to off target effects even observed in control cells no reproducible HCV phenotypes could be determined.

In conclusion, I could show that NS2 has strong cholesterol binding via a CRAC motif, which plays a critical role in the assembly of infectious HCV particles. I conclude that NS2 - cholesterol interaction might be necessary for the interaction between NS2 and the viral envelope proteins, thus recruiting the latter to cholesterol-rich HCV assembly sites.

Zusammenfassung

Das Hepatitis C Virus (HCV) induziert Leberentzündungen, die sich zu Leberzirrhosen und hepatozellulären Karzinomen entwickeln können. Im Jahr 2021 weisen schätzungsweise 58 Millionen Menschen chronische HCV Infektionen auf und im Jahr 2019 sind 290.000 Menschen an Konsequenzen von HCV-induziertem Leberversagen gestorben. Diese Daten stellen das HCV als eine große globale Gesundheitsbelastung dar. Mit der Entwicklung von direkt am Virus ansetzenden Medikamenten hat sich die Heilungsrate der behandelten Patienten drastisch erhöht. Der geringe Zugang zu Diagnose und Behandlung aufgrund hoher Kosten sowie das Auftreten arzneimittelresistenter Mutanten machen jedoch deutlich, wie wichtig die weitere Erforschung von HCV im Hinblick auf die Entwicklung eines prophylaktischen Impfstoffs und die breite Verfügbarkeit antiviraler Medikamente ist, um die globale Ausrottung von Hepatitis C zu erreichen. Zwei Aspekte, die noch nicht in ausreichender Tiefe aufgeklärt wurden, sind die Rolle von Cholesterol im HCV-Replikationszyklus und wie Lipidtröpfchen (LDs, von Engl. „Lipid droplets“) zum Zusammenbau infektiöser Viruspartikel beitragen könnten. Meine Doktorarbeit befasste sich daher mit zwei komplementären Aspekten. Die erste befasste sich mit dem Mechanismus, wie Cholesterol zur HCV-Replikation und Virusproduktion beiträgt.

Um diese Frage zu klären, untersuchte ich HCV-Proteine auf direkte Interaktion mit Cholesterol. Dazu wurde das photoaktivierbare und klickbare (PAC, von Engl. „photoactivatable and clickable“) Cholesterol zur Quervernetzung von eng benachbarten Proteinen verwendet. Ich fand heraus, dass das Nichtstrukturprotein 2 (NS2) am effizientesten mit PAC-Cholesterol quervernetzt wurde. Durch die anschließende systematische Untersuchung von 20 NS2-Mutanten auf PAC-Cholesterol-Quervernetzung und die 3D-Modellierung der NS2-Transmembran-domäne wurde ein sogenanntes CRAC-Motiv (von Engl. „cholesterol recognition amino acid consensus“) im dritten Transmembransegment von NS2 (Aminosäurerest 87-94) identifiziert. Das CRAC-Motiv ist verantwortlich für die NS2-Cholesterol-Interaktion, wobei der Aminosäurerest Tyr 91 den Hauptbeitrag zur Cholesterol-bindung leistete.

Die virologische Analyse von NS2-CRAC-Mutanten zeigte die wichtige Rolle der NS2-Cholesterol-Interaktion für die Produktion infektiöser Viren. Eine weitere Charakterisierung von NS2-CRAC-Mutanten unter Verwendung von

Immunfluoreszenz- (IF) und Co-Immunpräzipitationsassays lieferte Hinweise darauf, dass die Cholesterolbindung von NS2 für dessen Interaktion mit dem Hüllprotein E2 erforderlich sein könnte. Diese ist höchstwahrscheinlich notwendig, um E2 zur Produktionsstelle von HCV-Partikeln zu rekrutieren. Außerdem habe ich Beweise dafür gesammelt, dass die NS2-Cholesterol-Interaktion an der Modulation der späten Endosomenmobilität und der subzellulären Cholesterolkonzentration beteiligt sein könnte.

Der zweite Aspekt meiner Dissertation beschäftigte sich mit der Rolle von LDs bei der Assemblierung infektiöser HCV-Partikel. Das virale Protein *core*, welches das Kapsid bildet, und NS5A, eine Komponente des viralen Replikasekomplex, lokalisieren direkt auf LDs. Bemerkenswerterweise werden in der späten Phase des HCV-Replikationszyklus die viralen Hüllproteine zu NS5A-dekorierten LDs rekrutiert, und diese E2-/NS5A-doppelt positiven LDs werden eng von ER-Membranen umgeben. Da dieses Einfangen von LDs durch das endoplasmatische Retikulum (ER) von der Virusassemblierung abhängt, nahmen wir an, dass diese LDs Virion-Assemblierungsstellen entsprechen, was den Lipidtransfer von LDs zum ER ermöglicht und somit die Bildung von Lipid-umhüllten HCV-Partikeln fördert. Für die Etablierung von Kontakten zwischen ER und LDs wurde die Ras-verwandte kleine GTPase Rab18 als wichtiger Wirtsfaktor angesehen. Rab18 ist nicht nur dafür verantwortlich, ER-Membranen in engen Kontakt mit LDs zu bringen, sondern unterstützt auch den HCV-Replikationszyklus. Um den möglichen Beitrag von Rab18 zur HCV-Virionenproduktion zu untersuchen, habe ich Rab18-Knockout (KO)-Zelllinien generiert und detailliert charakterisiert. Wie erwartet, konnte ich die wichtige Rolle von Rab18 für die Herstellung von ER - LD-Kontakten bestätigen. Aufgrund von *Off-Target*-Effekten, die sogar in Kontrollzellen beobachtet wurden, konnten jedoch keine reproduzierbaren HCV-Phänotypen bestimmt werden.

Zusammenfassend konnte ich zeigen, dass NS2 eine starke Cholesterolbindung über ein CRAC-Motiv aufweist, das eine entscheidende Rolle bei der Assemblierung infektiöser HCV-Partikel spielt. Ich ziehe die Schlussfolgerung, dass die NS2-Cholesterol-Interaktion für die Interaktion zwischen NS2 und den viralen Hüllproteinen notwendig sein könnte, wodurch letztere zu cholesterolreichen HCV-Montagestellen rekrutiert werden.

Table of Content

Abbreviation

aa	amino acid
ASGR	asialoglycoprotein receptor
AP	adaptor protein
ATP	adenosine triphosphate
CCM	cholesterol consensus motif
CD81	cluster of differentiation 81
COVID19	coronavirus disease 2019
CRAC	cholesterol recognition amino acid consensus
DAA(s)	direct acting antivirals(s)
DAG	diacylglycerol
DMEM	Dulbecco's modified eagle medium
DMSO	dimethyl sulfoxide
DMV	double membrane vesicle
DNA	deoxyribonucleic acid
DRM(s)	detergent resistant membrane(s)
DTT	dithiothreitol
ER	endoplasmic reticulum
ERAD	ER-associated protein degradation
Erlin	ER membrane lipid raft-associated protein
ESCRT	endosomal sorting complex required for transport
FCS	fetal claf serum
GAP	GTPase activating protein
GAPDH	glyceraldehyde-3-phosphate degydrogenase
GDI	GDP dissociation inhibitor
GDP	guanine diphosphate
GEF	guanine nucleotide exchange factor
GM130	golgi matrix protein 130
gRNA	guide RNA
GTP	guanine triphosphate
HA	haemagglutinin
HBV	hepatitis B virus
HCC	hepatocellular carcinoma
HCV	hepatitis C virus
HRP	horseradish peroxidase
HTA(s)	host targeting antiviral(s)
IF	immunofluorescence
INF	interferon
Insig	insulin-induced gene
IP	immunoprecipitation
IRES	internal ribosome entry site
JFH1	Japanese fulminant hepatitis 1
kb	kilo base
kDa	kilo Dalton
KO	knockout
LAMP1	lysosomal associated membrane protein 1
LB	lysogeny broth
Ld	lipid-disordered
LD(s)	lipid droplet(s)
LDL	low density lipoprotein
LDLR	low density lipoprotein receptor
Lo	liquid-ordered
MβCD	methyl-β-cyclodextrin
MEM	minimum essential media
MS	mass spectrometry
NANBH	non-A and non-B hepatitis
NMR	nuclear magnetic resonance
NS	non-structural protein
NTR	non-translated region
ORF	open reading frame
PAC	photoactivatable and clickable
PBS	phosphate buffered saline
PCR	polymerase chain reaction
PFA	paraformaldehyde
pH	pondus Hydrogenii
PM	plasma membrane
RAS(s)	resistance-associated substitutions
RDRP	RNA-dependent RNApolymerase
RNA	ribonucleic acid
RT	room temperature
SARS-Cov-2	severe acute respiratory syndrome conronavirus 2
SCAP	SREBP cleavage activating protein
SDS	sodium dodecyl sulfate
shRNA	small hairpin RNA
siRNA	small interfering RNA
SREBP	sterol regulatory element-binding protein
SVR	sustained viral response
TAG	triacylglycerol
TCID50	tissue culture infectious dose 50
TMD	transmembrane domain
TMS	transmembrane segment
UTR	untranslated region
UV	ultraviolet
v/v	volume/volume
VLDL	very-low density lipoprotein
w/v	weight/volume
WB	western blot

1. Introduction

1.1. Cholesterol

1.1.1. Lipids and biological membranes

1.1.1.1. General aspects of biological membranes

Biological membranes are 6 to 10 nm thick and sequester a specific space from another (i.e. the cytoplasm and the extracellular space). Moreover, they compartmentalize different biological systems in eukaryotic cells in forms of subcellular organelles, where ion- and molecule exchanges are limited (selective permeability). Consequently, membranes are electrically polarized supporting several processes occurred through membranes [1].

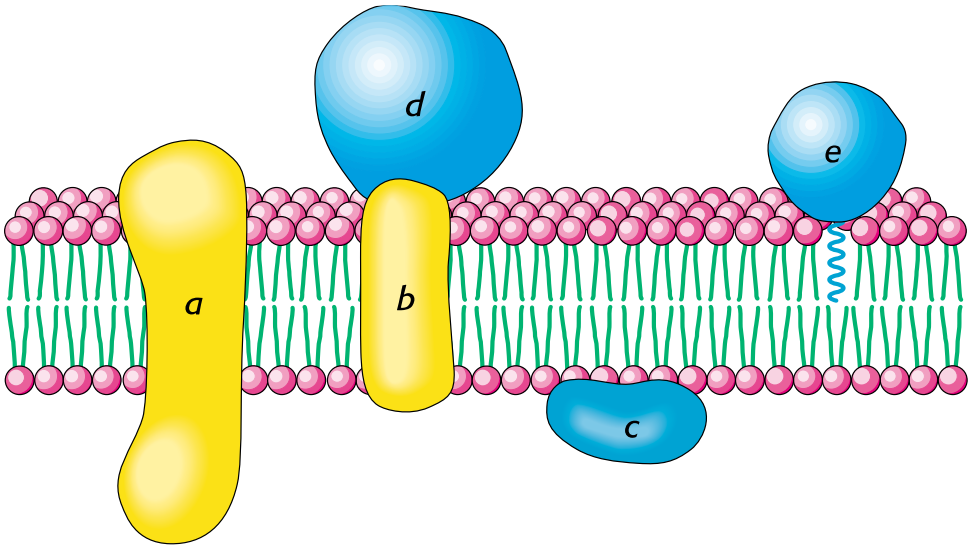

Fig. 1.1. Biological membranes. Biological membranes consist of lipids, which have a hydrophilic head (red) and hydrophobic fatty acid chains (green), and proteins (a-e). The proteins a and b are integral membrane proteins interacting with the lipid bilayer intensively. The peripheral membrane proteins c, d and e associate with membranes via the head of lipids, interaction with other integral membrane proteins and covalently linked lipid anchor, respectively. Adapted from Stryer Biochemistry [2].

The major components of membranes are lipids and proteins (Fig. 1.1.). They associate together non-covalently and easily can diffuse laterally [3], whereas vertical flipping does not occur often, which keeps the asymmetry between the outer- and the inner layers according to their compositions [4]. Membrane lipids contain a hydrophilic and a hydrophobic part and can spontaneously form closed bimolecular layer in aqueous media, designated a lipid bilayer, which serves as a barrier for hydrophilic

molecule exchanges [2]. Membrane proteins determine the functionality of specific membranes. [1].

1.1.1.2. Fatty acids

The hydrophobicity, an essential characteristic for lipids, is mostly derived from fatty acids. Fatty acids are long hydrocarbon chains with no (saturated) or more than one C=C double bond mostly in *cis*-configuration (unsaturated) containing a carboxylic acid at the end. Fatty acids in biological systems have 14 to 24 C-atoms, where fatty acids with 16 and 18 C-atoms such as palmitic-, stearic- and oleic acid exist most frequently [2]. The characteristics of fatty acids are depending on their chain length and the number of C=C double bonds. The longer the hydrocarbon chains and the less unsaturated a fatty acid is, the higher is the melting point of the fatty acid due to tighter packages and increasing van der Waals interaction between fatty acid chains. Fatty acids with short chains have less van der Waals interactions and the presence of C=C double bonds hinders tight packaging sterically [2, 5].

1.1.1.3. Three major membrane lipids

1) Phospholipids exist in all biological membranes. They consist of four components: 1) one or more fatty acids, 2) a platform such as a glycerol or a sphingosine, which other components are linked to, 3) a phosphate group and 4) an alcohol connected to the phosphate (Fig. 1.2.). While fatty acids form hydrophobic barriers, the other components of phospholipids are hydrophilic allowing interactions with aqueous environment [2]. Phospholipids built on a glycerol, which consists of three C-atoms with an alcohol group for each C-atom, are phosphoglycerols. The simplest form of phosphoglycerols is diacylglycerol-3-phosphate. Other phosphogylcerols are generated via ester bond between the phosphate group and a hydroxy group of another molecule such as serin, ethanolamine, choline and inositol resulting in phosphatidylserine, -ethanolamine, - choline and -inositol, respectively [6]. An example of phospholipids built on the sphingosine is sphingomyelin (Fig. 1.2). Sphingosine is an amino alcohol with an unsaturated hydrocarbon chain. Sphingomyelin is generated by linking a fatty acid to the amino group of the sphingosine and by linking a choline to the phosphate group via an ester bond [2, 7].

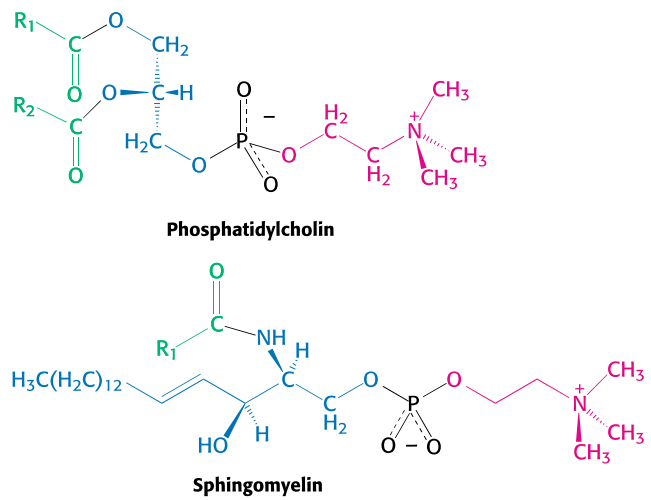

Fig. 1.2. Phospholipids. Glycerols and sphingosines (blue) are platforms for phospholipids, which contain hydrophobic fatty acid chains via ester- and amid bond (green), respectively. Both types of phospholipids also have a phosphate group (black), which can be connected to other alcohol molecules such as choline (pink) via an ester bond. Adapted from Stryer Biochemistry [2].

2) Glycolipids are derived from sphingosines. Glycolipids differ from phospholipids built on sphingosines by the presence of one or more carbohydrate units which are linked to the phosphate group of sphingosines via a glycosidic bond. The simplest version of glycolipids is cerebroside containing either a glucose or a galactose linked to the phosphate group. Gangliosides, an example for a complex glycolipid, have up to seven carbohydrate units. Glycolipids are asymmetric and localize at the extracellular site of membranes [2].

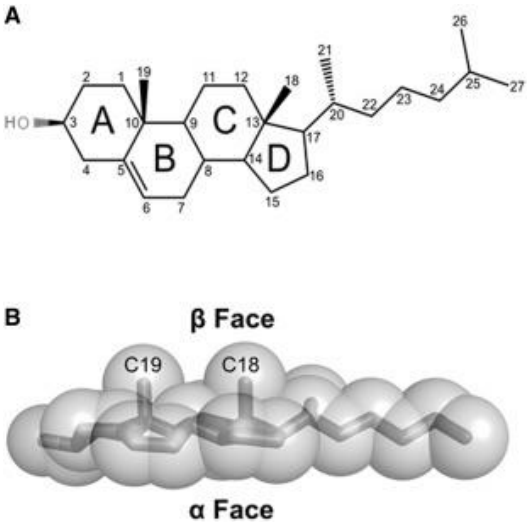

Fig. 1.3. Cholesterol. A. Chemical structure of cholesterol. C-atoms are numbered from 1 to 27. The four hydrocarbon rings are marked as A to D. **B.** Space filling and stick representation of cholesterol. Adapted from Marlow et al. [8].

3) Cholesterols have a completely different structure compared to the other two major membrane lipids (Fig. 1.3.). Cholesterol is a steroid consisting of four connected hydrocarbon rings, which is rigid with an almost flat front face (alpha-face) and a more corrugated back face (beta-face) [9]. At the end of the steroid, there is a more flexible

iso-octyl tail and at the other site of the steroid a hydroxy group, which is the only hydrophilic part of a cholesterol [2].

In membranes, a cholesterol unit localizes parallel to phospholipids [2]. The hydroxy group of the cholesterol interacts with the hydrophilic part of phospholipids via hydrogen bridges and the hydrophobic part with fatty acid chains of phospholipids. The rigid ring structure of cholesterol limits the *transgauche* isomerizations of the fatty acid chains increasing their structural orders and reducing diffusion dynamics and fluidity generating a liquid-ordered (Lo) phase [10], which decreases diffusion dynamics of membrane proteins as well [9]. The presence of cholesterol in lipid bilayers affect further characteristics of membranes such as the bending ability and the compressibility [11].

Cholesterol interacts with long, saturated phospholipids within a complex mixture of lipids such as cellular membranes. This interaction pattern of cholesterol leads to the segregation of lipids according to their chemical characteristic such as the melting point and the fluidity resulting in cholesterol-rich Lo domains surrounded by cholesterol poor liquid-disordered (Ld) domains [12]. In biological membranes, Lo domains are called as lipid rafts enriched in cholesterol and sphingolipids [13], which are small, dynamic and transient [14]. Due to tightly packed cholesterol and other lipid species, lipid rafts show characteristic features, among others, being resistant to mild detergent like triton X100, which makes studies of lipid rafts possible by isolating detergent resistant membranes (DRMs) [15].

Addition to the interaction with long saturated phospholipids, the presence of cholesterol straightens out the fatty acid chains of neighbored phospholipids making the lipid bilayer of the Lo domain thicker than that of the Ld domains [16]. The difference of the lipid bilayer thickness between two domains causes a discontinuity at the border and this generates a line tension, which is related to the membrane curvature in the domain boundary [17, 18]. Therefore, line tensions support budding [19, 20], formation of new vesicles [21] as well as fusion events [22].

Cholesterol intrinsically induces negative curvatures in lipid bilayers due to its small hydrophilic head compared to its much bigger hydrophobic body suggesting that cholesterol supports highly curved membrane structures such as lipid stalks during fusion events [9].

1.1.2. Cholesterol protein interaction

Cholesterol affects the structural and functional characteristics of integral membrane proteins 1) by changing physical properties of lipid bilayers and 2) by direct interaction via specific cholesterol binding motifs of membrane proteins [9]. Regarding to the first point, the presence of cholesterol in lipid bilayers increases the order of fatty acid chains from phospholipids reducing the free volume in lipid bilayers. This affects membrane protein conformations and shifts conformational equilibria [23], as it has been shown among others with rhodopsin. Rhodopsin takes two conformations, metarhodopsin I and II (MI and MII). Upon addition of cholesterol into lipid bilayers, the conformational equilibrium shifts to MI, which is detectable by changes of light emissions [24, 25]. Another interesting example for the role of cholesterol according to the first point is, that the Lo/Ld separation stabilizes the structure of the M2 proton channel in the influenza envelop membrane. M2 consists of a transmembrane domain and an amphipathic helix [26]. The amphipathic helix is stabilized by cholesterol in the Lo-phase, whereas the transmembrane domain with a shorter length prefers to be in the Ld-phase leading to their localization at Lo/Ld-boundary, which supports efficient budding of influenza virus [27]. Regarding to the second point (direct cholesterol protein interaction), there are several cholesterol binding motifs reported [28]. A common feature of these motifs is that they consist of three characteristic amino acid residues: a basic (K or R), an aromatic ((Y,L or W) and an aliphatic residue (I, L or V) interacting with the hydroxy group via hydrogen bridges, with the ring structure via stacking CH-Pi interaction and with the iso-octyl chain of cholesterol via van der Waals interaction, respectively. A well-studied motif is the cholesterol recognition amino acid consensus (CRAC) motif (Fig. 1.4A.). The CRAC motif is defined as (L/V)-X_{1-5}-(Y)-X_{1-5}-(K/R) from the N-terminus to the C-terminus of proteins, where the linker X_{1-5} between the three key amino acid residues is standing for one to five random residues [28]. The flexible number of possible linker amino acid residues allows the tyrosine residue within CRAC motif to be able to interact with four different rings of cholesterol [29]. The possible length of CRAC motif ranges from 5 to 13 amino acid residues. The length of 13 amino acid residues within an α-helix corresponds approximately to the cholesterol length (20 Å) [30]. As an example for direct interaction between cholesterol and protein, the peripheral-type benzodiazepine receptor interacts with cholesterol via a CRAC motif, which is involved in the uptake of cholesterol [31].

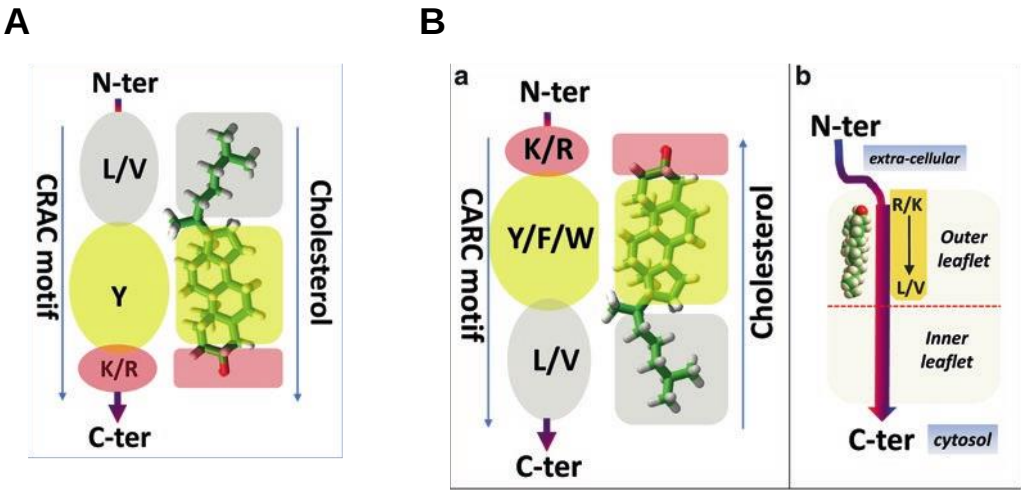

Fig. 1.4. CRAC and CARC motifs. A. CRAC motif consists of an aliphatic (L/V in grey), an aromatic (Y in yellow) and a positively charged amino acid (K/R in red) from the N-terminus to the C-terminus, which interact with the iso-octyl, the ring and the hydroxy group of cholesterol, respectively. **B. a)** CARC motif consists of a positively charged amino acid (K/R in red), an aromatic (Y in yellow) and an aliphatic (L/V in grey) from the N-terminus to the C-terminus. **b)** Localization of a CARC motif within lipid bilayer. The dashed line separates the outer- and inner leaflet. Figures adapted from Fantini et al. [28].

Interestingly, in several cases, a single residue within the CRAC motif plays the key role in cholesterol interactions [32-34] and often the highest energetic contribution to cholesterol protein interactions is assigned to the CH-pi interaction pronouncing the particular importance of the aromatic residues within the CRAC motif [35]. Another cholesterol recognition motif CARC is an inverted CRAC motif, which consists of the same three amino acid residues except the aromatic residue (Fig. 1.4B). It allows not only Tyr, but also Phe or Trp to be included into the motif: (K/R)-X_{1-5}-(Y/F/W)-X_{1-5}-(L/V) [28]. For example, beta(2)-adrenergic receptor can interact with cholesterol via its CARC motif, which seems to stabilize the structure of the receptor [36]. Other type of cholesterol interaction motif is the CCM, an abbreviation for the cholesterol consensus motif. The CCM motif is not a linear sequence of amino acid residues such as the CRAC or CARC but is distributed between two transmembrane segments. The first segment contains Lys/Arg, Trp/Tyr, and Ise/Val/Leu, which face to the same side of the α-helix. The second segment supports the cholesterol-protein interaction via its aromatic residue Tyr or Phe interacting with the cholesterol from the opposite site [9]. This type of cholesterol interaction motif is observed from the haemagglutinin (HA) of influenza viruses. Mutations of amino acid residues belonging to the CCM motif show a delay in processing of HA in Golgi, such as acquisition of Endo H (endoglycosidase H)- resistant carbohydrates and proteolytic cleavage [37].

1.1.3. Photoactivatable cholesterol species as tools to study direct interactions between cholesterol and proteins

Proper studies of cholesterol interactions of integral membrane proteins by performing X-ray crystallography and NMR analysis are complex and difficult among others due to the low expression level, solubility and non-physiological conditions used for structural studies, although it has been improved a lot during last years [38, 39]. Instead, photoactive labeling of lipid species has been considered as a useful tool to study lipid-protein interactions at the molecular level starting from 1975 [40].

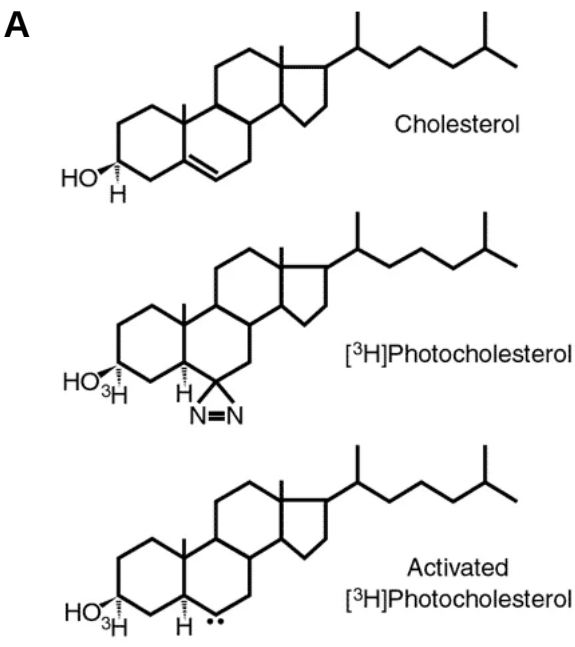

Fig. 1.5. Tritium [^{3}H]-labeled photoactivatable cholesterol. A. From the top: physiological cholesterol, [^{3}H]-labeled photoactivatable cholesterol and activated form of [^{3}H]-labeled photoactivatable cholesterol. Figure adapted from Thiele et al. [41]. **B.** Activation of a diazirine group by irradiating UV-light resulting in a reactive carbene group which forms a covalent linkage to its interaction partner. Figure adapted from Lepage et al. [42].

In 2000, Thiele et al. generated a photoactivatable cholesterol by dissolving Δ5 double bond and by replacing C-6 hydrogen with a diazirine ring (Fig. 1.5. A), which can be activated to a reactive carbene upon UV-light irradiation resulting in crosslinking to

close interaction partner (Fig. 1.5**.** B) [41]. After incorporation of photoactivatable cholesterols into cells by feeding, proteins interacting with cholesterols are covalently linked to the photoactivatable cholesterols. For detection of cholesterol-protein complex, the hydrogen atom at C-3 of cholesterol has been replaced by tritium (^{3}H) [41]. However, considering laborious handling of ^{3}H, photoactivatable cholesterol has received an alternative labeling, an alkyne (Fig. 1.6. A), which can be covalently linked to affinity tags containing an azide group such as biotin azide by copper-mediated click reaction (Fig. 1.6. B).

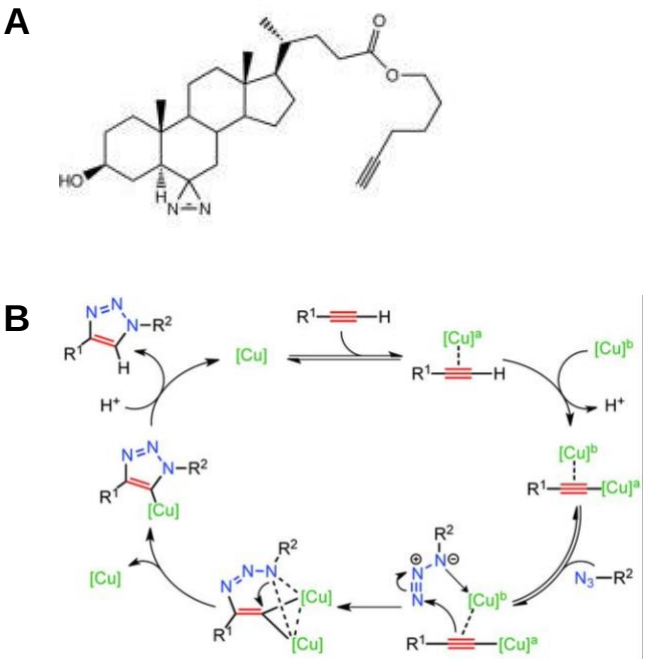

Fig. 1.6. Photoactivatable and clickable cholesterol. A. Structure of the bifunctional cholesterol. Figure adapted from Hulce et al. [43]. **B.** Copper-mediated click reaction between an alkyne and an azide. Figure adapted from Worrell et al. [44].

By using this bifunctional cholesterol, Hulce et al. could identify cholesterol interacting proteins, whose previously reported functions are involved in cholesterol biosynthesis, transport and cholesterol level regulation [43].

1.2. Hepatitis C Virus (HCV)

1.2.1. General aspects of HCV

1.2.1.1. Hepatitis

The definition Hepatitis describes a liver inflammation. The causes of hepatitis can be toxic substances such as alcohol or drugs, autoimmune- and metabolic diseases as well as infection with viruses and bacteria. But in most cases, hepatitis is mediated by infection with one of five main hepatitis viruses referred as type A, B, C, D and E. Acute infection can be asymptomatic. However, it also induces symptoms such as jaundice (yellowing of the skin and eyes), dark urine, extreme fatigue, nausea, vomiting and abdominal pain. Infection with hepatitis virus B (HBV) and C (HCV) often cause chronical liver inflammation which increase the risk of liver cirrhosis and hepatocellular carcinoma (HCC) development [45].

1.2.1.2. Discovery of HCV

In 1975, Feinstone at al. reported for the first time about patients having transfusion-associated hepatitis not positive for hepatitis A and B [46]. Then 14 years later, the RNA genome of so called non-A and non-B hepatitis (NANBH) agent was discovered [47], which is currently known as HCV.

1.2.1.3. Classification of HCV

HCV belongs to the genus Hepacivirus within the family Flaviviridae. Virions are 40-60 nm in diameter, with approximately 9-13 kb of positive-sense and non-segmented RNA genomes. Members of Flaviviridae mostly encode a single core protein and two or three envelope glycoproteins. Addition to Hepacivirus, Flavivirus (i.e. Dengue virus), Pestivirus (i.e. Bovine viral diarrhea virus 1) and Pegivirus (i.e. Pegivurs C) belong to the family Flaviviridae [48].

1.2.1.4. Genetic heterogeneity of HCV: quasispecies and genotypes

HCV genome replication depends on error-prone RNA-dependent RNA polymerase (RDRP), where an associated repair mechanism does not exist. This leads to mutations during viral replication resulting in genetic heterogeneity. The heterogeneity

of HCV results in emergences of quasispecies and genotypes. The term quasispecies refers to genetic diversities of a virus population within an infected patient. In contrast to that, the term genotype describes genetically different virus isolates [49].

There are at least six major genotypes of HCV designated as genotype 1-6, which were identified by sequence and phylogenetic analysis. Each genotype differs from the other genotypes in 30-35% of nucleotide sites in average. There are more variable regions such as that encoding envelop proteins, E1 and E2 and more conserved regions such as that encoding capsid core as well as the 5' UTR within HCV genome. Despite the genetic heterogeneity, different HCV genotypes contain colinear genes of similar or identical size within the open reading frame (ORF) and the transmission dynamics, persistence and disease development are similar. Furthermore, each HCV genotype includes several subtypes, where the difference between subtypes is about 20-25% in average. Subtypes are connoted with lowercase alphabets such 1a, 1b and 2a [50].

The heterogeneity of HCV genomes supports viruses to escape immune response in chronical infection and different genotypes and subtypes contribute to varied resistance to some of the currently available antiviral drugs [51]. Therefore, determination of genotypes/subtypes of HCV genomes in patients is important for planning therapy [52].

1.2.1.5. Epidemiology

In 2021, World Health Organization (WHO) estimated that there are 58 million people having chronical infection with HCV. Chronic HCV infection is globally distributed: the Eastern Mediterranean- (12 million), the European- (12 million), the South-East Asia- (10 million), the Western Pacific- (10 million), the African- (9 million) and the America region (5 million) [53]. According to the genotype distribution, genotype 1 with 46.2% of all HCV cases is the most prevalent virus, which is followed by genotype 3 with 30.1%. A total of 22.8% of all HCV cases are derived from genotype 2, 4 and 6. The genotype 5 is responsible for <1% of all HCV cases [54]. Interestingly, HCV genotypes often are specific for certain regions, except globally spread 1, 2 and 3 (Fig. 1.7) [54, 55].

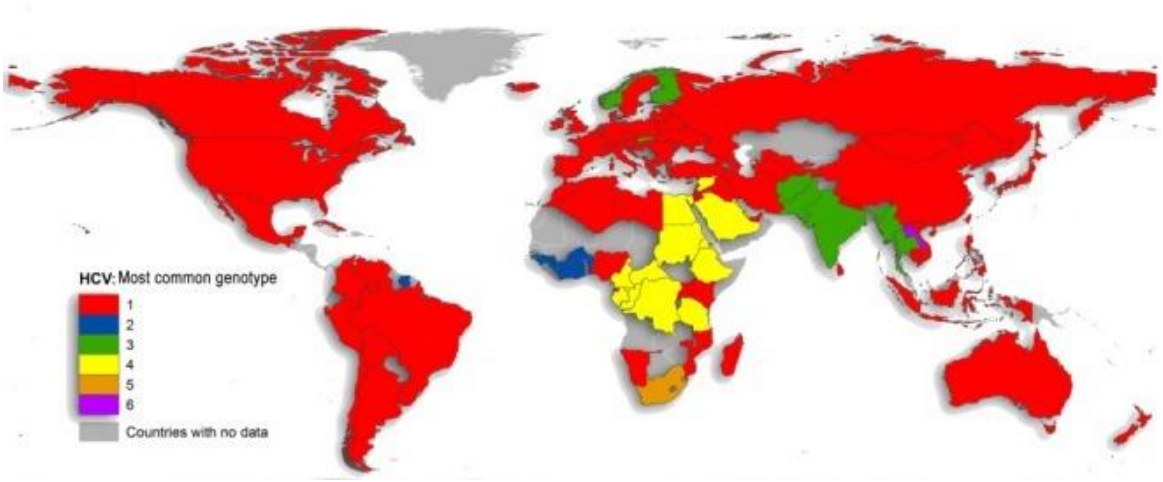

Fig. 1.7. Distribution of HCV genotypes. Data from 1217 studies representing 117 countries covering 90% of the global population. Adapted from Messina et al., 2015 [54].

Every year, about 1.5 million new infections are estimated to occur. Transmission of HCV occurs through blood contacts. Common causes of HCV transmission are: 1) reuse and no proper sterilization of medical equipment such as syringes and needles, 2) transfusion of blood containing infectious viruses. 3) drug abuse via injection with used syringes and needles. Apart from that, virus transmissions from an infected mother to her baby during birth and during sexual activities leading to blood contacts are considered be potential transmission routes, although these are rare cases [53].
Infection with HCV often is asymptomatic and for 30% of infected people, viruses are cleared within 6 months of infection by their own immune response. However, for approximately 70% (55-85%) of HCV-infected individuals, it develops to chronical infection. Among 15% to 30% of patients with a chronic infection will have cirrhosis within 20 years. In 2019, roughly 290 000 people died from HCV infection, mostly due to cirrhosis and HCC [53]. Currently, there is an indication that COVID19 increases the mortality of patients with cirrhosis (40%) compared to unselected populations (5.8%), cirrhosis patients prior to COVID19 (5.4%) and patients with cirrhosis and influenza (18%) suggesting the need of studies about co-infection with HCV and SARS-Cov-2 [56].

1.2.1.6. Testing and diagnosis

An infection with HCV can be diagnosed by two steps of tests. Firstly, the serological presence of antibodies specific for HCV is assessed. In case of a positive result, result must be confirmed by second test, where the presence of viral RNA is detected, since

individuals who had acute HCV infection often show HCV-specific antibodies despite of virus clearance. After diagnosis, the degree of liver damage (Fibrosis and cirrhosis) must be determined by liver biopsy or non-invasive methods. Early diagnosis is important to prevent severe consequences of HCV chronic infection and further virus transmission [53].

1.2.1.7. Treatment

Since 1990, interferon α (INF-α) has been used to treat HCV-infected patients, which supports anti-viral response [57]. The success of interferon treatment is evaluated by measuring sustained viral response (SVR). SVR refers to a state where no virus can be detected 24 weeks after anti-viral treatment [58]. The effectiveness of INF-α treatment has been improved when it was combined with ribavirin, a guanosine analogue. The major mode of action is either direct incorporation into viral genome or into RDRP, thereby inhibiting viral RNA replication. Apart from that, ribavirin is reported to inhibit guanosine production. Although it does not decrease SVR efficiently in its monotherapy, using of ribavirin is recommended for every HCV genotype in combinatory therapies [59]. Pegylation of INF-α enhances the rate of SVR from the combination therapy with ribavirin up to 40-50% for genotype 1 and around 80% for genotype 2 and 3, because it extends its half-life and prevent the clearance of drug, however, not affecting cellular activity [60]. Despite of previously reported success of interferon treatment against HCV infection, there are many uncomfortable side effects and patient compliance to antiviral therapy has been decreased. This has been resulted in therapies without interferon treatment, which should take shorter time with minimum side effects [59].

Apart from INF-α and ribavirin, direct acting antivirals (DAAs) have been developed, which specifically target essential viral activities. DAAs include inhibitors of viral proteases such as NS3/4 (glecaprevir and voxilaprevir) and NS5A (velpatasvir and pibrentasvir), and inhibitors of viral RDRP, NS5B (sofosbuvir). Combination therapies of these DAAs such as sofosbuvir/velpatasvir and glecaprevir/pibrentasvir display upto 95% of SVR pan-genotypically [58]. However, there have been several observations of resistance-associated substitutions (RASs) due to emerging DAA-resistant HCV variants demonstrating the necessity of vaccines against HCV [61, 62]. Since discovery of HCV, there were attempts to generate vaccines against HCV. However,

the genetic heterogeneity and the ability to escape adaptive immune response of HCV reflect the hurdle of vaccine research [63].

Additionally, host targeting antivirals (HTAs) have been developing for cure of HCV-infected patients. The main two focuses of the development are 1) to support immune response activation and 2) to inhibit host pathways essential for virus replication cycle [59].

1.2.2. Molecular biology of HCV

1.2.2.1. HCV genome organization

HCV genome is a positive-strand RNA, which contains an open reading frame (ORF) encoding a polyprotein consisting of around 3000 amino acids. This corresponds to ten viral proteins after processing [64, 65]. This ORF is flanked by non-translated regions (NTRs) with high order structures, one for each end of the ORF (Fig. 1.8.) [64]. These NTRs are essential for viral RNA replication [66]. In the 5' NTR, an internal ribosome entry site is localized, which enables the translation of the polyprotein in a cap-independent manner [67]. The HCV polyprotein is cleaved during and after translation by host and viral proteases resulting in ten membrane-associating proteins (Fig. 1.8. and Fig. 1.9.) [65]. The first three proteins from the N-terminus of the polyprotein, capsid core, envelop proteins E1 and E2 are components of viral particles, therefore called as structural proteins.

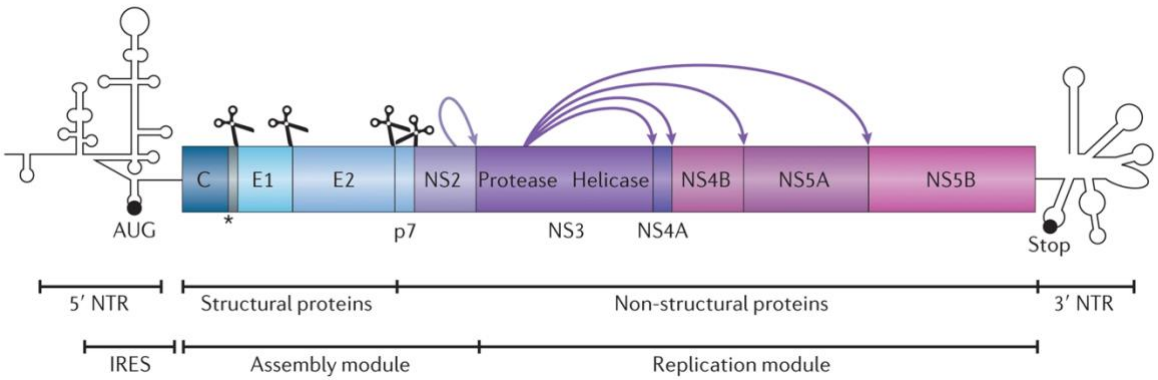

Figure 1.8. HCV genome organization and polyprotein cleavage. HCV genome contains an ORF flanked by a NTR at each end of ORF. A part of the 5' NTR functions as IRES for the translation control of HCV genome. The ORF encodes a polyprotein, which is co- and post-translationally cleaved by host (marked with scissors) as well as viral proteases NS2 and NS3/4A (marked with arrows). Each viral protein can be assigned to structural/non-structural proteins and/or assembly-/replication modules depending on the presence in viral particle and on the major functions, respectively. Figure adapted from Bartenschlager et al., 2013 [68] .

The other proteins not contained in viral particles are called as non-structural proteins. These are P7, NS2, NS3, NS4A, NS4B, NS5A and NS5B. Since P7 and NS2 are essential for infectious viral particle assembly, they belong to the assembly module together with core, E1 and E2 [69]. The rest of the non-structural proteins (NS3-NS5B) is sufficient for a proper viral RNA replication [70]. Therefore, these proteins are grouped as a replication module [68]. However, all non-structural proteins are required for infectious viral particle assembly too [71].

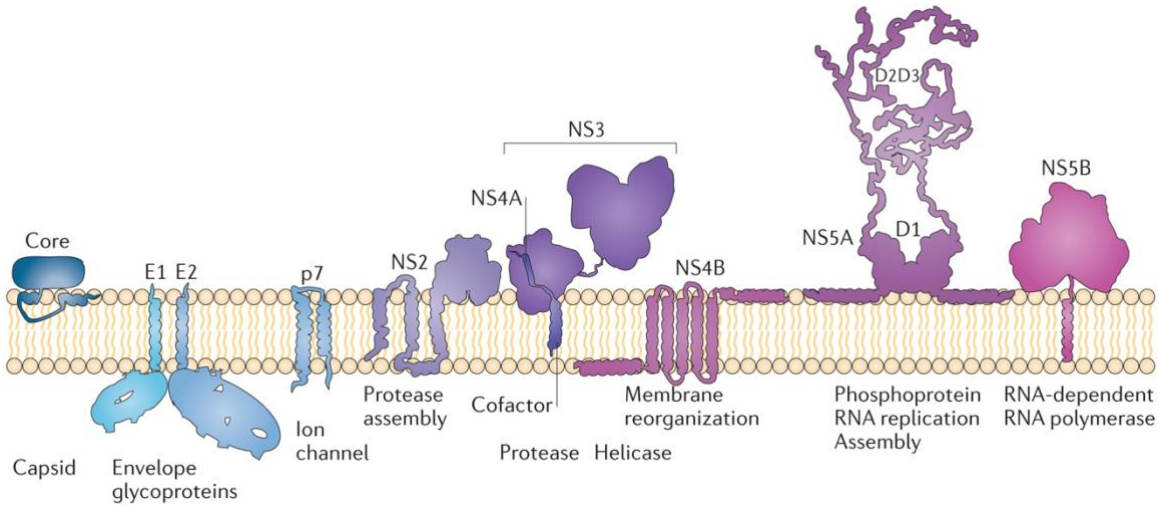

Fig. 1.9. Membrane topology models and main functions of each HCV protein. Almost every viral protein associates with membrane by a or several transmembrane segments except core, NS3 and NS5A. Core and NS5A contain amphipathic α-helices, which mediate their membrane interaction. NS3-membrane association occurs via a small α-helix and via the cofactor NS4A intercalating into the N-terminal protease domain of NS3. NS5A is shown as homodimer. Figure adapted from Bartenschlager et al., 2013 [68].

1.2.2.2. Overview of viral proteins

HCV core is the building material of the viral nucleocapsid. There are two essential cleavage events for functional core: the first cleavage by a signal peptidase separates the immature core (191 aa) from the polyprotein [72] and the second cleavage by a signal peptide peptidase serves as a maturation step resulting in the mature 21 kDa core protein of 177 aa released from ER to target to LDs [73]. A mature core consists of two domains. The N-terminal domain 1 (aa 1-117) is hydrophilic and responsible for RNA binding as well as RNA folding, which is based on the high number of positively charged aa residues within domain 1 [74, 75]. Moreover, the homo-oligomerization of the core and the interaction with the envelop protein E1 are mediated by the domain 1 as well [76, 77]. The domain 2 contains two α-helices (aa 119-136 and 148-165), which

are connected to each other via a hydrophobic loop, and it is responsible for the LD-localization of core proteins [78].
There are additional core variants due to alternative reading frame via ribosomal frame shift. However, the role of these core variants in the HCV replication cycle is not known [75].

The envelope glycoproteins E1 and E2 are type I transmembrane proteins which are 35 and 70 kDa, respectively. E1 and E2 form a noncovalent heterodimer and consist of an N-terminal ectodomain localizing in the ER-luminal site (around 160 and 360 aa for E1 and E2, respectively) and a short C-terminal transmembrane domain (TMD) of around 30 aa [75]. The ectodomain is highly glycosylated and the TMD contributes to E1-E2 non-covalent heterodimerization. E1 and E2 are involved in virus assembly, virus entry and fusion with endosomal membranes, which requires abilities to adapt different conformations depending on functional necessity [75].

The viroporin P7 is an integral membrane protein of 7 kDa consisting of 63 aa, which has two transmembrane α-helices. These two α-helices are linked via a positively charged cytosolic loop [79]. P7 is not required for HCV RNA replication, but it is essential for infectious virus assembly and release. The importance of P7 for the HCV assembly on the one hand is based on its interaction with other viral proteins, such as NS2 as well as E1 and E2 for virus envelopment, on the other hand on its ability to from oligomers (hexamers and/or heptamers), which serve as ion channel complexes regulating pH-values [80]. The ion channels consisting of P7 prevent unwished conformational changes of nascent virions in an acidic environment by lowering the acidity to ensure the maturation of virus [75].

NS2 is an integral protein consisting of 217 aa with a molecular weight of 23 kDa. It has a N-terminal transmembrane domain (aa 1-94) consisting of three transmembrane segments (aa 4-23, 27-49 and 72-94) and a small α-helix (aa 61-70) as well as a C-terminal cytosolic domain (aa 94-217) [81], which can form a homodimer and acts as a cysteine protease together with the N-terminal one-third of NS3 [75]. The protease activity is derived from the catalytic triade His 143, Glu 163 and Cys 184, which is responsible for the cleavage of the junction between NS2 and NS3. In the dimer form, His 143 and Glu 163 are localized on one monomer and Cys 184 localizes on the other

monomer [82]. Although NS2 is dispensable for the HCV RNA replication, the cleavage mediated by NS2 is essential for the release of functional NS3 for proper viral RNA replication [75].

NS2 is essential for HCV virus assembly, where the protease activity is not required [83, 84]. The importance of NS2 in the virus assembly is suggested to be based on its interaction with other viral factors belonging to assembly module such as E2 and P7 as well as NS3, which is a component of viral RNA replicase complex. Thereby, NS2 might recruit the replicase complex to the place of the virus assembly [81]. Another aspect of NS2 importance for the virus assembly is its localization on lipid rafts, which have been studied by isolating detergent resistant membranes (DRMs). For NS2 DRM localization, presence of functional P7 is essential. Disrupted NS2-DRM association impairs DRM localization of E2 leading to an assembly defect indicating that DRMs serve as virus assembly platforms [85]. Additionally, the palmitoylation of NS2 via Cys 113 seems to be important for the DRM localization of NS2 [86]. Moreover, NS2 is important for envelopment of HCV as well. HCV is suggested to exploit the endosomal sorting complex required for transport (ESCRT) machinery for its envelopment [87, 88]. There, the K63-linked polyubiquitination of NS2 via Lys 27, Lys 172 and Lys 173 mediated by a RING-finger E3 ligase March8 fulfills the late domain function, recruiting HRS, an initiator of ESCRT, to the HCV assembly platform. Beside ubiquitination, NS2 can be phosphorylated at Ser 168 mediated by the protein kinase CK2 which targets NS2 for the proteasomal degradation [89].

NS2 is not only important for virus assembly, but also for virus release. NS2 interacts with adaptor proteins (APs) AP-1A, AP-1B and AP-4. The interaction between NS2 and APs is mediated by two dileucine motifs of NS2 consisting of Leu 202, Leu 203, Leu 216 and Leu 217. AP-1A is responsible for Golgi-endosome trafficking and AP-1B as well as AP-4 are involved in basolateral sorting within post-Golgi compartments. All three APs mediate the virus release and the cell-free spread of virus via interacting with NS2. But only AP-1B and AP-4 are involved in cell-to-cell spread [90].

Moreover, the NS2 seems to manipulate cell cycle [91, 92], to inhibit apoptosis [93] and to escape host immune responses by altering the cytokine gene expression [94, 95]. Additionally, NS2 impairs host RNAi interferences by interaction with double stranded RNAs (dsRNAs) and small interfering RNA (siRNAs) via its Cys 184 [96]. Interestingly, NS2 downregulates HCV protein translation by inducing ER-stress [97] and decreases viral RNA replication [98]. How far this ER-stress induction and

subsequent consequences can affect the viral replication cycle remained to be investigated.

NS3 consists of 631 aa with molecular weight of 70 kDa. NS3 acts as a serine protease with the first N-terminal 180 aa and as an NTPase/RNA helicase with the remaining C-terminal aa [75]. The protease activity of NS3 is important for cleavage of HCV polyproteins and the helicase activity for unwinding single- and/or double-stranded RNA in an inchworm or ratchet-like manner [99]. The linker connecting the protease and the helicase within NS3 is required for virus assembly possibly by mediating NS3 interactions with other viral and/or host factors [100]. NS3 exists as a noncovalent complex with **NS4A**, which is a cofactor for the NS3 serine protease consisting of 54 aa with molecular weight of 16 kDa. The N-terminal part of NS4A (aa 1-21) is a transmembrane α-helix responsible for the NS3-4A membrane localization as an integral protein complex. The central part consisting of aa 21-32 is a β-strand interacting with NS3. The C-terminal acidic NS4A (aa 40-54) associates with other viral RNA replicase components [75].
NS3-4A is localized not only in ER, but also recruited to mitochondrial membranes and/or to ER-mitochondria contact sites, where it impairs host innate immune response by cleaving the mitochondrial antiviral-signaling protein (MAVS), adaptor of pattern recognition receptors (PRRs) for dsRNA such as Retinoic acid-inducible gene I (RIG-I) and Melanoma Differentiation-Associated protein 5 (MDA5) responsible for induction of interferon-β expression [75].

NS4B is a hydrophobic 27 kDa integral membrane protein consisting of 261 aa. NS4B contains a N-terminal part (aa 1-69), a central part with four predicted transmembrane segments and a C-terminal part (aa 191-261). Each of the N- and C-terminal parts has two amphipathic α-helices facing to the cytoplasm, which contribute to membrane association of NS4B with the central transmembrane domain [75]. The most studied function of NS4B is the generation of the membranous web, deformed membrane structures consisting of membranous vesicles, where the viral RNA replication occurs [75, 101]. As a part of the viral RNA replicase, NS4B interacts with other viral proteins belonging to the replication module and possibly with viral RNA as well [102]. Moreover, NS4B seems to act as a NTPase [103] and it is important for the virus assembly, too

[104]. NS4B can form oligomers and the oligomerization is important for the membranous web formation and HCV RNA replication [75].

NS5A is a 56-58 kDa membrane-associated phosphoprotein composed of 447 aa, which is essential for the viral RNA replication and for the virus assembly. NS5A consists of its N-terminal amphipathic α-helix and C-terminal cytosolic domain. The N-terminal amphipathic α-helix allows NS5A association on membranes and on LD. The cytosolic domain of NS5A can be divided in three highly structured domains, which are linked via two low complexity sequences (LCS1 and LCS2) [105]. Highly structured domain 1 (D1, aa 36-213) can bind RNA [106], associate with LDs [107] and is essential for membranous web formation [108]. Moreover, D1 is suggested to form a dimer [109] and the folding state of D1 is kept by zinc binding and disulfide bonds [110]. The domain 2 (D2, aa 250-342) and 3 (D3, aa 356-447) are unstructured and widely dispensable for the viral RNA replication [69]. However, D3 is required for virus assembly [111]. Additionally, D3 is involved in interaction with core and in viral RNA transfer to the virus assembly site [112, 113].
NS5A is distinguished between the basal- (56 kDa) and the hyperphosphorylated (58 kDa) states. The central and the C-terminal parts of NS5A are the places, where the basal phosphorylation occurs, whereas the hyperphosphorylation occurs in LCS1 [75]. Depending on its phosphorylated form, NS5A seems to interact with different host factors, which supports the viral RNA replication and virus production [114].

NS5B is a 68 kDa RNA dependent RNA polymerase (RDRP) with 591 aa, which mediates the viral RNA replication. NS5B consists of a N-terminal catalytic domain (aa 1- 530) which is connected to its C-terminal anchor (aa 570-591) responsible for the membrane association [75]. During viral RNA replication, NS5B generates a negative-stranded RNA from the original viral RNA. Upon RNA polymerase reaction with the negative-stranded RNA as template, a new copy HCV genome is created. [115].

1.2.2.3. Cell culture tools for studying HCV replication cycle

Ten years after the discovery of HCV genome, the first cell culture system was established in 1999 [70], which has allowed thorough investigation of nature of the HCV RNA replication which opened the way for antiviral drug development [116]. This system is known as a subgenomic replicon and includes a reporter gene encoding

neomycin phosphotransferase and/or luciferase followed by the minimal HCV genome essential for viral RNA replication, which encodes from NS3 to NS5B of the genotype 1b, Con1. The expression of the reporter and the HCV RNA replicase is under control of the IRES of HCV and of encephalomyocarditis virus (EMCV), respectively and the whole system is flanked by 5'- and 3'-NTR of HCV genome [70]. Passaging of single hepatoma Huh7 cell clones positive for HCV subgenomic RNA replication has revealed cell culture adaptive mutations enhancing the viral RNA replication. Furthermore, it established individual cell clones with higher permissiveness for HCV such as Huh7 Lunet and Huh7.5, which are cured from replicating subgenomic replicon with IFN-α treatment [117, 118]. First replicon, which does not need any adaptive mutation for high replication, is derived from the genotype 2a JFH1 [119]. However, infectious virus production using full length virus genome from JFH1 was not efficient in cell culture, which has been compensated by several adaptive mutations for higher virus production [120, 121]. Further attempts to gain high virus titer from cell culture systems resulted in generation of a chimeric HCV consisting of genotype 2a J6CF genome encoding core to the first transmembrane segment of NS2 and of JFH1 genome encoding the remaining NS proteins, which is called as Jc1. By using this chimeric construct, 10-fold higher infectious titer can be achieved compared to wt JFH1 [122]. A reporter system JcR2a derived from Jc1 was generated by inserting renila luciferase into the 5'-end of Jc1, which is flanked by genes encoding 16 N-terminal aa of core (5'-end) and encoding the foot-and-mouth disease virus (FMDV) 2a peptide for proteolytic separation of the reporter from the HCV polyprotein [123].

1.2.2.4. HCV replication cycle and its close relationship to cholesterol

HCV entry. One of the main features of HCV is that viral particles are highly lipidated by association with low-density and very-low-density lipoproteins (LDL and VLDL) containing various apolipoproteins such as ApoE [69, 124, 125]. Lipidomic analysis of HCV Jc1 particles revealed that more than 60% of virus lipid content consisting of cholesterol and cholesterol ester resembles to LDL lipid composition (20% and 44%, respectively) [126]. This highly lipidated virus, therefore called as lipoviroparticles, interacts among others with LDL-receptors on the surface of hepatocytes, which capture virus close to the cell surface with other receptors such as heparan sulfate proteoglycans (HSPGs). Then, interactions with further receptors such as scavenger receptor class B member1 (SRB1) and tetraspanin CD81 help viral particles to form

an entry complex with tight junction protein claudin1 (CLDN1) and occludin (OCLN), which supports clathrin-mediated endocytosis of HCV [127]. The virus entry depends on proper localization of these receptors on membrane microdomains with high concentration of cholesterol, lipid rafts [128]. Interestingly, CD81 function as a receptor mediating HCV entry is depending on its conformation which is depending on its interaction with cholesterol [129, 130].

HCV RNA replication. After endocytosis of HCV, viral genome is released into cytoplasm and the viral proteins are expressed at the rough ER. There, non-structural proteins NS3-N5B are sufficient for viral RNA replication [70] and their localization on lipid raft seems to be essential, since depletion of cholesterol disrupts HCV RNA replication [131]. Furthermore, the expression of NS3-NS5B might recruit host factors to lipid raft probably for exploiting them to support HCV replication cycle [132]. A functional RNA replication complex consists of viral RNA, HCV RDRP NS5B and RNA replication organelles (ROs), double membrane vesicles (DMVs). DMVs are generated by NS3-NS5B supported by several host factors [127]. Among others, due to structural similarities, the autophagy machinery has been subjected to investigations to understand the mechanism of DMV generation. An interesting aspect of the autophagy related to cholesterol is the specific autophagosome cholesterol association in lipid rafts upon HCV replication, which appears to be important for HCV RNA replication [133].

Although DMVs are originated from ER, they contain high concentration of cholesterol in contrast to the low cholesterol level in ER [134]. There are several host factors reported to induce accumulation of cholesterol on DMVs such as oxysterol-binding protein (OSBP), VAMP-associated protein A and B (VAPA and VAPB,) which exchange phosphatidylinositol 4-phosphate (PI4P) for cholesterol via non-vesicular transport [135]. Additionally, Stöck et al. reported direct cholesterol transports from endo/lysosomes to ER at their contact sites for viral RNA replication [136]. Components of HCV RNA replicase complex also regulates cholesterol level by manipulating host factors involved in the cholesterol biosynthesis [137, 138].

HCV assembly and release. The components of the assembly module, core, E1, E2, P7 and NS2, localize on lipid raft and this localization is essential. Disrupting their lipid raft localization by depletion of cholesterol impairs infectious virus production [85].

Virus assembly is thought to occur in close proximity to lipid droplets (LDs), which are storage organelles for neutral lipids such as triacylglycerols and cholesterol esters [69]. Core and NS5A localize on LDs [139, 140]. Moreover, envelop proteins E2 and non-structural proteins NS2, NS3, NS4B and NS5A are closely localized to LD indicating LDs as platforms, where the assembly- and the replication modules are recruited together [81, 141]. Ultrastructural studies of LDs positive for E2 and NS5A representing assembly- and replication modules, respectively, are tightly surrounded by ER membranes connected with DMVs [142]. HCV RNAs synthesized from DMVs might be transported to the assembly platform via interaction with NS5A. Subsequent encapsidation and envelopment of viral RNA occurs in a coupled way [113]. Importantly, there are indications that components of the VLDL assembly and its secretion might be involved in the HCV assembly, such as ApoE, ApoB and microsomal triglyceride transfer protein (MTTP) [125, 143]. However, HCV seems to be secreted not via VLDL secretion pathway, but via the canonical TGN-endosomal secretion pathway [90, 144, 145].

1.2.2.5. Lipid droplets in HCV replication cycle

Lipid droplets consist of a hydrophobic core, which is sequestered from the cytoplasm by a monolayer of phospholipids as well as peripheral and integral membrane proteins. Components of the hydrophobic core of LDs are neutral lipids such as triacylglycerols (TAG) and cholesterol esters (CE), which are synthesized in ER by diacylglycerol acyltransferase (DGAT1 and DGAT2) and acyl-CoA:cholesterol O-acyltransferase (ACAT1 and ACAT2), respectively [146]. Neutral lipids form a lens-like structure between lipid leaflets, if they reach certain concentration (5-10 mol% for TAG) [147, 148].

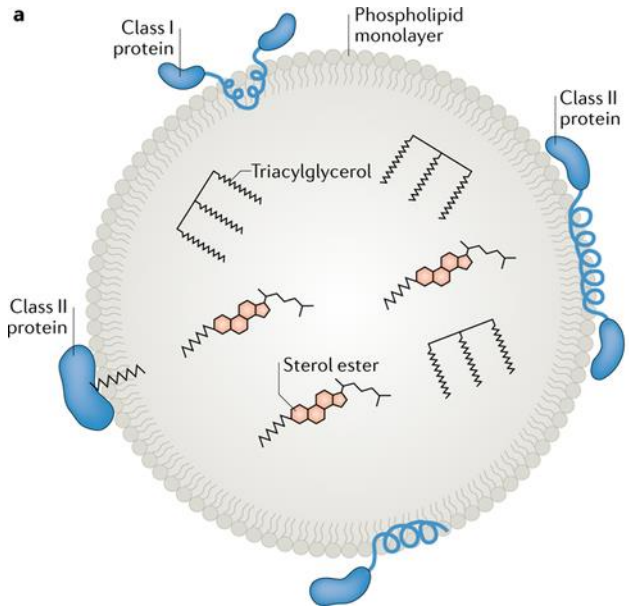

Fig. 1.10. Lipid droplet (LD). A LD consists of a hydrophobic core sequestered from the cytoplasm by the phospholipid monolayer. The hydrophobic core contains neutral lipids such as triacylglycerol and sterol ester. On the phospholipid monolayer, there are proteins interacting with LD via hairpin structures, lipid anchors or amphipathic helices. Adapted from Olzmann and Carvalho, 2019 [146].

LDs function as organelles for neutral lipid storage or as sources for phospholipids depending on nutrition and/or cell growth. In case of a nutritional deficiency or a cellular growth, TAG from LDs are hydrolyzed by lipolysis or by lipophagy to cover the cellular needs of phospholipids [146]. In contrast to that, in phospholipid abundance, LDs store free fatty acids in forms of TAG and therefore protect cells from lipotoxicity. An excess of free fatty acid can disrupt membrane structures as detergent and they can be used for generation of more complex lipid species, which are cytotoxic in high concentrations, such as ceramide, acylcarnitine and diacylglycerol. The disability of storing free fatty acids in LDs leads to diseases related to lipotoxicity such as type 2 diabetes and non-alcoholic fatty liver disease [149, 150]. Furthermore, there are indications for the roles of LDs in the protection against ER stress and mitochondrial damage during autophagy [146].

In the LD biogenesis, budding of LDs is depending on the phospholipid composition of ER membranes, especially phosphatidic acid (PA) and diacylglycerol (DAG) [151-153]. The phospholipid composition is responsible for the membrane tension and for the directionality of budding: lipid species with a negative curvature such as DAG and phosphatidylethanolamine (PE) tend to show LDs embedded in ER, those with a positive curvature such as lysolipids enhances emerging of LDs from ER [154]. Therefore, different lipid compositions with different membrane curvatures between ER monolayers decides for the direction of LD budding [146]. Furthermore, correct budding of LDs requires LD- and ER-localizing proteins such as fat storage-inducing transmembrane (FIT) proteins, perilipin1 (PLIN1) and seipin [155-157]. Apart from the

lipid composition and the LD-ER localizing proteins, the membrane surface tension derived from the physical force between the hydrophobic core of LDs and the aqueous cytoplasm side is important for budding of LDs [158].

Expansions of LDs occur through 1) fusion of LDs, 2) neutral lipid transfer at ER-LD contact sites and 3) on-site biosynthesis of neutral lipids [146]. During the expansion of LDs, the phospholipids synthesis is increased to cover the increasing LD surface. For example, CTP:phosphocholine cytidylyltransferase-α (CTTα), a rate-limiting enzyme in phosphatidylcholine (PC) synthesis, is recruited to LDs and activated by fatty acid-mediated LD expansion resulting in higher concentration of PC [159].

After budding, some of LDs are detached from ER in higher eukaryotes, which is a reversible process. However, the exact mechanism of the selective detachment is not well elucidated [146]. LD-ER reassociation depends on COPI coatomer complex. The components of COPI coatomer are recruited to LDs and cause budding of small droplets of around 60 nm in diameter. Due to increasing surface/hydrophobic core volume ratio, the surface tension of the original LDs grows making LD-ER fusion more favorable [160, 161].

Analysis of LD associating proteins revealed that the LD-proteomes depend on the cell type and methods used. However, there are 100-150 commonly found proteins mostly involved in lipid metabolism, membrane trafficking and protein degradation. Proteins from the perilipin (PLIN) family also belong to the invariable LD-proteomes [146, 162]. LD proteins interact with LDs via hairpin structure, amphipathic α-helices or lipid anchors and can be divided in class I and class II. Class I includes those, which are able to localize both on the surface of ER and of LD. Class II proteins are directly transported to LDs from cytoplasm anchoring into the LD monolayer [146]. There are evidences, that the localization of class I proteins between ER and LDs might be regulated by interaction with other ER proteins [163-165] and/or by the ER-associated protein degradation (ERAD) pathway, which degrades proteins on ER with higher conformational instability, while these proteins stay more stable on LD monolayers [146]. Class II proteins might compete for the LD-association with the phospholipid monolayer of LDs as shown in molecular dynamics simulations [166, 167]. Especially In case of high surface tension, phospholipid monolayers do not fully cover all surface of LDs allowing class II proteins to localize on LDs.

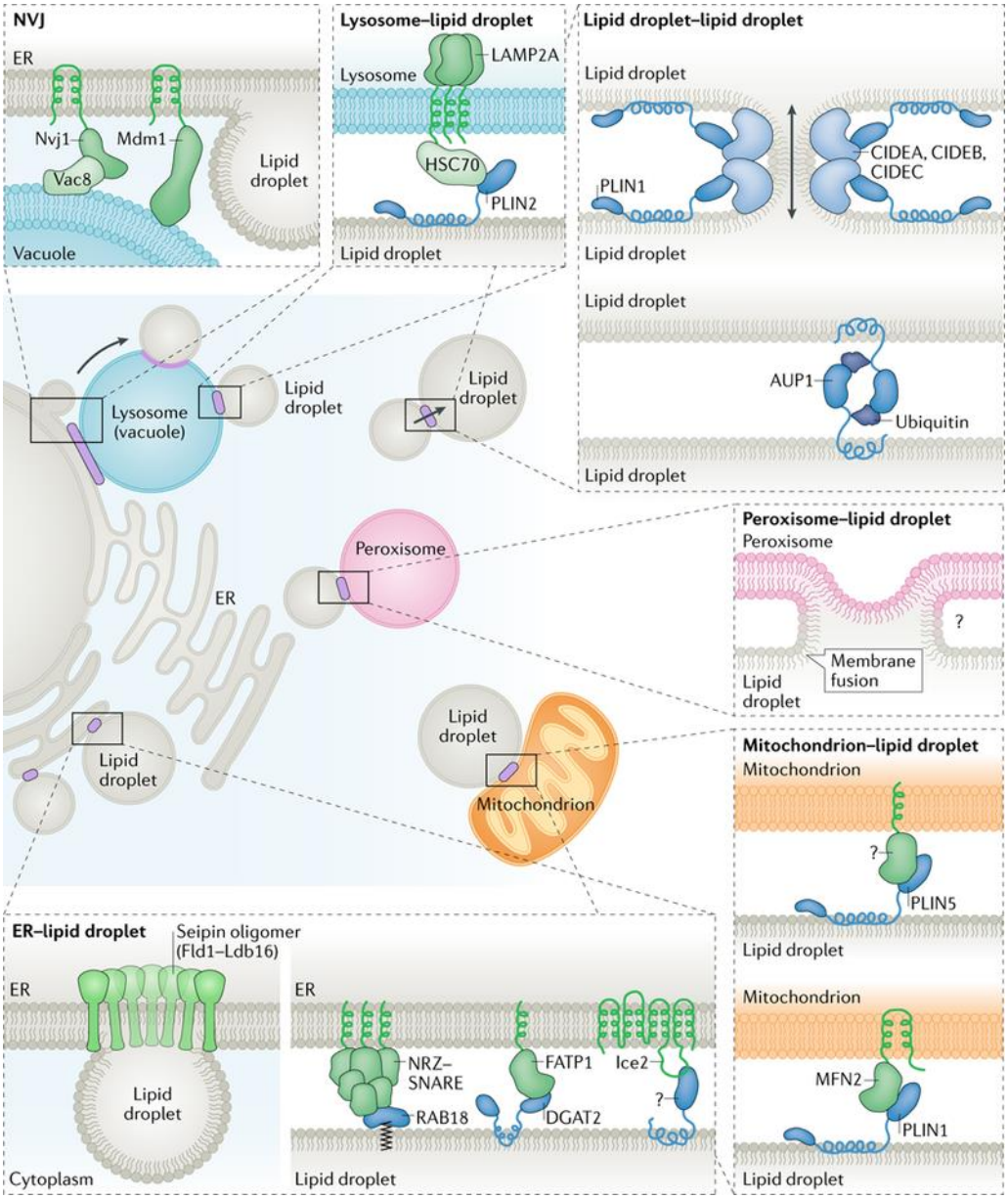

Fig. 1.11. Tether complex between LDs and other subcellular organelles. LDs are reported to interact with almost every subcellular organelle. These contacts usually occur not only between a LD and one another organelle, but between LDs and multiple organelles. However, the exact mechanisms are not well elucidated. The known proteins involved in tethering complex between LDs and other organelles are shown: those on LDs in blue and those on the other organelles in green. Not identified components of certain tethering complex is shown with question marks. AUP1, ancient ubiquitous protein 1; CIDEA, cell death-inducing DFFA-like effector A; DGAT2, diacylglycerol acyltransferase 2 protein; ER, endoplasmic reticulum; FATP1, fatty acid transport protein 1; HSC70, heat shock cognate 71 kDa protein; Ice2, inheritance of cortical ER protein 2; L AMP2A, lysosome-associated membrane protein 2A; Mdm1, structural protein MDM1; MFN2, mitofusin 2; NVJ, nuclear ER–vacuole junction; NRZ, NAG–RINT1–ZW10 complex; Nvj1, nuclear vacuolar junction protein 1; PLIN, perilipin; Vac8, vacuolar protein 8. Adapted from Olzmann and Carvalho, 2019 [146].

Immunofluorescence studies using COS-7 cells indicate that although some LDs are detached from ER, most of LDs (85%) are connected to ER [168]. These connections are established via either transient membrane bridges or via non-membranous tethering complexes [146, 168]. For LD-ER association, Seipin [169], diacylglycerol-O-

acyltransferase 2 (DGAT2) with fatty acid transport protein1 (FATP1) [170], Rab18 with NAG-RINT1-ZW10 (NRZ) complex, its associated sNAREs (Syntaxin18, USE1 and BNIP1) [171] and inheritance of cortical ER protein 2 (Ice2) [172] are required and these are considered as part of tethering complexes. Apart from LD-ER contacts, LDs also can associate with different subcellular organelles, such as Golgi, mitochondria, lysosomes and peroxisomes via either transient membrane bridges or non-membranous tethering complexes [146, 168]. These LD contacts to other organelles serve as a platform for lipids-, metabolites-, ions exchange reactions [173] and as a control tower of organelle division, trafficking and inheritance [168, 174].

1.2.2.6. Rab18 and LD-ER association for HCV

Rab18 is a small GTPase and belongs to the Ras-related Rab family. As other members of this family, Rab18 functions as a molecular switch: the GTP-bound state of Rab18 is activated allowing interaction with effector proteins, whereas GDP-bound Rab18 is not able to interact with its effectors. The GTP-bound form associates with membranes by its prenylated C-terminal cysteine residue [175] and recruits its effector proteins to exert biological functions. The switch from the GTP- to GDP-bound states occurs via GTP-hydrolysis, which is usually triggered by GTPase activating (GAP) proteins (i.e. TBC1D20), since the intrinsic GTP-hydrolysis activity of Rab proteins is very low. After GTP-hydrolysis, the GDP-bound form dissociates from membrane by interacting with GDP dissociation inhibitor (GDI). Then, GDP in the small GTPase is exchanged to GTP, which is mediated by guanine nucleotide exchange proteins (GEFs) such as Rab3GAP and this leads the Rab protein back to membrane for reinserted state[176].

Mutations in Rab18 cause a genetic disease called Warburg-Micro syndrome, which include symptoms like severe mental retardation, absence of the corpus callosum, hypogenitalism and multiple ovular problems indicating its essential role in organ development [176].

Rab18 expression is increased upon adipogenic differentiation of 3T3-L1 cells. Rab18 overexpression leads to increased lipogenesis and its depletion inhibits insulin-induced lipogenesis [177]. Not only for the fat accumulation, but also for the LD metabolism, Rab18 plays an important role. Rab18 localizes on LDs and this is triggered upon stimulation of lipolysis [178]. As mentioned previously, Rab18 can induce LD-ER apposition [179], probably by interacting with NAG-RINT1-ZW10 (NRZ) tethering

complex and SNAREs (Syntaxin18, Use1, BNIP1) on ER [171] and this LD-ER contacts might serve as sites where lipid- and protein exchanges between LDs and ER occur. [146]. Interestingly, this LD-ER apposition can be observed upon HCV replication specifically for LDs positive for E2 and NS5A, representing virus assembly- and viral RNA replication modules, respectively [142]. The observed Rab18 NS5A interaction, which might recruit HCV RNA replicase complex to LDs, suggests that Rab18 might be involved in HCV-induced LD-ER apposition [180]. This indication for the importance of Rab18 in LD-ER apposition upon HCV replication cycle is further supported by the facts that Rab18 depletion decreases viral RNA replication and that Rab18 overexpression increases infectious virus particle production and release [180].

1.3. Aim of study

The general aim of this study was to elucidate host virus interaction during HCV assembly. Cholesterol is an important component of biological membranes which regulates functions of membrane proteins in different manners. Coherently, for many steps in the HCV replication cycle, the importance of cholesterol was demonstrated. However, detailed mechanisms, how cholesterol is involved in viral propagation, remains to be investigated. To reveal the role of cholesterol in HCV replication cycle, I started with identifying direct interaction between cholesterol and HCV proteins. I used bifunctional cholesterol species which enable capturing the cholesterol protein interaction via photo-crosslinking and specific labeling via radioactive tritium or clickable functional group at cholesterol. Among tested viral proteins, NS2 showed the most efficient crosslinking to the bifunctional cholesterol. I aimed 1) to identify the NS2 domains responsible for its cholesterol interaction, 2) to characterize the importance of NS2 cholesterol for HCV replication cycle by introducing alanine substitutions of amino acid residues of NS2 responsible for its cholesterol interaction and 3) to elucidate the detailed mechanism how NS2 cholesterol interaction can contribute to HCV propagation. According to the third point, I tried to study the importance of NS2 cholesterol interaction for NS2 interactions a) with other viral proteins and b) with host factors based on the NS2 proteomics data from our lab.

In the second project, I aimed to elucidate the mechanism for establishing ER-wrapping of E2-/NS5A double positive LDs, which were proposed as possible HCV assembly sites. In terms of establishing ER-LD contacts, a small GTPase Rab18 has been considered to be important: Rab18 mediates ER LD interaction and has been shown to be involved in HCV viral RNA replication and virus production. To investigate possible role of Rab18 in virus assembly, I tried to generate Rab18 KO cell lines and characterized them for their genotypes and virus phenotypes. Subsequent ultrastructural analysis of NS5A-positive LDs within KO cell lines should create better insight of the mechanism how possible HCV assembly sites are established.

2. Materials and methods

2.1. Materials

2.1.1. Antibodies and dyes

Table 2.1. Primary antibodies

Antibody	Type	WB	IF	Supplier/catalogNo.
α-β-actin	Mouse IgG1	1:4000	n.t.	Merck (Darmstadt, Germany)/A5441
α-Calnexin	Rabbit polyclonal	1:2000	1:100	Enzo Life Science (Farmingdale, USA)/ADI-SPA-865
α-Caveolin1	Rabbit polyclonal	1:1000	n.t.	Cell Signalling Technology (Danvers, USA)/3238
α- HCV Core (C7/50)	Mouse IgG1	1:1000	1:200	Gift from Darius Moradpour, Universität Lausanne
α-HCV E2	Rat	1:50	1:20	Gift from J.A. Mckeating
α-Erlin2	Rabbit polyclonal	1:1000	n.t.	Cell Signalling Technology (Danvers, USA)/2959
α-Erlin2	Rabbit polyclonal	n.t.	1:200	Thermo Fisher Scientific (Waltham, USA)/PA5-51669
α-Flotillin1	Rabbit IgG	1:1000	n.t.	Cell Signalling Technology (Danvers, USA)/D2V7J
α-GAPDH	Rabbit IgG	1:1000	n.t.	Cell Signalling Technology (Danvers, USA)/D16H11
α-GM130	Rabbit IgG	n.t.	1:3200	Cell Signalling Technology (Danvers, USA)/D6B1
α-HA	Mouse IgG1	1:10000	1:200	Merck (Darmstadt, Germany)/H3663
α-Lamp1	Rabbit IgG	1:1000	1:200	Cell Signalling Technology (Danvers, USA)/9091S
α-HCV NS3	Rabbit polyclonal	1:3000	n.t.	Homemade
α-HCV NS4B	Rabbit polyclonal	1:1000	n.t.	Homemade
α-HCV NS5A	Mouse IgG2α	1:10000	n.t.	Gift from Charles Rice, Rockefeller University New York City
α-Rab18	Rabbit polyclonal	1:1000	1:200	Proteintech (Manchester, UK)/11304-1-AP
α-SREBP2	Rabbit polyclonal	1:1000	1:200	Abcam (Cambridge, USA)/ab30682

Table 2.2. Secondary antibodies

Antibody	Specificity	Type	IF	Supplier
AlexaFluor®647 (A31571)	Anti-mouse IgG (H+L)	donkey	1:1000	Thermo Fisher Scientific (Waltham, USA)
AlexaFluor®568 (A10037)	Anti-mouse IgG (H+L)	donkey	1:1000	Thermo Fisher Scientific (Waltham, USA)
AlexaFluor®488 (A21042)	Anti-mouse IgM	goat	1:1000	Life technologies (Waltham, USA)
AlexaFluor®647 (A31574)	Anti-rabbit IgG (H+L)	donkey	1:1000	Thermo Fisher Scientific (Waltham, USA)

AlexaFluor®568 (A10042)	Anti-rabbit IgG (H+L)	donkey	1:1000	Thermo Fisher Scientific (Waltham, USA)
AlexaFluor®488 (A21206)	Anti-rabbit IgG (H+L)	donkey	1:1000	Thermo Fisher Scientific (Waltham, USA)
AlexaFluor®647 (A21247)	Anti-rat IgG (H+L)	goat	1:1000	Life technologies (Waltham, USA)
AlexaFluor®568 (A11077)	Anti-rat IgG (H+L)	goat	1:1000	Thermo Fisher Scientific (Waltham, USA)
AlexaFluor®488 (A21208)	Anti-rat IgG (H+L)	donkey	1:1000	Thermo Fisher Scientific (Waltham, USA)
Anti-mouse HRP	Anti-mouse IgG	goat	1:10000	Merck (Darmstadt, Germany)
Anti-rabbit HRP	Anti-rabbit IgG	goat	1:5000	Merck (Darmstadt, Germany)
Anti-rat HRP	Anti-rat IgG	goat	1:5000	Merck (Darmstadt, Germany)

Table 2.3. Dyes

Dyes	Specificity	IF	Supplier
HSC LipidTox™ Deep Red neutral lipid stain	Neutral lipid (mostly stored in lipid droplets)	1:1000	Thermo Fisher Scientific (Waltham, USA)
Filipin III	Free cholesterol	250 µg/ml	Merck (Darmstadt, Germany)
DAPI	DNA	1:3000	Thermo Fisher Scientific (Waltham, USA)

2.1.2. Buffers and solutions

Table 2.4. Buffers and solutions used for protein work

Buffer/solution	Composition
Bradford Reagent	100 mg Coomassie Brilliant Blue G250 dissolved in 50 ml 95% Ethanol and mixed with 100 ml 85% (w/v) phosphoric acid
10x TGS running buffer	150 mM Tris, 1.92 M Glycine, 1% (w/v) SDS
Resolving gel buffer	1.5 M Tris-HCl (pH 8.8), 0.4% (w/v) SDS
Stacking gel buffer	1 M Tris-HCl (pH 6.8), 0.8% (w/v) SDS
Western Blot blocking buffer	5% Skim milk powder in 1x PBS
Western Blot washing buffer	0.5% (v/v) Tween-20 in 1x PBS
Western Blot antibody incubation buffer	1% Skim milk poweder in 1x PBS
4x LDS (Thermo Fisher Scientific)	106 mM Tris HCl, 141 mM tris Base, 2% LDS, 10% glycerol, 0.51 mM EDTA, 0.22 mM SERVA Blue G250, 0.175 mM phenol red pH 8.5

Table 2.5. Buffers and solutions used for nucleic acid work

Buffer/solution	Composition
NEB buffer 1	10 mM Bis Tris Propane-HCl, 10 mM $MgCl_2$, 1 mM DTT (pH 7.0 at RT)
NEB buffer 2	10 mM Tris-HCl, 10 mM $MgCl_2$, 50 mM NaCl, 1 mM DTT (pH 7.9 at RT)
NEB buffer 3	50 mM Tris-HCl, 10 mM $MgCl_2$, 100 mM NaCl, 1 mM DTT (pH 7.9 at RT)
NEB buffer 4	20 mM Tris-acetate, 10 mM magnesium acetate, 50 mM potassium acetate, 1 mM DTT (pH 7.9 at RT)
TAE (50x)	2 M Tris-HCl, 2 M acetic acid, 50 mM EDTA pH 8.3
Transcription buffer RRL (5x)	400 mM HEPES (pH 7.5), 60 mM $MgCl_2$, 10 mM Spermidine, 200 mM DTT

Table 2.6. General buffers and solutions

Buffer/solution	Composition
Cytomix	120 mM KCl, 2 mM Potassium phosphate buffer (pH 7.6), 25 mM HEPES (pH 7.6), 0.15 mM $CaCl_2$, 5 mM $MgCl_2$, 2 mM EGTA, adjusted to pH 7.6 with KOH (2 mM ATP and 5 mM glutathione freshly added before use)
Cacodylade buffer	50 mM Sodium cacodylate (pH 7.2)
EM fixative	25% Gluteraldehyde, 50 mM KCl, 2 mM $MgCl_2$, 2 mM $CaCl_2$, 2% sucrose in 50 mM cacodylade buffer
Immunofluorescence blocking buffer	3% (w/v) fatty acid free BSA in 1x PBS
Immunofluorescence antibody incubation buffer	1% (w/v) fatty acid free BSA in 1x PBS
Phosphate buffered saline (PBS) (x10)	80 mM Na_2HPO_4, 20 mM NaH_2PO_4, 2.4 M NaCl, 2.7 mM KCl, 1.76 mM K H_2PO_4
TCID50 detection substrate (Carbazol)	0.4 g 3-amino-9-ethyl carbazole dissolved in 125 mM N,N-dimethyl-formamide stored at 4 °C in darkened area
TCID50 Acetate solution	75 mM 0.5 M NaAcetate, 30 ml 0.5 M acetic acid, 945 ml dH_2O
TCID50 detection solution	5 ml Acetate solution, 1.5 ml carbazole, 20 µl peroxide
4% Paraformaldehyde (PFA)	4 g PFA dissolved in 10 ml PBS

Table 2.7. Buffers and solutions for luciferase activity assays

Buffer/solution	Composition
Coelenterazine stock solution	5 mg dissolved in 11.6 ml methanol, aliquots stored at -80 °C
Luciferin stock solution	1 mM Luciferin, 25 mM glycylglycin, stored at -80 °C
Luciferase assay buffer	15 mM Potassium phosphate (pH 7.8), 15 mM $MgSO_4$, 4 mM EGTA, 25 mM gylcylglycin (pH 7.8) (1 mM DTT and 2 mM ATP in case of Firefly luciferase measurement freshly added before use)
Luciferase lysis buffer	1% (v/v) Triton X100, 10% glycerol, 15 mM $MgSO_4$, 4 mM EGTA, 25 mM
TAE (50x)	2 M Tris-HCl, 2 M acetic acid, 50 mM EDTA pH 8.3, gylcylglycin (pH 7.8) (1 mM DTT freshly added before use), stored at 4 °C

2.1.3. Plasmid constructs

Table 2.8. pTM-based expression constructs

Name	Description	Reference
pTM ApoE	Expression of HA-tagged ApoE	Dr. Long
pTM ASGR-Myc-HA	Expression of asialoglycoprotein receptor 1 with a Myc and with a HA tag	Self made
pTM Caveolin-HA	Expression of caveolin1 with a 3x HA tag	Self made
pTM core-HA_JFH	Expression of HCV JFH1 HA-tagged core	Self made
pTM NS4B_38HA-Q31R_JFH	Expression of HCV JFH1 NS4B 38HA containing the Q31R pseudoreversion	Dr. Paul
pTM spE1-spHA-linker-E2 J6	Expression of HCV J6 E1 and HA-tagged E2	Self made
pTM spHAF_NS2_JFH	Expression of N-terminally HA- and FLAG-tagged HCV JFH1 NS2	Dr. Vlastimil
pTM JFH1_NS3_JFH	Expression of HCV JFH1 NS3	Self made
pTM NS5AHADII	Expression og HA-tagged NS5A	Dr. Zayas

Table 2.9. pTM-based HCV JFH1 NS2 mutant expression constructs

Name	Description	Reference
pTM spHAF_NS2_JFH L22A	Expression of HA- and FLAG-tagged NS2 L22A	Self made
pTM spHAF_NS2_JFH Y26A	Expression of HA- and FLAG-tagged NS2 Y26A	Self made
pTM spHAF_NS2_JFH K27A	Expression of HA- and FLAG-tagged NS2 K27A	Self made
pTM spHAF_NS2_JFH Q49A	Expression of HA- and FLAG-tagged NS2 Q49A	Self made
pTM spHAF_NS2_JFH E50A	Expression of HA- and FLAG-tagged NS2 E50A	Self made
pTM spHAF_NS2_JFH W51A	Expression of HA- and FLAG-tagged NS2 W51A	Self made
pTM spHAF_NS2_JFH Q56A	Expression of HA- and FLAG-tagged NS2 Q56A	Self made
pTM spHAF_NS2_JFH R58A	Expression of HA- and FLAG-tagged NS2 R58A	Self made
pTM spHAF_NS2_JFH R61A	Expression of HA- and FLAG-tagged NS2 R61A	Self made
pTM spHAF_NS2_JFH D62A	Expression of HA- and FLAG-tagged NS2 D62A	Self made
pTM spHAF_NS2_JFH L86A	Expression of HA- and FLAG-tagged NS2 L86A	Self made
pTM spHAF_NS2_JFH L87A	Expression of HA- and FLAG-tagged NS2 L87A	Self made
pTM spHAF_NS2_JFH G88A	Expression of HA- and FLAG-tagged NS2 G88A	Self made
pTM spHAF_NS2_JFH P89A	Expression of HA- and FLAG-tagged NS2 P89A	Self made
pTM spHAF_NS2_JFH Y91A	Expression of HA- and FLAG-tagged NS2 Y91A	Self made
pTM spHAF_NS2_JFH L92A	Expression of HA- and FLAG-tagged NS2 L92A	Self made
pTM spHAF_NS2_JFH L93A	Expression of HA- and FLAG-tagged NS2 L93A	Self made
pTM spHAF_NS2_JFH R94A	Expression of HA- and FLAG-tagged NS2 R94A	Self made

Table 2.10. pFK-based viral vectors

Name	Description
pFK-JFH1-ad-XbaI_HA-Flag-NS2_dg	Full length HCV JFH1 with three adaptive mutations enhancing virus titer without affecting viral RNA replication [120]. It contains a HA- and a FLAG-tag at the N-terminal site of NS2.
pFK_i389RLuc2A-Core-3'Jc1	From 5'-UTR: 2x the first 16 aa of core, Renilla luciferase, foot and mouth disease virus (FMDV) 2a peptide as cleavage site and Full length HCV chimera Jc1 consisting of J6CF (core to NS2) and JFH1 (the rest). Monocistronic expression [123].

pFK_i389LucNS3-3'_JFH1_dg	From 5'-UTR: HCV IRES, the first 16 aa of core, Firefly luciferase, EMCV IRES and HCV JFH1 NS3-NS5B. Bicistronic expression [122].
pFK_i389neoNS3-3'_dg_JFH1_NS5A-aa2359_mCherry_NS3-K1402Q	Subgenomic replicon of HCV JFH1 with mCherry tagged NS5A [181].

Table 2.11. pFK-based JFH1 ad HAF-NS2 mutants

Name	Description	Reference
pFK JFH1 ad. HAFNS2 L86A	Expression of full length HCV JFH1 ad HAF-NS2 L86A	Self made
pFK JFH1 ad. HAFNS2 L87A	Expression of full length HCV JFH1 ad HAF-NS2 L87A	Self made
pFK JFH1 ad. HAFNS2 G88A	Expression of full length HCV JFH1 ad HAF-NS2 G88A	Self made
pFK JFH1 ad. HAFNS2 P89A	Expression of full length HCV JFH1 ad HAF-NS2 P89A	Self made
pFK JFH1 ad. HAFNS2 Y91A	Expression of full length HCV JFH1 ad HAF-NS2 Y91A	Self made
pFK JFH1 ad. HAFNS2 L92A	Expression of full length HCV JFH1 ad HAF-NS2 L92A	Self made
pFK JFH1 ad. HAFNS2 L93A	Expression of full length HCV JFH1 ad HAF-NS2 L93A	Self made
pFK JFH1 ad. HAFNS2 R94A	Expression of full length HCV JFH1 ad HAF-NS2 R94A	Self made
pFK JFH1 ad. HAFNS2 L87A Y91A	Expression of full length HCV JFH1 ad HAF-NS2 L87A Y91A	Self made
pFK JFH1 ad. HAFNS2 L86A L87A Y91A	Expression of full length HCV JFH1 ad HAF-NS2 L86A L87A Y91A	Self made
pFK JFH1 ad. Core-p7 IRES NS3-NS5B	Expression of full length HCV JFH1 ad without NS2	Self made

Table 2.12. Retroviral vectors

Name	Description
pWPI-blx	Vector for lentiviral transduction mediating expression of inserts of interests driven by the E2a promotor containing blasticidin resistant gene as a selection marker.
pCMV-dR8.91	Packaging plasmid expressing gag-pol for lentivirus production
pMD-G	Expression plasmid for VSV envelope protein for lentivirus production

2.1.4. Chemicals and compounds

Table 2.13. Chemicals and reagents

Name	Description
Acrylamide: Bisacrylamide Mix (29:1) 40%	Sigma Aldrich (Darmstadt, Germany)
Agarose	Thermo Fisher Scientific (Waltham, USA)
Albumin, from bovine serum (BSA), fatty acid free	Sigma Aldrich (Darmstadt, Germany)
Amersham Hyperfilm ECL	GE Healthcare Life Sciences (Uppsala, Sweden)
Coomassie Brillian Blue G250	Serva Electrophoresis GmbH (Heidelberg, Germany)
Coelenterazine	PJK (Kleinblittersdorf, Germany)
D-Luciferin	PJK (Kleinblittersdorf, Germany)
DMSO	Roth (Karlsruhe, Germany)
Dithiolthreitol (DTT)	Sigma Aldrich (Darmstadt, Germany)
ECL Plus Western Blot Detection System	Amersham/Perkin-Elmer (Darmstadt, Germany)
EDTA	Merck (Darmstadt, Germany)
Ethanol p.A.	Sigma Aldrich (Darmstadt, Germany)
HEPES	Thermo Fisher Scientific (Waltham, USA)
Hydrogen Peroxide	Roth (Karlsruhe, Germany)
Fluoromount G	Southern Biotechnology Associates (Birmingham, USA)
Fetal Calf Serum	PAA Laboratories (USA)
GeneRuler 1 kb DNA Ladder	Thermo Fisher Scientific (Waltham, USA)
Glutathione	Sigma Aldrich (Darmstadt, Germany)
Glycerol	Roth (Karlsruhe, Germany)
Glycyl-glycine	Sigma Aldrich (Darmstadt, Germany)
Isopropanol p.A.	Sigma Aldrich (Darmstadt, Germany)
Methanol p.A.	Sigma Aldrich (Darmstadt, Germany)
Beta-Mercaptoethanol	Roth (Karlsruhe, Germany)
Prestained protein marker	New England Biolabs (Frankfurt, Germany)
Immobilon®-P	Millipore (Darmstadt, Germany)
rNTPs	Roche (Mannheim, Germany)
Skim Milk	Roth (Karlsruhe, Germany)
Sodium dodecylsulfate	Applichem (Darmstadt, Germany)
TEMED	Applichem (Darmstadt, Germany)
Triton X100	Merck (Darmstadt, Germany)
Tween 20	Roth (Karlsruhe, Germany)
L(+)-Ascorbic Acid powdered BioChemica	Applichem (Darmstadt, Germany)
Copper (II) sulfate pentahydrate	Sigma Aldrich (Darmstadt, Germany)
Methyl-beta-cyclodextrin	Santa Cruz Biotechnology (Dallas, USA)
Tris[(1-benzyl-1H-1,2,3,-triazol-4-yl)methyl]amin (TBTA)	Roth (Karlsruhe, Germany)
Biotin azide	Sigma Aldrich (Darmstadt, Germany)

2.1.5. Media and antibiotics

Table 2.14. Chemicals and reagents

Media/supplements	Composition
Ampicillin stock solution	100 mg/ml in dH_2O, filter sterilized, stored at -20°C
Blasticidin stock solution	5 mg/ml in ddH_2O, filter sterilized, stored at -20°C
DMEM complete	Dulbecco's modified minimal essential medium (DMEM) (GIBCO) supplemented with 2 mM L-glutamine (GIBCO), 1x nonessential amino acids (GIBCO), 100 µg/ml streptomycin (GIBCO), 10% fetal calf serum (Heat inactivated) (PAA), 100 U/ml penicillin (GIBCO), stored at 4 °C
Geniticin G418 stock solution	100 mg/ml in dH_2O, filter sterilized, stored at -20°C
Lysogeny broth (LB)	10 g Bacto- Trypton, 2.5 g NaCl, 5 g Yeast extract, total volume of 1 l
LB-Agar	10 g Bacto- Trypton, 2.5 g NaCl, 5 g Yeast extract, 20 g Agar, total volume of 1 l
OptiMEM	0.05% trypsin, 0.02% EDTA in 1x PBS (GIBCO), autoclaved, stored at 4 °C
Trypsin solution	100 mM Tris-HCl (pH 8.3), 500 KCl, 15 mM $MgCl_2$, 0.01% (w/v) gelatine
LDL, human (Merck)	Liquid in 150 mM NaCl, pH 7.4 with 0.01% EDTA, filter sterilized, stored at 4°C

Table 2.15. Antibiotics

Antibiotics	Composition
Ampicillin	Roche (Mannheim, Germany)
Blasticidin	Thermo Fisher Scientific (Waltham, USA)
Geniticin sulfate G418	Thermo Fisher Scientific (Waltham, USA)
Zeocin	Sigma Aldrich (Darmstadt, Germany)

2.1.6. Emzymes and kits

Table 2.16. Enzymes

Name	Supplier
Calf Intestinal Phosphatase (CIP)	New England Biolabs (Frankfurt, Germany)
DNaseI	Promega (Mannheim, Germany)
NEB DNA restriction enzymes	New England Biolabs (Frankfurt, Germany)
rRNasin® RNase inhibitor	Promega (Mannheim, Germany)
T4 DNA Ligase	Fermentas (St. Leon-Rot, Germany)
T7 RNA polymerase	Promega (Mannheim, Germany)

Table 2.17. Kits

Kits	Supplier
Nucleobond ® PC100	Machery-Nagel (Düren, Germany)
Nucleospin ® Extract II	Machery-Nagel (Düren, Germany)
Nucleospin ® Plasmid	Machery-Nagel (Düren, Germany)
Molecular Probes™ Amplex™ Red Cholesterin-Assay-Kit	Thermo Fisher Scientific (Waltham, USA)

2.1.7. Oligonucleotides

Table 2.18. Primers for pTM-based plasmids

Name	Sequence (5´-3´)
For_pTM core-HA JFH	GATCCCATGGCCATGAGCTACCCATACGATGTTCCAGATTAC
Rev_pTM core-HA JFH	GC ACTAGTTCAAGCAGAGACCGG
For_pTM E1E2-HA JFH	GATC GGATCCATG CCCGGTTGCTCCTTTTCT
Rev_pTM E1E2-HA JFH	GC TTAATTAACTA TGCTTCGGCCTGGC
For_pTM Cav-HA	GATC GGATCCATG TCTGGGGGCAAATAC
Rev_pTM Cav-HA_1	GACGTCATAGGGATAGCCCGCATAGTCAGGAACATCGTATGG GTATCTAGATATTTCTTTCTGCAAGTTGATGC
Rev_pTM Cav-HA_2	GCTTAATTAATCAAGCGTAATCTGGAACGTCATATGGATAGGA CCCTGCATAGTCCGG GACGTCATAGGGATAGCCC
For_pTM ASGR-HA	GATCCCATGG ATGACCAAGGAGTATCAAGACCTTC
Rev_pTM ASGR-HA	GCACTAGTTTAAACCGCATAATCCGGCACATCATACGGATACA GGATATCATTTGCTGCCAG

Table 2.19. Primers for genomic PCR

Name	Sequence (5´-3´)
Rab18_Ex1_F3	CAGCTCACTCTGCTGAAGGGCT
Rab18_Ex1_R3	CCAAGACCTGGATGAAATCACA
Rab18_Ex4_F	GATC CACTTGTCAGTAAGCGAACACAT
Rab18_Ex4_R	GC CATACACATTTCAATCCTATTAACAT

Table 2.20. Primers for pWPI plasmids for expression of Rab18 with silent mutation

Name	Sequence (5´-3´)
F_Rab18	GATC GTTTAAACCCATGGACGAGGACGTGC
R_Rab18	GC ACGCGTTCATAACACAGAGC
R_shR1_1	GAGCATTGAGTGTTTCCTGGCAAATTTCAGG CCTTCATTTCTATCGAC
F_shR1_2	GCC AGG AAA CAC TCA ATG CTC TTTATAG AGGCAAGTGCAAAAACCTGT
R_shR4	AGTTTACTAGTACGCGTTCATAGAACCGAAC AGTATCCGCCGCAGGCTCCTCCTCCTTGGCCTTCTTCC

Table 2.21. Primers for introducing mutations into HCV NS2

Name	Sequence (5´-3´)
New pTM F	AATACCATGGGTCGGGTGGTC
New pTM R	ACTTAATTAATTATCAAAGGAGCTTCCACCC
NS2_JFH1ad_For	GATC GAAGCAGCTCTAGAGAAGTTGGTCGTC
NS2_JFH1ad_Rev	GCGTGGCCCCTAGGGCAGAGCAC
L22A_Rev	CGGGGTGGCTGTGAAGAGGGTGATCAATATCAA
L22A_For	TTCACAGCCACCCCGGGGTATAAGACCCTCCTC
Y26A_Rev	GGTCTTAGCCCCCGGGGTGAGTGTGAAGAGGGT
Y26A_For	CCGGGGGCTAAGACCCTCCTCGGCCAGTGTCTG
K27A_Rev	GAGGGTCGCATACCCCGGGGTGAGTGT
K27A_For	GGGTATGCGACCCTCCTCGGCCAGTGTCT
Q49A_Rev	CCACTCCGCAATCATGGCTTCCCCCAGG
Q49A_For	ATGATTGCGGAGTGGGTACCACCCATGCA
E50A_Rev	TACCCACGCCTGAATCATGGCTTCCCCCAG
E50A_For	ATTCAGGCGTGGGTACCACCCATGCAGG
W51A_Rev	TGGTACCGCCTCCTGAATCATGGCTTCCCCCAG
W51A_For	CAGGAGGCGGTACCACCCATGCAGGTGCGCGGC
Q56A_Rev	GCGCACCGCCATGGGTGGTACCCACTCCTG
Q56A_For	CCCATGGCGGTGCGCGGCGGCC
R58A_For	GCCGCCGGCCACCTGCATGGGTGGTACC
R58A_Rev	CAGGTGGCCGGCGGCCGCGATGG
R61A_Rev	GCCATCGGCGCCGCCGCGCACCTGCATGGGTGG
R61A_For	GGCGGCGCCGATGGCATCGCGTGGGCCGTCACT
D62A_Rev	GATGCCAGCGCGGCCGCCGCGCACCTGCATGGG
D62A_For	GGCCGCGCTGGCATCGCGTGGGCCGTCACTATA
L86A_Rev	CCCAAGCGCCGCCAAAAGCCATTTGGTAATGT
L86A_For	TTGGCGGCGCTTGGGCCTGCTTACCTCTTAAG
L87A_Rev	AGGCCCAGCCAACGCCAAAAGCCATTTGGTAAT
L87A_For	GCGTTGGCTGGGCCTGCTTACCTCTTAAGG
G88A_Rev	AGCAGGCGCAAGCAACGCCAAAAGCCATTTG
G88A_For	TTGCTTGCGCCTGCTTACCTCTTAAGGGCCG
P89A_Rev	GTAAGCAGCCCCAAGCAACGCCAAAAGC
P89A_For	CTTGGGGCTGCTTACCTCTTAAGGGCCGCT
Y91A_Rev	TAAGAGGGCAGCAGGCCCAAGCAACGCCAAAAG
Y91A_For	CCTGCTGCCCTCTTAAGGGCCGCTTTGACACAT
L92A_Rev	CCTTAAGGCGTAAGCAGGCCCAAGCAACGCCAA
L92A_For	GCTTACGCCTTAAGGGCCGCTTTGACACATGTG
L93A_Rev	GGCCCTTGCGAGGTAAGCAGGCCCAAGCAACGC
L93A_For	TACCTCGCAAGGGCCGCTTTGACACATGTGCCG
R94A_Rev	AGCGGCCGCTAAGAGGTAAGCAGGCCCAAGCAA
R94A_For	CTCTTAGCGGCCGCTTTGACACATGTGCCGTAC
R_LY87-91AA	TAAGAGGGCAGCAGGCCCAGCCAACGCCAAAAGCC ATTTGGTAAT
F_ LY87-91AA	GGGCCTGCTGCCCTCTTAAGGGCCGCTTTGACA
R_LLY86-91AAA	AGGGCAGCAGGCCCAGCCGCCGCCAAAAGCCATTTGGTAA TGTC
F_ LLY86-91AAA	GCTGGGCCTGCTGCCCTCTTAAGGGCCGCTTTGACA
JFH1 Core-p7 IRES NS3-NS5B_1F	CACCATGATCCTGGCGTAC

JFH1 Core-p7 IRES NS3-NS5B_1R	GGGGAGGGAGAGTTAGGCATAAGCCTGCCGGG
JFH1 Core-p7 IRES NS3-NS5B_2F	CGGCAGGCTTATGCCTAACTCTCCCTCCCCCC
JFH1 Core-p7 IRES NS3-NS5B_2R	CAAGGTCAGCTTGCATGC

2.1.8. Instruments

Table 2.22. Instruments

Name	Supplier
Spinningdisc confocal microscope ERS-6	PerkinElmer (Baesweiler, Germany)
Intas Science imager	Intas Science Imaging Instruments GmbH (Göttingen, Germany)
Luminometer Lumat LB 9507	Berthold Technologies (Bad Wildbad, Germany)
Luminometer Mithras LB940	Berthold Technologies (Bad Wildbad, Germany)

2.1.9. Transfection reagents

Table 2.23. Instruments

Name	Supplier
Mirus TransIT Transfection Reagent	Mirus Bio (Madison, USA)
OptiMEM	Thermo Fisher Scientific (Waltham, USA)

2.1.10. Cell culture

Eukaryotic cell lines

Cell lines	Description	Uses
HEK-293T	Human embryonic kidney cells expressing SV40 large T antigen supporting replication of, among others, lentivirus	Lentivirus production
Huh7.5	Human hepatoma cell clone cured from subgenomic HCV RNA replication by IFNalpha treatment leading to high permissiveness for genomic and subgenomic HCV RNA replication.	HCV infection
Huh7/Lunet CD81H	Human hepatoma cells ectopically expressing CD81, derived from Huh7/Lunet cells.	Uses for main experiments and imaging
Huh7/Lunet T7	Human hepatoma cells ectopically expressing T7 RNA polymerase.	Transfection with pTM expression vector
Huh7/Lunet CD81H Rab18 KO	Huh7/Lunet CD81H cells with knocked out Rab18	Assessing viral RNA replication and virus production

Bacterial cells

Cell	Description	Uses
E. Coli DH5α	Chemically competent *E. Coli* (F^-, φ80dlacZΔM15, Δ(lacZYA- argF)U169, deoR, recA1, endA1, hsdR17(rK-, mK+), phoA, suE44, λ-, thi-1, gyrA96, relA1)	Transformation with plasmids for cloning

2.2. Methods

2.2.1. Cell culture

Cell expansion, storage and thawing

Plated cells were washed with 1x PBS once and trypsinized (0,05% trypsin, 0,02% EDTA in 1xPBS) for 5 min at 37°C. Afterwards, cells were collected in complete DMEM and used for further expansion or for storage. For storing, trypsinized cells in complete DMEM were pelleted at 700 g for 5 min at RT, resuspended in cryo-solution containing 90% (v/v) fetal-calf serum and 10% (v/v) DMSO and filled into the cryo-tubes (Greiner). The tubes were stored in freezer at -80 °C and moved into liquid nitrogen container for long-term storage.

For thawing, frozen cells in cryo-solution in cryo-tubes were incubated in water bath at 37 °C, until cell suspension is thawed. Then, cell suspension was mixed with 10 ml of complete DMEM. After pelleting cells by centrifuging at 700 g for 5 min at RT, cell pellets were resuspended in complete DMEM and plated on cell culture dishes, which were incubated at 37 °C with 5% CO_2.

Manipulation of cellular lipid metabolism

For activating SREBP2 pathway, a counter reaction upon cholesterol starvation, cells were incubated in DMEM with 10% delipidated FCS for 3 h at 37 °C with 5% CO_2. For providing cells with excess of cholesterol, cells were incubated with either DMEM or OptiMEM with 100 µg/ml LDL for 3 h.

Cholesterol extraction from cells

For extracting cholesterol from cells, cells were incubated in DMEM with 10% delipidated FCS and 1% methyl-beta-cyclodextrin for 7 h at 37 °C with 5% CO_2.

2.2.2. Nucleic acid standard methods

Polymerase chain reaction (PCR)

For amplifying DNA inserts for cloning, PCR was done by using thermocycler. The PCR reaction mixture consisted of 1x PhusionFlash High-Fidelity MasterMix (Thermo Scientific), 2,5 µM of forward- and reverse primers and 0,5 µg template DNA. The program for the PCR is listed below:

Step	Temperature [°C]	Duration [sec]	Repeats
1. Denaturation	95	10	
2. Denaturation	95	1	
3. Annealing	55	5	30x
4. Elongation	72	15 for 1 kb	
5. Final elongation	72	1 min	
6. Termination	4	hold	

Agarose gel electrophoresis and gel extraction

Agarose gel electrophoresis allows separation of DNA fragments according to their sizes. Agarose gel was made of 1% agarose in 1X TAE buffer (40 mM TRIS, 1 mM EDTA and 40 mM acetic acid). For visualization of DNA fragments, staining solution 10x Midori Green Direct (NIPPON genetics) was added to DNA samples directly before loading onto gels. As size references, DNA ladder GeneRuler 1kb (ThermoScientific) was mixed with Midori Green Direct and loaded onto gels. The separation was done at 120 V for 30 min and visualized on a blue/green LED transilluminator (MNIPPON genetics). For cloning purposes, gel containing DNA fragments were cut out and DNA fragments were extracted using the NucleoSpin® Gel and PCR Clean-up kit (Macherey-Nagel) according to the manufacturer's instruction.

Restriction digestion

For generating specific ends for DNA inserts as well as vector DNAs, DNA samples were digested with restriction enzymes supplied by New England Biolabs according to the manufacturer's instructions with a reaction volume of 30 µl. After PCR, whole purified DNA fragments were subjected to the digestion. After digestion, 70 µl of water was added to the reaction and digested PCR products were purified by using the NucleoSpin® Gel and PCR Clean-up kit (Macherey-Nagel) according to the

manufacturer's instruction. In case of digesting plasmid DNA, 5 µg DNA was subjected to the digestion. After plasmid DNA digestion, calf intestine alkaline phosphatase (New England Biolabs) was added to the samples to dephosphorylate 5' phosphates for preventing self-ligation of digested plasmid DNA. Then digested plasmid DNA was purified by performing gel electrophoresis and subsequent gel extraction.

Ligation

Ligation of DNA inserts and vector DNA was done by using the T4 DNA ligase (New England Biolabs). For ligation, 1 U of T4 DNA ligase, 1x ligase buffer and DNA inserts and vector in a 1:3 ratio were mixed in a final volume of 10 µl. As control, a reaction without DNA inserts was prepared. Then the reaction was done at 16 °C overnight.

Transformation of competent *E. Coli* DH5α

After ligation, 30 µl of competent *E. Coli* DH5α cell suspension, which was thawed on ice, was mixed with 10 µl of ligation product on ice. Then, cell suspension was subjected to the heat shock at 42 °C for 1 min and to followed cooling down on ice for 1 min. Afterwards, 300 µl of LB medium was added and cell suspension was incubated at 37 °C at 800 rpm for 30 min. Subsequently, cells were pelleted by centrifuging the suspension at 4500 rpm for 1 min at RT. Cell pellet was resuspended in 50 µl of LB medium and plated on LB agar plates containing antibiotics for clonal selection of transformed cells which form colonies. Plates were incubated at 37°C overnight.

In case of transformation with purified plasmid DNA, 500 ng of plasmid DNA was mixed with 30 µl of competent *E. Coli* DH5α cell suspension. Then, cell suspension was subjected to the heat shock at 42 °C for 1 min and to followed cooling down on ice for 1 min. Afterwards, cell suspension was directly plated on LB agar plates containing antibiotics and incubated at 37°C overnight.

Plasmid DNA isolation and purification from *E. Coli* DH5α

For isolating plasmid DNA to check the success of cloning, a transformed bacteria colony from LB agar plates was picked and transferred to 5 ml LB medium containing antibiotics. After overnight incubation at 37 °C in a shaker, plasmid DNAs were isolated from bacteria cells by using NucleoSpin® Plasmid (Macherey-Nagel) according to the manufacturer's instruction based on alkaline lysis and DNA isolation by silica adsorption.

For isolating plasmid DNA in a bigger extent, a transformed bacteria colony from LB agar plates was picked and transferred to 300 ml and 800 ml of antibiotics containing LB medium for high- and low copy plasmids, respectively. After overnight incubation at 37 °C in a shaker, plasmid DNAs were isolated from bacteria cells by using NucleoBond® XtraMaxi (Macherey-Nagel) according to the manufacturer's instruction based on alkalin lysis and DNA isolation by anion exchanges.
For sequencing, isolated DNA samples were sent to GATC (Eurofins genomics).

In vitro transcription

Before the actual *in vitro* transcription, 10 µg plasmid DNA were linearized by incubating with the restriction enzyme MluI and purified by using the NucleoSpin® Gel and PCR Clean-up kit (Macherey-Nagel) according to the manufacturer's instruction. Then in vitro transcription was done with purified plasmid DNA in 80 mM HEPES/KOH (pH 7.5), 12 mM $MgCl_2$, 2 mM spermidine, 40 mM dithiothreitol (DTT), 1.5625 mM of each ribonucleoside triphosphate, 1 U/µl RNasein (Promega) and 0.8 U/µl of T7 RNA polymerase (homemade) in a total volume of 200 µl by incubating at 37 °C for 3 h. After addition of 0.4 U/µl of T7 polymerase, the reaction was further incubated for 2 h at 37 °C. Subsequently, 10 U RNAse free DNAse (Promega) was added, and the reaction was incubated for 40 min at 37 °C for stopping in vitro transcription. Purification of generated transcripts was done by performing acidic phenol/chloroform extraction at 4 °C and by isopropanol precipitation at room temperature. The RNA precipitates were resolved in RNAse free water and the quality of RNAs was assessed by performing agarose gel electrophoresis.

Quantification of nucleic acid concentration

The concentration of DNA and RNA was measured based on the light absorbance at 260 nm of samples. The measurement was done by using the NanodropLite Spectrophotometer (Thermo Fisher Scientific). For assessing the purity of samples, the absorbance at 280 nm was measured additionally indicative for the presence of proteins in samples. If the ratios between absorbance at 260 nm and 280 nm, A 260/280, are around 1,8 and 2 for DNA and RNA samples, respectively, it is considered as pure.

DNA transfection by lipofection

Transfection with DNA was done by using TransIT®-LT1 Reagent (Mirus Bio) according to the manufacturer's instruction, which is based on the principle of lipofection.

RNA transfection by electroporation

Electroporation of Huh7/Lunet CD81 high cells was done for transferring RNAs into cells. Cells were detached, washed once with 1x PBS, and resuspended in cytomix containing 120 mM KCl, 0.15 mM $CaCl_2$, 10 mM K_2HOP_4/KH_2PO_4 (pH 7.6), 25 mM HEPES, 2 mM EGTA, 5 mM $MgCl_2$ and freshly added 2 mM ATP as well as 5 mM glutathione. The final cell concentration was 10^7 cells/ml. Two different gab cuvettes and three different electroporation set ups were used depending on the cell suspension volume and on the amount of RNA as described below:

RNA [µg]	Cell suspension [µl]	Gab cuvette [mm]	High capacity [µF]	Voltage [V]
2.5	100	0.2	500	166
5	200	0.2	975	166
10	400	0.4	975	270

After electroporation, cell suspension was transferred to 4 ml complete medium per 100 µl cell suspension.

2.2.3. Protein analysis standard methods

Protein concentration determination by Bradford assay

Protein concentration was measured by using Coomassie-Brillant-Blue G-250 and its binding to cationic and apolar amino acid residues in an acidic milieu. Upon building complexes with amino acid residues, Coomassie-Brillant-Blue G-250 changes its light absorbance maximum from at 470 nm to at 595 nm, which serves as a quantitative indication for protein concentration in samples. To have reference values, 20 µl of BSA solved in HPLC water with concentration from 0 to 20 µg/ml was prepared and mixed with 1ml of 1x Coomassie-Brillant-Blue G-250. After 10 min of incubation, the absorbance at 595 nm was measured, which were used for generating BSA standard curve. For estimating protein concentration of samples, the absorbance at 595 nm was

measured and resulted values were transformed to protein concentration by using the BSA standard curve.

Sodium Dodecyl Sulfate PolyAcrylamide Gel Electrophorese (SDS PACE)

For protein separation through SDS PAGE, protein samples are incubated with sodium- or lithium dodecyl sulfate at 95 °C, where proteins become denatured. Negatively charged dodecyl sulfates bind to linearized proteins and the amount of bound dodecyl sulfates and the negative charges are proportional to the size of proteins. Based on this, proteins with different sizes were separated in 12%/14% acrylamide gel upon an electric field. As references of protein sizes, a pre-stained protein marker was loaded beside actual protein samples.

Western Blot analysis

Proteins separated by their sizes in acrylamide gel by performing SDS PAGE were transferred onto a PVDF membrane (PerkinElmer Life Sciences) for 1 h at 350 mA by using wet-transfer-system. After transfer, membranes were blocked by incubating in 5% milk in 1x PBS for 30 min at RT and subsequently incubated with primary antibodies in 1% milk in 1x PBS for overnight at 4 °C. Then membranes were washed 3x with 0.5% Tween in 1x PBS and incubated with secondary antibodies conjugated to horseradish-peroxidase in 1% milk in 1x PBS for 30 min at RT. After 3x wash with 0.5% Tween in 1x PBS, signals were developed by addition of Clarity ECL blotting substrate (Bio-Rad) onto membranes and detected by using the Advanced ECL imaging system (Intas Science Imaging Instruments). Quantification of signal intensities was done by using LabImage1D (Kapelan Bio-Imaging).

2.2.4. Biochemical assays

Wessel-Flügge precipitation

The precipitation method allows discarding detergents and remaining lipids from cell lysates: 1x volume supernatant was mixed vigorously with 4x volume methanol, 2x volume chloroform and 3x volume µl water; after centrifugation at 16000 g at 4 °C for 2 min, upper fraction was discarded and 3x volume methanol was added. Protein

precipitates were pelleted by centrifuging at 16000 g at 4 °C for 5 min and resuspended in proper volume of 4% SDS in 1x PBS.

Photoactivatable and clickable (PAC) cholesterol binding assay

Confluent Huh7/Lunet cells in 6-well plate were fed with 10 µM PAC cholesterol in DMEM with 10% delipidated FCS for 1 h at 37 °C. After 3x wash with 1x PBS, cells were covered with 1 ml of 1x PBS, irradiated with UV light for 5 min at 4 °C for generating protein-PAC cholesterol complexes. Then cells were harvested by scratching followed by centrifugation at 3000 g at 4 °C for 4 min. The cell pellets were subsequently resuspended in 100 µl of 1% triton, 0.1% SDS in 1x PBS containing protease inhibitor cocktail (Sigma Aldrich) and incubated on rotating wheel for 1 h at 4 °C. After centrifugation at 16000 g at 4 °C for 8 min, the supernatant was subjected to Wessel-Flügge precipitation. Protein precipitates were resuspended in 25 µl 4% SDS in 1xPBS by incubating at 37 °C at 800 rpm for 10 min. For the click chemistry reaction of biotin azide to protein-PAC cholesterol complexes, 25 mM $CuSO_4$ (water), 2.5 mM TBTA (DMSO), ascorbic acid (water) and 1 mM biotin azide (DMSO) were added to protein samples in a final volume of 125 µl and incubated at 37 °C at 800 rpm for 3 h. Then 1.4 ml of ice cold methanol was added to the reaction and incubated at -80 °C overnight for protein precipitation. The precipitates were pelleted by centrifuging at 16000 g at 4 °C for 10 min, washed with ice cold methanol and resuspended in 10 µl 4% SDS in 1x PBS by incubating it at 37 °C at 800 rpm for 10 min. After addition of 190 µl 1x PBS, samples were centrifuged at 10000 g for 1 min to exclude insoluble protein aggregates from further processes. 160 µl of samples was subjected to pull down by adding 20 µl High Capacity Neutravidin Agarose Resin (Thermo Scientific) slurry in 0.2% SDS in 1x PBS which was incubated at RT on rotating wheel for 1 h. 30 µl of remained samples (input) was mixed with 10 µl of 4x LDS sample buffer and boiled at 95 °C for 5 min, which served as input for the pull down. After pull down, agarose resin was washed ten times with 1% SDS in 1x PBS by centrifuging at 500 g for 1 min. To elute bound protein-PAC cholesterol-biotin complexes, resin was boiled with 1) 25 µl NuPAGE® 2x LDS sample buffer (Invitrogen) and with 2) 20 µl 2x LDS sample buffer at 95 °C each for 15 min resulting in a final eluate volume of 45 µl. The PAC cholesterol crosslinking efficiency was assessed by analyzing the quantitative presence of proteins of interests in the input and in the eluate by performing SDS PAGE and western blot with subsequent signal quantification.

Floatation assay

Confluent Huh7/Lunet cells in 10 cm plate were washed with cold 1x PBS and harvested in a buffer A containing 25 mM Tris-HCl [pH 7,5], 150 mM NaCl and 5 mM EDTA with protease inhibitor. Pelleted cells (600 g for 5 min at 4°C) were resuspended in 1 ml of buffer A and lysed by passing through a 25-gauge needle 20 times. For each condition, 300 µl cell lysate was put into separate 1,5 ml tube and triton-X100 was added to a final concentration of 1%. Subsequently, samples were incubated either on ice for 30 min, or at 37°C for 30 min. Then, 400 µl 100% Optiprep was added to make 40% of optiprep-cell suspension, which was added to the 60 mm tubes for SW60 ti rotors. On top of 40% Optiprep cell suspension, 1,2 ml of 30%, 1,2 ml of 26% and 0,8 ml of 6% Optiprep diluted with the buffer A were added. After ultracentrifugation at 42 k rpm for 4 h at 4°C, ten fractions with 400 µl volume were taken, where 100 µl 100% TCA was added for precipitation for overnight at 4°C. Precipitated proteins were pelleted at 16000g for 30 min at 4°C. The pellet was resuspended in 50 µl of 2xLDS buffer containing 100 µM DTT and boiled for 5 min at 95°C.

Detergent resistant membrane (DRM) isolation

Confluent Huh7/Lunet cells in 6-well plate were washed with the buffer A containing 25 mM Tris HCl (pH 7.5), 150 mM NaCl and 250 mM EDTA and harvested by scratching in 400 µl of buffer A containing 0.05% triton X100 and protease inhibitor cocktail (Sigma Aldrich), which were kept on ice for further processes. Then, cells were lysed by 10x passing through 22-gauge needles. 150 µl of cell lysate was subjected to incubation at 4 °C for 30 min and DRMs were pelleted by centrifuging the cell lysates at 16000 g at 4 °C for 5 min. The genomic DNAs in pellets were digested by incubating with Benzonase® Nuclease (EMD Millipore Corp.) in 2 mM $MgCl_2$ in 50 µl 1x PBS at 37 °C at 800 rpm for 20 min. Then proteins from DRMs and from non-DRMs were precipitated by performing Wessel-Flügge precipitation. Subsequently, the precipitates were resolved in 10 µl of 4% SDS in PBS at 37 °C at 800 rpm for 10 min, where 15 µl 1x PBS and 25 µl of 2x LDS containing 100 mM DTT were added afterwards. The samples finally were boiled at 95 °C for 5 min. The presence of proteins of interest in DRM (insoluble fraction) and non-DRM (soluble fraction) was evaluated by performing SDS PAGE and western blot.

Immunoprecipitation

For immunoprecipitating HA-tagged NS2 from HCV JFH1, $8*10^6$ Huh7/Lunet cells overexpressing CD81 were electroporated with 20 µg *in vitro* transcripts from JFH1 containing N-terminally HA- and FLAG-tagged NS2 and plated on a 15 cm dish. After 72 h, cells were lysed in 500 µl lysis buffer containing 100 mM NaCl, 20 mM Tris (pH 7.5), 0.5% DDM and protease inhibitor cocktail (Sigma Aldrich) by rotating at 4 °C for 30 min. Then, insoluble protein aggregates and cell debris were discarded by centrifuging at 20000 g at 4 °C for 30 min. After measuring protein concentration in the cell lysate by performing Bradford assay, protein concentration of each sample was adjusted to each other and 450 µl of the lysate was incubated with 100 µl slurry of pre-equilibrated anti-HA agarose resins (Sigma Aldrich) on rotating wheel at 4 °C for overnight. As input 45 µl cell lysate was mixed with 15 µl NuPAGE® 4x LDS sample buffer (Invitrogen) and boiled at 95 °C for 5 min. After 3x wash with lysis buffer, resins were boiled in 100 µl 2x LDS sample buffer at 95 °C for 5 min (eluate). The success of immunoprecipitation of HA-tagged NS2 and its known co-precipitates were assessed by analyzing inputs and eluates performing SDS PAGE and western blot.

Quantification of cholesterol concentration

For measuring cellular cholesterol level, cells were lysed in 1% triton, 0.1% SDS in 1x PBS and subjected to cholesterol measurement by using Amplex Red Cholesterol Assay Kit (Invitrogen) according to manufacturer's instruction. Shortly, cholesterol oxidase and cholesterolester esterase were added to cell lysate resulting in H_2O_2 production. Subsequent addition of Amplex Red will react with H_2O_2 resulting in the final product resorufin, which has absorption and emission wavelength of 571 nm and 585 nm, respectively. The emission at 585 nm indicative for cholesterol concentration was measured with fluorescent plate reader.

Cell viability measurement

For assessing cell viability, subcellular ATP level as indicator for cellular metabolic activity was quantified by using Cell titer glo® Luminescent (Promega). Cell titer glo® Luminescent contains Firefly luciferase and its substrate luciferin. Firefly luciferase catalyzes reactions of luciferin with ATP resulting, among others, in light, which is indicative for the amount of present ATP. For performing the assay, cells were plated on 96-well plate. At given time point, Cell titer glo® was added to cells with the same

volume as the cell culture medium and samples were incubated at RT for 10 min. The measurement was done with the plate luminometer (Mithras LB 940; Berthold Technologies).

2.2.5. Virological methods

Lentivirus production

For lentivirus production, $1x10^6$ HEK 293T cells were plated on 6 cm dish. 24 h after, cells were transfected with plasmids encoding lentiviral components and Rab18 silent mutant as following: The transfection mixture consisted of 6.4 µg packaging plasmid pCMV (gag-pol), 2.1 µg envelope plasmid pMD2.G and 6.42 µg of the transfer plasmid pWPI encoding Rab18 with silent mutation in 500 µl water. The mixture A was mixed with 500 µl of 2x HBS and incubated for 30 min at RT. Subsequently the mixture was added to cells by dropping the solution onto 4 ml of freshly changed cell culture medium (DMEM). 6 h after transfection, medium was changed (5 ml) and 48 h and 72 h after transfection, cell culture medium containing lentiviruses were collected, filtered (0.45 µm) and stored at -80 °C.

Lentiviral transduction of cells

Huh7/Lunet CD81H Rab18 KO cells were transduced with lentivirus encoding Rab18 with silent mutation. $4x10^4$ cells were plated on a 12 well plate. After 24 h, 1 ml supernatant containing lentiviruses replaced the given cell culture medium and incubated for 8 h. Afterwards, Medium was changed to fresh DMEM. 48 h after lentiviral transduction, transduced cells were selected by adding selection marker. As control, non-transduced cells were exposed to selection as well. Selected cells were stored at -80 °C.

Assessing viral RNA replication and virus production

For assessing viral RNA replication and virus production, IVT transcripts of full-length HCV JC1/JFH1 chimera additionally encoding Renilla luciferase reporter, JcR2a, were used for electroporating cells. Electroporated cells were plated on 24 well plates and 4 h, 24 h, 48 h and 72 h after electroporation, cells were washed with 1x PBS and lysed in 150 µl of lysis buffer containing 1% triton X100, 25 mM Gly-Gly (pH 7.8), 15 mM

$MgSO_4$, 4 mM EGTA and 1 mM DTT. 30 µl of cell lysates were pipetted into luminometer tubes. Then, 50 µl of 1.5 µM coelenterazine (PJK) in the lysis buffer without ATP and DTT was injected into the luminometer tubes automatically by using the luminometer Lumat LB9507 (Berthold Technologies). The measurement of luciferase activity was done in duplicates and took 20 s per round.

For assessing virus production of electroporated cells, cell culture medium was collected and filtered (0.45 µm) at 24 h, 48 h and 72 h after electroporation. Then Huh7.5 cells, which were seeded on 24 well plates one day before infection, were incubated with collected medium containing viruses for 4 h. Afterwards, medium was changed to DMEM and 72 h after infection, cells were lysed and subjected to Renilla luciferase activity measurement as described above. Finally, resulted values were divided by values from the assessment of viral RNA replication, which indicates the ability of virus production.

For assessing viral RNA replication only, IVT transcripts of HCV JFH1 subgenomic replicon additionally encoding Firefly luciferase were used. Electroporated cells were plated on 24 well plates. 4 h, 24 h, 48 h and 72 h after electroporation, cells were washed with 1x PBS and lysed in 150 µl of lysis buffer containing 1% triton X100, 25 mM Gly-Gly (pH 7.8), 15 mM $MgSO_4$, 4 mM EGTA and 1 mM DTT. For the measurement, 30 µl cell lysate was mixed with 200 µl of 0.2 mM luciferin in 25 mM Gly-Gly in luminometer tubes, which were subjected to measurement with the luminometer Lumat LB9507. The measurement of luciferase activity was done in duplicates and took 20 s per round.

Determination of extracellular and intracellular viral titers

$2x10^6$ Huh7/Lunet cells overexpressing CD81 were electroporated with 5 µg IVT transcripts of HCV JFH1 ad. HAF-NS2 and diluted in 8 ml of DMEM. $3.75x10^5$ cells were plated on a well of 6 well plates with final DMEM volume of 2.5 ml. After 72 h, supernatants were collected and filtered (0.45 µm) for assessing extracellular virus titer. For determining intracellular viral titers, cells were harvested and resuspended in 500 µl DMEM. Then cell lysates were generated by subjecting cell suspensions to 5x freezing-thawing cycle. Then, supernatants and cell lysates were used to infect Huh7.5 cells with serial dilution (Limiting-dilution assay). For the infection $4x10^4$ Huh7.5 cells were seeded on each well of 96 well plates one day before infection. After 72 h of infection, cells were fixed with ice cold methanol and infected cells were visualized by

immunostaining of NS5A. Virus titer units are given as 50% tissue culture infective dose (TCID50) per ml.

HCV Core ELISA

For quantification of HCV core by performing ELISA, samples were sent to the central laboratory for diagnostic at the university clinic Heidelberg. For sample preparation, $2x10^6$ Huh7/Lunet CD81H cells were electroporated with 5 µg IVT transcripts of HCV JFH1 ad. HAF-NS2 and diluted in 8 ml of DMEM. $3.75x10^5$ cells were plated on a well of 6 well plates with final DMEM volume of 2.5 ml. 72 h after electroporation, extracellular core sample was prepared by diluting filtered (0.45 µm) cell culture supernatant for 1:10 in 0.5% triton X100 in 1xPBS. Intracellular core sample was prepared by diluting cell lysate, which was generated by addition of 300 µl 0.5% triton X100 in 1xPBS to each well, for 1:200 in 0.5% triton X100 in 1xPBS.

2.2.6. Imaging

Immunofluorescence

For immunofluorescence, Huh7/Lunet CD81H cells were used. Depending on experimental time span 2-3*10^4 cells were seeded on 24 well plate with cover slips and at earliest 24 h after seeding cells were fixed with 4% PFA for overnight at 4°C. Then, fixed cells were permeabilized in 0.5% triton X100 at RT for 5 min. After 3x of wash with 1x PBS, cells were blocked with 3% BSA in 1x PBS and incubated with primary antibody in 1% BSA in 1x PBS for overnight at 4 °C. After 5x of wash with 1x PBS, incubation with secondary antibody in 1% BSA in 1x PBS was done for 1 h at RT. After 5x of wash with 1x PBS, cells were mounted with DAPI Fluoromount-G® (Sounthern Biotechnology). For visualizing fluorescently tagged proteins in cells, the whole process was done without permeabilization. Images were acquired with a Leica SP8 confocal laser-scanning microscope.

Neutral lipid staining with Bodipy or LipidTox

For visualization of neutral lipids mostly accumulating in lipid droplets via light microscopy, fluorescent dye Bodipy493/503 or HSC LipidTOX™ Neutral lipid stain (Thermo Fisher Scientific) were used. Sample preparation was done as described

above for “Immunofluorescence”. The only additional step is the 20 min incubation at RT with 20 mg/ml Bodipy495/503 or LipidTOX™ (excitation at 647 nm) in 1x PBS depending on wished detection light channel before mounting cells.

Free cholesterol staining using filipin III

For visualizing endogenous cholesterol in light microscopy, filipin III (Sigma Aldrich) was used. After fixing cells with 4% PFA, cells were incubated in 1.5 mg/ml glycine in 1x PBS for 30 min at RT and subsequently with 250 µg/ml filipin III in 1x PBS containing primary antibody for overnight at 4 °C. After 5x wash with 1x PBS, cells were incubated with 250 µg/ml filipin III in 1x PBS containing secondary antibody for 1 h at RT. After 5x of wash with 1x PBS, cells were mounted with DAPI Fluoromount-G® (Sounthern Biotechnology). Images were acquired with a Leica SP8 confocal laser-scanning microscope.

PAC cholesterol staining

Cells were fed with 10 µM PAC cholesterol in DMEM with 10% delipidated FCS containing media for 1 h. After 2x wash with 1x PBS, cells were fixed with 4% PFA in 1x PBS for overnight at 4 °C, permeabilized with 0.5% triton X100 for 5 min at RT and washed with 1x PBS. Then, the click reaction of Alexa 488 azide to PAC cholesterol was done by incubating cells in reaction buffer containing 25 mM $CuSO_4$ (water), 2.5 mM TBTA (DMSO), ascorbic acid (water) and 2 mM Alexa488 azide (DMSO) for 30 min at 37 °C. After 5x wash with 1x PBS, cells were further treated for immunostaining of proteins of interests as described above.

Image analysis: colocalization of two signals

For quantifying colocalization of two signals, acquired images from the Leica SP8 confocal laser-scanning microscope were deconvoluted by using AutoQuant X3 (Media Cybernetics). Afterwards, deconvoluted images were segmented by using ilastik (ilastik) and Mander’s overlap coefficient were assessed by using Coloc2 at Fiji.

Correlative Light and Electron Microscopy (CLEM)

Huh7/Lunet CD81H Rab18 KO cell clones were electroporated with IVT encoding HCV JFH1 subgenomic replicon containing mCherry-tagged NS5A and seeded on glass-bottom culture dishes containing gridded cover slips (MatTek Corporation). 48 h after

electroporation, cells were fixed with 4% PFA and 0.2% GA in 1x PBS for 30 min at RT and washed 3x with 1x PBS. Then, lipid droplets were stained with LipidTox^{TM} Deep Red Neutral Lipid Stain (Invitrogen) and subsequently fluorescence images were acquired from cells with positive mCherry signals by using Leica SP8 confocal laser-scanning microscope. For recognition of cells of interests during EM sample preparation, images were taken in the transmitted light channel using differential interference contrast (DIC). Afterwards, cells were further fixed for EM sample preparation in buffer containing 2.5% GA, 2% sucrose, 50 mM sodium cacodylate buffer (CaCo), 50 mM KCl, 2.6 mM Mg Cl_2 and 2.6 mM $CaCl_2$ for 30 min on ice. After 3x wash with 50 mM CaCo, cell components were stained for EM by incubation with 2% osmium tetroxide in 25 mM CaCo for 40 min on ice followed by 3x wash with EM grade water and incubation with 0.5% uranyl acetate in water overnight at 4 °C. Further steps for sample embedding, polymerization, sectioning and counterstaining were done by Uta Haselmann as described by Lee et al. [142]. EM images were acquired by using a JEOL JEM-1400. For correlation of fluorescent images with EM images, lipid droplets were considered as fiducial marker.

2.2.7. Statistical analysis

GraphPad Prism was used for statistical analysis with unpaired Student's t-test (***, $p<0.001$; **, $P<0.01$; *, $p<0.05$).

3. Result

3.1. Identification of HCV proteins interacting with cholesterol and characterization of protein-cholesterol interaction for HCV replication cycle

3.1.1. Tritium (H3)-labeled cholesterol as tool for studying protein-cholesterol interaction

Cholesterol is an important lipid species for Hepatitis C Virus (HCV) since it is involved in many steps during virus replication cycle: virus entry [128, 130], viral RNA replication [131, 134-136] and assembly of infectious viral particles [85, 182]. However, exact mechanisms how cholesterol is participating in these events are poorly understood. To elucidate the role of cholesterol during HCV replication cycle, a tool might be useful which can detect possible interactions of viral proteins with cholesterol. In this point of view, David Paul, previous PhD student in our lab, came to a cholesterol species, which contains a diazirine group localized at C-6 and a tritium localized at C-3 of cholesterol (Fig. 3.1A). The diazirine group is for crosslinking proteins in close proximity (≤3Å) to this cholesterol species by UV irradiation and the C-3 tritium is used for detection of crosslinked proteins [41]. Considering that NS4B is a component of viral RNA replicase complex with the largest transmembrane domain and that it localizes to the DMVs, which are highly enriched with cholesterol [134], NS4B is expected to show high cholesterol crosslinking efficiency compared to chosen controls NS2 and NS5A. However, the preliminary data resulted from photoaffinity-labeling assay using this tritium-labeled cholesterol in collaboration with AG Brügger indicated more efficient cholesterol binding of NS2 compared to NS4B and NS5A. This led to the idea that the NS2-cholesterol interaction should be important for its function in HCV replication cycle. Based on this idea, I started my PhD with validating the preliminary data with the goal, elucidation of the role of NS2 cholesterol interaction for HCV replication cycle. Huh7/Lunet cells stably expressing T7 RNA polymerase (Lunet T7 cells) were transfected with pTM plasmids with T7 promoter encoding either HA-tagged NS2, NS4B or NS5A. 3xHA-tagged caveolin1, a well-known cholesterol binding protein served as positive control [183] and HA-tagged asialoglycoprotein receptor 2 (ASGR), a plasma membrane protein [184], which does not show photocrosslinking was used as negative control. After transfection, cells were incubated with tritium labeled photoactivatable cholesterol and irradiated with ultraviolet light for crosslinking. After lysis, lysates were subjected to immunoprecipitation against HA epitope and analyzed by western blot and digital autoradiography. From the digital autoradiography, high

signal intensities for NS2 and for the positive control Caveolin1 could be observed, while the signals from NS4B, NS5A and the negative control ASGR were low (Fig. 3.1B). To be able to estimate the crosslinking efficiency of tested proteins, the band intensities from digital autoradiography were set in ratio to that from WB developed for HA (denoted as 3H/HA) and normalized to that of NS2. This clearly showed that NS2 crosslinking efficiency is comparable to that of the positive control caveolin1 and higher than NS4B and NS5B (Fig. 3.1B).

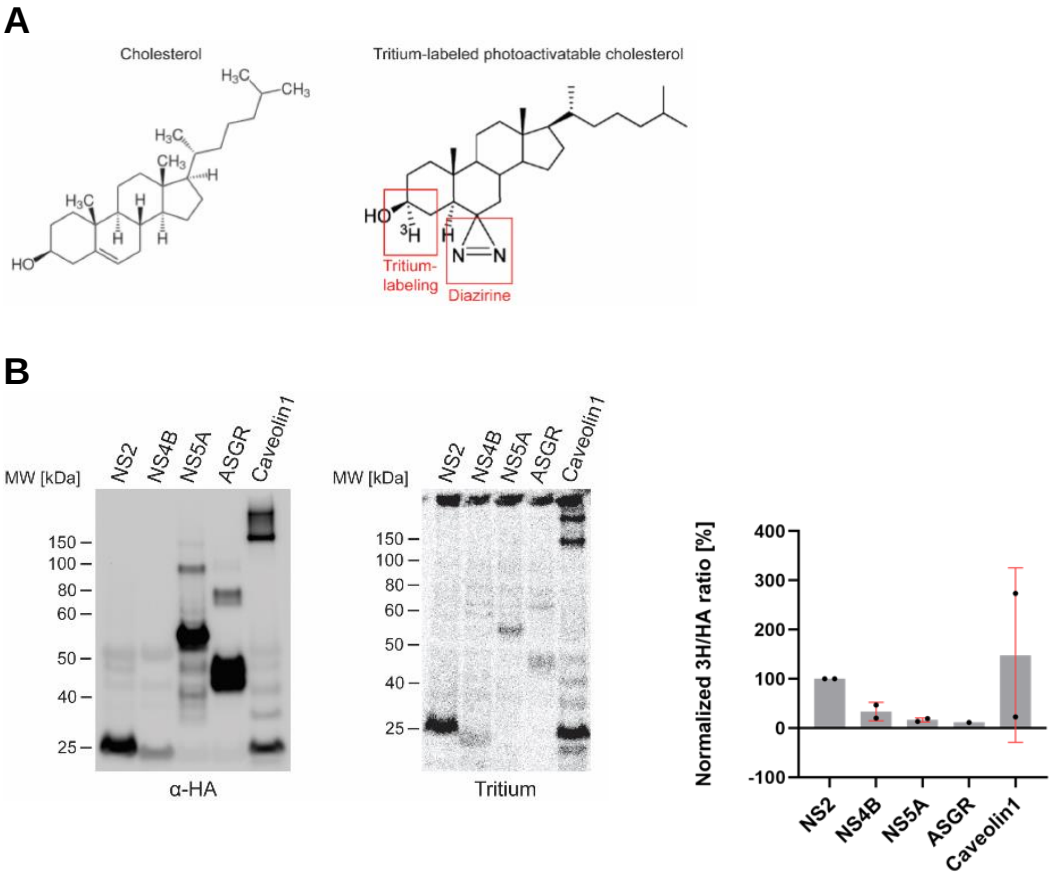

Figure 3.1. ^{3}H (tritium)-labeled photoactivatable cholesterol as tool for studying HCV proteins and cholesterol interaction. A. Comparison of cholesterol with tritium-labeled photoactivatable cholesterol. Tritium labeled photoactivatable cholesterol (right) contains tritium which replaced hydrogen at C-3. Additionally, a diazirine ring for photocrosslinking is located at C-6 which results in dissolving of C=C double bond between C-5 and C-6 compared to the physiological cholesterol (left). **B. Tritium-labeled photoactivatable cholesterol binding assay.** Huh7/Lunet cells expressing T7 polymerase ectopically (T7) were transiently transfected with indicated constructs encoded in pTM vector containing a T7 promoter. 4 h after transfection, tritium labeled photoactivatable cholesterol was added. 24 h after transfection, cells were ultraviolet irradiated, lysed, subjected to immunoprecipitation against the HA epitope and analyzed by western blot (first blot) and digital autoradiography (second blot). Ratios between tritium signal intensities and HA epitope signal intensities were calculated and normalized to values of NS2 (=100%). N=2.

3.1.2. Photoactivatable and clickable (PAC) cholesterol as a tool for studying protein cholesterol interaction.

To avoid the complexity of handling radioactive tritium-labeled cholesterol a commercially available non-radioactive cholesterol species, photoactivatable and clickable (PAC) cholesterol, was considered as an alternative cholesterol species for cholesterol protein interaction studies.

3.1.2.1. Experimental set up

PAC cholesterol contains a diazirine group and an alkyne group (Fig. 3.2A) for crosslinking proteins in close proximity (≤3Å) to PAC cholesterol by UV irradiation and for click chemistry to an affinity tag such as biotinazide, respectively [43]. Biotinylated protein-PAC cholesterol can be selectively isolated by performing pull down with streptavidin agarose resins. Subsequent quantitative analysis of input and eluate from pull down enables estimation of crosslinking efficiency of proteins of interest which is indicative for protein cholesterol interaction efficiency (Fig. 3.2B).

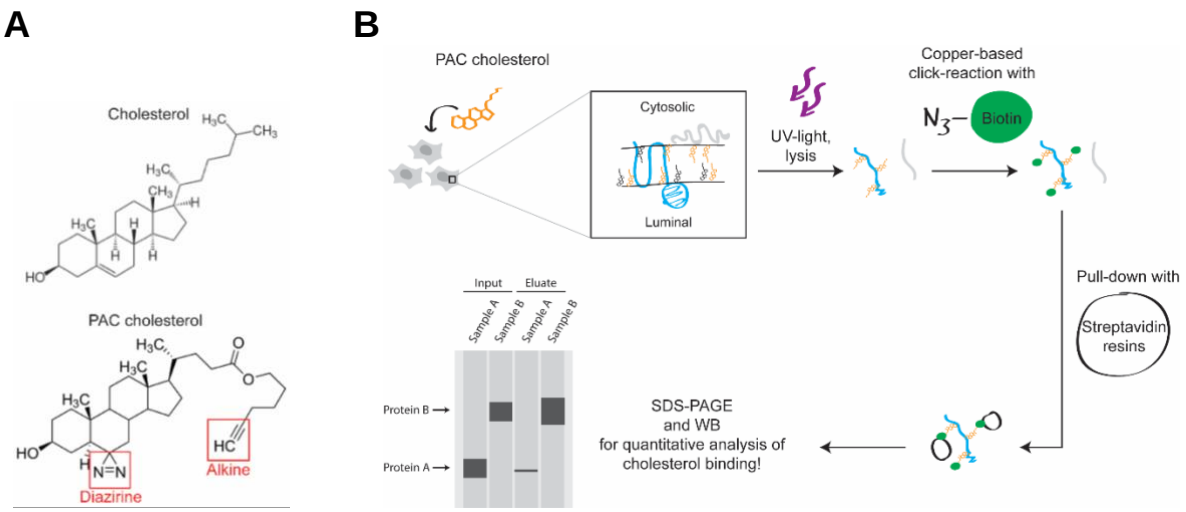

Figure 3.2. Photoactivatable and clickable (PAC) cholesterol as tool for studying HCV protein cholesterol interaction. A. Comparison of PAC cholesterol with the physiological cholesterol. Addition to diazirine ring for photocrosslinking at C-6, PAC cholesterol has an alkyne group for a click-reaction to an affinity tag containing an azide group. **B. Principle of PAC cholesterol binding assays.** Cells are fed with PAC cholesterol, irradiated with UV-light for crosslinking of PAC cholesterol to proteins in close proximity (≤3Å) and lysed. Cell lysates are subjected to click reaction with an affinity tag such as biotin azide. Resulted PAC cholesterol-protein-biotin complexes (inputs) were selectively isolated by performing pull down with streptavidin resins. Eluates from pull down and inputs are quantitatively analyzed by SDS-PAGE and WB allowing estimation of PAC cholesterol crosslinking efficiency of each tested protein.

Firstly to confirm the concentration dependent crosslinking efficiency [43], Huh7/Lunet cells expressing CD81 ectopically (CD81H) were incubated in 3 µM or in 10 µM of PAC cholesterol for 1 h. To test the importance of lipid presence in the medium for incorporation of PAC cholesterol into cells, two medium conditions were set: either DMEM with lipidated FCS (complete DMEM) or with delipidated FCS. The crosslinking specificity was assessed by performing PAC cholesterol binding assay ± UV irradiation and/or ± PAC cholesterol. As a positive control, crosslinking of caveolin1 to PAC cholesterol was tested. As observed with tritium-labeled cholesterol, caveolin1 was detected in eluate fraction in the PAC cholesterol binding assay, which was specific for + UV and + PAC cholesterol (Fig. 3.3). In contrast to caveolin1, Erlin2, which is known ER lipid raft marker, was not detectable in eluate fraction (Fig. 3.3) indicating protein specific PAC cholesterol crosslinking. The intensity of caveolin1 band in the eluate fraction from the condition with 10 µM PAC cholesterol was higher than that in the condition with 3 µM PAC cholesterol confirming concentration dependent crosslinking efficiency. Moreover, in the condition of delipidated FCS, caveolin1 band in the eluate showed higher intensity compared to the condition with lipidated FCS indicating more efficient PAC cholesterol incorporation into cells. Considering the result from this experiment, further PAC cholesterol binding assays were done with 10 µM PAC cholesterol in DMEM with delipidated FCS.

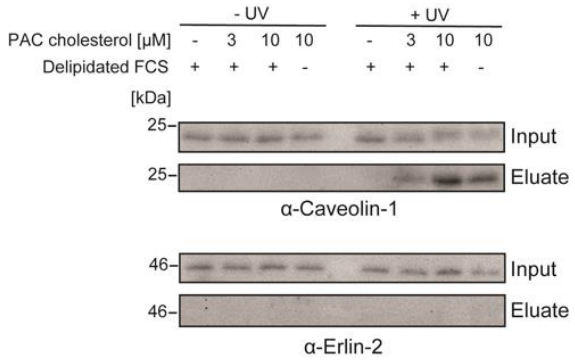

Figure 3.3. Experimental set up for PAC cholesterol binding assay. Huh7/Lunet cells expressing CD81 ectopically (CD81H) were incubated with 3 µM or 10 µM PAC-cholesterol in DMEM with delipidated FCS as well as with 10 µM PAC cholesterol in DMEM with lipidated FCS for 1 h. As a negative control, no PAC cholesterol was added to DL-DMEM. These four different conditions were subjected either to no irradiation (- UV) or to UV irradiation (+ UV). A representative WB from two independent experiments.

3.1.2.2. Subcellular distribution of PAC cholesterol

To estimate how comparable PAC cholesterol and physiological cholesterol are according to their subcellular distributions, I performed immunofluorescence experiments. CD81H cells were fed ± 10 µM of PAC cholesterol for 1 h in DMEM with delipidated FCS. After fixing cells, PAC cholesterol was stained with fluorescent dye Alexa488-azide, which was covalently linked to PAC cholesterol by copper mediated click-reaction. Filipin was used as a cholesterol marker for the samples which are not treated with PAC cholesterol. Then, these two different cholesterol signals were analyzed for their colocalization with signals from subcellular organelle markers such as Calnexin, GM130 and LAMP1 for ER, golgi and late endosome, respectively (Fig. 3.4). 13%, 7% and 21% of filipin signals colocalized with that from ER, golgi and endosomes, respectively, whereas 1%, 11% and 13% of PAC cholesterol signals colocalized with that from ER, golgi and late endosomes, respectively. Although late endosomes seemed to be the subcellular organelles with the highest concentration of both cholesterol species, these data indicated that endocytosed PAC cholesterol is not yet distributed as physiological cholesterol within 1 h of incubation.

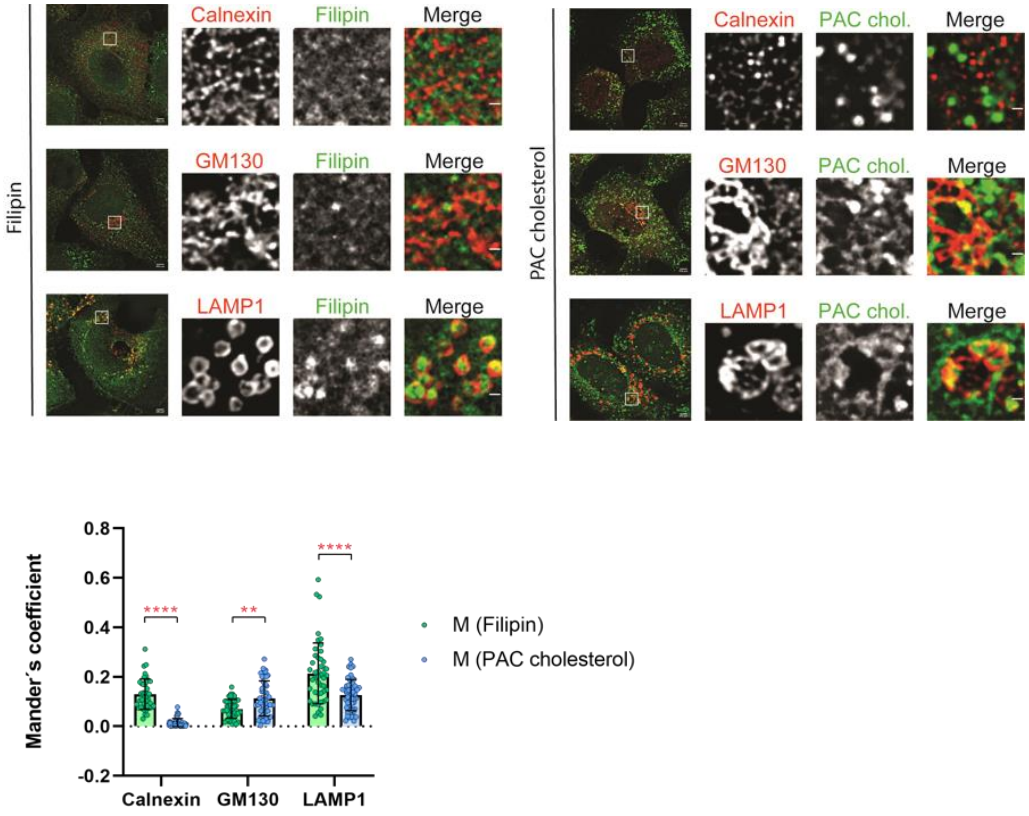

Figure 3.4. Subcellular localization of PAC cholesterol compared to physiological cholesterol. Huh7/Lunet CD81H cells plated on cover slips were incubated with 10 µM PAC-cholesterol for 1 h

and fixed with 4% PFA. After permeabilization with 0,5% triton x100, cells were subjected to click-reaction with Alexa488-azide, incubated with primary and secondary (Alexa647) antibodies for staining subcellular organelles as indicated in the figure. In case of physiological cholesterol staining with filipin, cells were incubated with primary and secondary (Alexa647) antibodies in presence of 250 µg/ml filipin without permeabilization step. Images were taken with confocal spinning disc. Scale bar: 100 µm (left) and 500 nm (right). Images were deconvoluted (Autoquant) and segmented (Ilastik). Then, Mander´s coefficient was calculated (Coloc2 in FIJI). N=2.

3.1.2.3. Screening for HCV proteins cross-linked to PAC cholesterol

After establishing the experimental set up, HCV proteins were screened for their PAC cholesterol crosslinking efficiency (Fig. 3.5A). CD81H cells were electroporated with RNA encoding HCV JFH1 with three adaptive mutations in NS5A and NS5B enhancing virus production [120] and HA- and FLAG-tagged NS2 [81] (JFH1 ad. HAF-NS2). 48 h after electroporation, cells were subjected to PAC cholesterol binding assay. Among tested viral proteins (core, E2, NS2, NS3, NS4B and NS5A), E2, NS2 and NS4B were detectable in the eluate fraction on WB, where NS2 showed the highest eluate/input ratio indicating the most efficient PAC cholesterol crosslinking. Coherently, IF experiments indicated that NS2 was the most efficiently labeled viral protein. (Fig. 3.5B and 3.5C). Considering that cholesterol interaction of tested proteins might be affected by interaction with other viral proteins, Lunet T7 cells were transfected with pTM plasmids encoding core, E1E2, E2, NS2, NS3, NS4B or NS5A and subjected to PAC cholesterol binding assay. In the absence of other viral protein, NS2 still showed the highest eluate/input ratio indicating its high PAC cholesterol crosslinking efficiency (Fig. 3.5D).

A

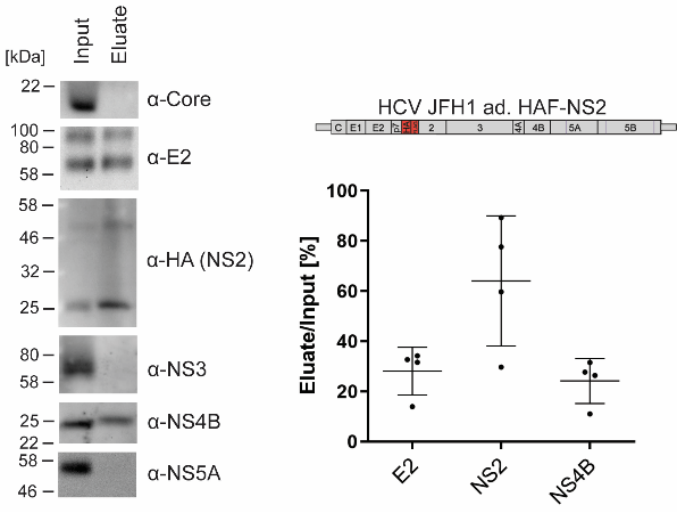
[kDa]
Input
Eluate
22
100
80
58
α-Core
α-E2
58
46
32
25
α-HA (NS2)
80
58
α-NS3
25
22
α-NS4B
58
46
α-NS5A
HCV JFH1 ad. HAF-NS2
C
E1
E2
p7
NS2
3
4A
4B
5A
5B
Eluate/Input [%]
100
80
60
40
20
0
E2
NS2
NS4B

B

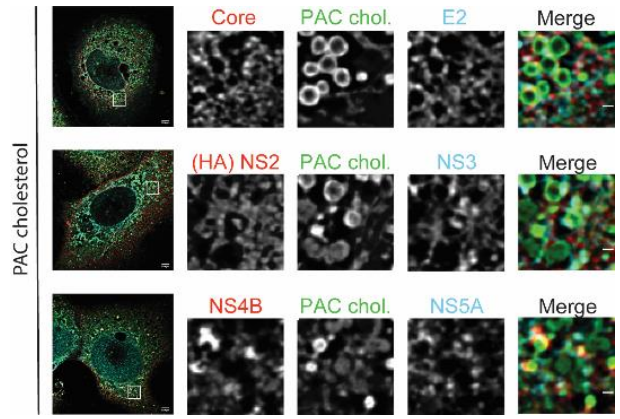
PAC cholesterol
Core
PAC chol.
E2
Merge
(HA) NS2
PAC chol.
NS3
Merge
NS4B
PAC chol.
NS5A
Merge

C

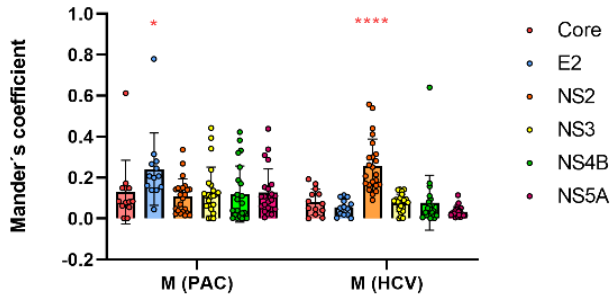
Mander´s coefficient
1.0
0.8
0.6
0.4
0.2
0.0
-0.2
*
****
M (PAC)
M (HCV)
Core
E2
NS2
NS3
NS4B
NS5A

D

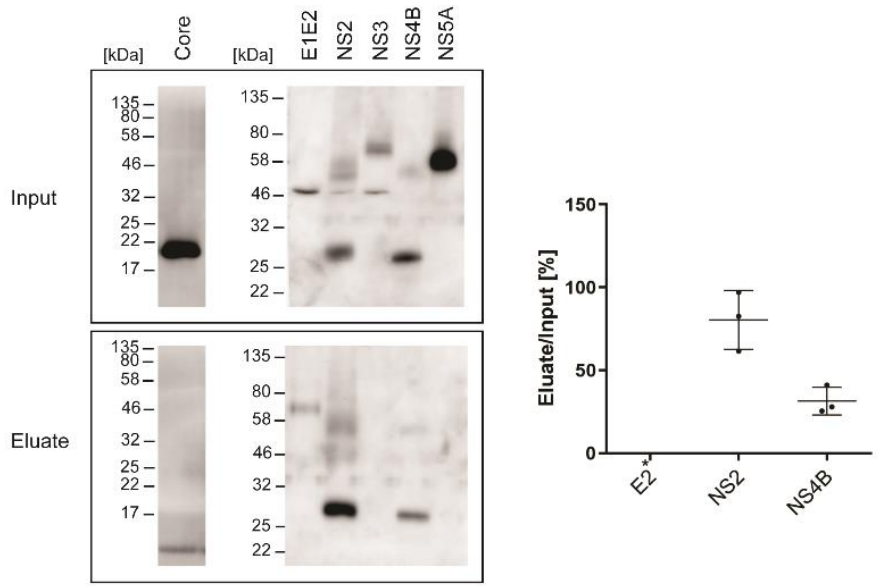

Figure 3.5. PAC cholesterol crosslinking to HCV proteins. A. Screening for HCV proteins crosslinked to PAC cholesterol. Huh7/Lunet CD81H cells were electroporated with RNA encoding full length HCV JFH1 with HA and FLAG (in red) linked NS2 and three adaptive mutations (in dark grey) within NS5A and NS5B for enhancing virus production (JFH1 ad. HAF-NS2). After 48 h, cells were subjected to PAC cholesterol binding assay. N=4. **B and C. Colocalization of HCV proteins with PAC cholesterol.** 72 h after electroporation with RNA encoding JFH1 ad. HAF-NS2, Huh7/Lunet CD81H cells were fixed with 4% PFA. After permeabilization with 0,5% triton x100, cells were subjected to click-reaction with Alexa488-azide, incubated with primary and secondary antibodies as indicated in the figure (red=Alexa647, Cyan=Alexa568). Images were taken with confocal spinning disc. Scale bar: 100 µm (left) and 500 nm (right). N=1. **C.** Images were deconvoluted (Autoquant) and segmented (Ilastik). Then, Mander´s coefficient was calculated (Coloc2 in FIJI). N=1. **D. Sole expression of each HCV protein and their PAC cholesterol crosslinking efficiency.** Huh7/Lunet T7 cells were transiently transfected with expression vector pTM containing T7 promoter encoding HA-tagged HCV proteins as indicated in the figure. After 24 h, cells were subjected to PAC cholesterol binding assay. N=3.

3.1.2.4. PAC cholesterol cross-linking efficiency of HCV NS2 compared to host factors

For comparison of PAC cholesterol crosslinking efficiency of NS2 with that of other known cholesterol binding host factors, Lunet T7 cells were transfected with pTM plasmids encoding NS2, caveolin1 (CAV), ASGR or apolipoproteinE (ApoE) and subjected to PAC cholesterol binding assay (Fig. 3.6). As indicated previously with tritium-labeled cholesterol, caveolin1 was efficiently crosslinked to PAC cholesterol, whereas ASGR exhibited a weak signal. Interestingly, the PAC cholesterol crosslinking efficiency of NS2 even was higher than that of caveolin1. Another host factor ApoE's PAC cholesterol crosslinking efficiency was close to that of ASGR, which was

surprising, because ApoE is part of lipoproteins, where it might have contact to cholesterol [185].

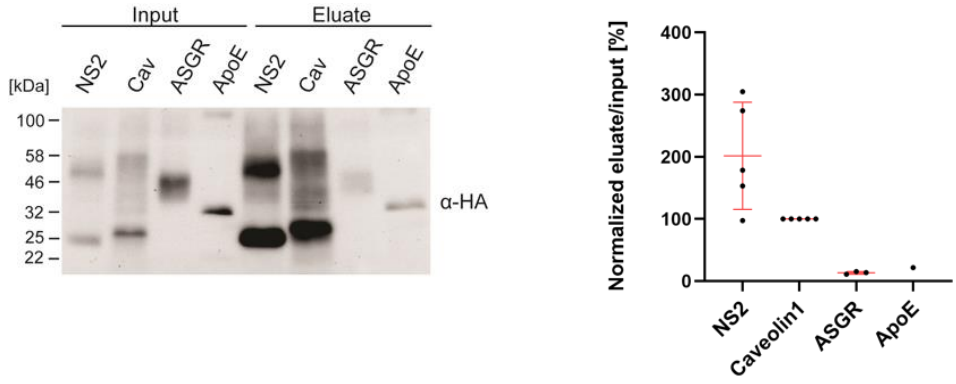

Figure 3.6. HCV NS2 is crosslinked to PAC cholesterol efficiently. Huh7/Lunet T7 cells were transiently transfected with expression vector pTM containing T7 promoter encoding HA-tagged HCV NS2, caveolin1 (Cav), asialoglycoprotein receptor (ASGR) and apolipoprotein E (ApoE). After 24 h, cells were subjected to PAC cholesterol binding assay. N=4.

3.1.2.5. Screening for amino acid residues within NS2 transmembrane domain responsible for PAC cholesterol cross-linking

Previous results showing efficient PAC cholesterol crosslinking of NS2 led to the question, which domains of NS2 is responsible for the PAC cholesterol crosslinking. To address the question, amino acid sequences of NS2 transmembrane domain with three transmembrane segments (Fig. 3.7B) from four different HCV genotypes were aligned (Fig. 3.7C) and checked for existence of potential Cholesterol Recognition Amino acid Consensus (CRAC) motifs (L/I-X_5-Y-X_5-K/R; X_5: 1-5 random amino acids) (Fig. 3.7A), which is assumed to mediate protein-cholesterol interaction [35]. A possible CRAC motif including either aa86-aa94 (**L**LGPA**Y**LL**R**) or aa87-aa94 (**L**GPA**Y**LL**R**) and a CRAC-like motif denoted as pseudo-CRAC motif including aa22-aa27 (**L**TPG**YK**) were found. Moreover, a hydrophilic loop between second and third transmembrane segments including aa49-aa62 (**QEW**VPPM**Q**V**R**GG**RD**) might interact with cholesterol via a hydrogen bond with the hydroxy group of cholesterol. Based on this finding, selected amino acid residues were substituted with alanine (Fig. 3.7C) and cloned into pTM plasmids.

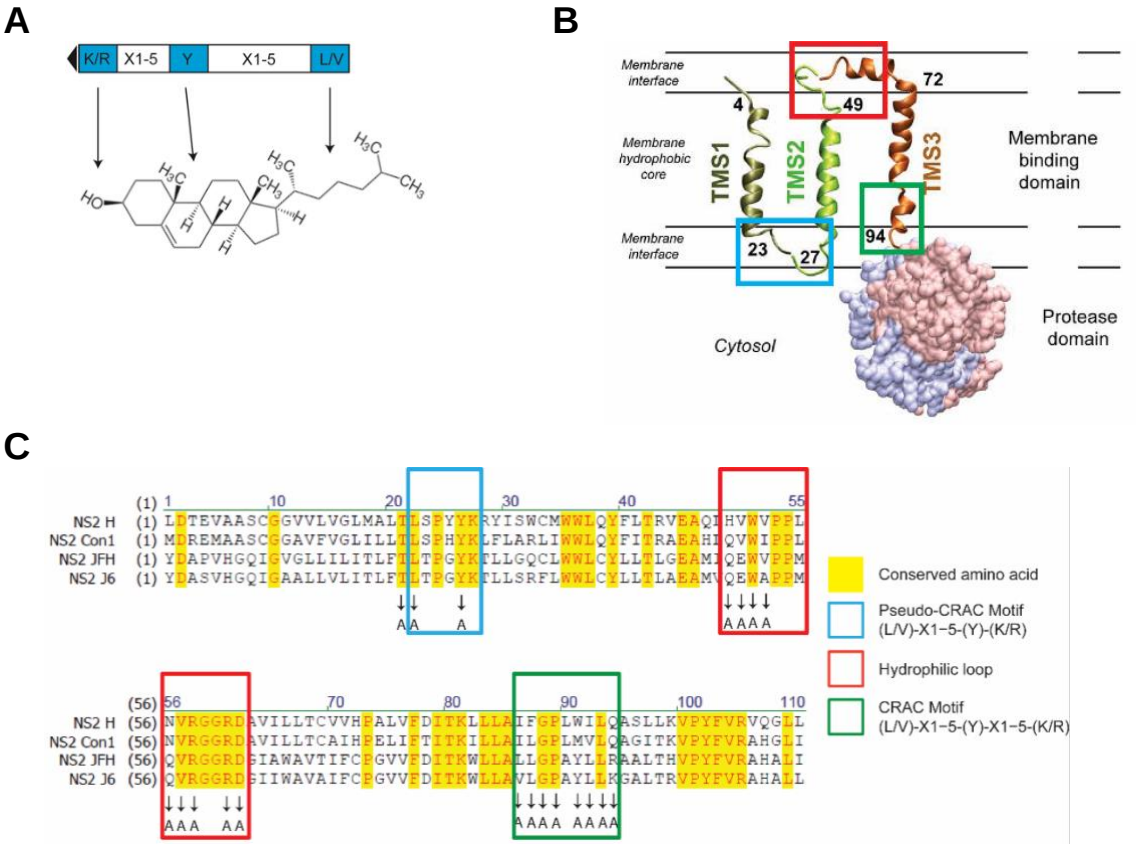

Figure 3.7. Possible Cholesterol Recognition Amino acid Consensus (CRAC) motif within NS2 transmembrane domain. A. CRAC motif. A CRAC motif is consisting of an aliphatic amino acid such as leucine and isoleucine interacting with aliphatic chain of cholesterol, an aromatic amino acid such as tyrosine interacting with ring structure of cholesterol and a charged amino acid such as lysine and arginine interacting with the hydroxyl group of cholesterol [29]. **B. Topology model of NS2 based on NMR and X-ray crystallography.** NS2 contains a transmembrane domain with three transmembrane segments and a cytosolic domain, which forms a dimer with that of another NS2 (Model adapted from Jirasko et al., 2010) [81]. **C. Alignment of amino acid (aa) sequences of NS2 transmembrane domain from four different HCV genotypes.** Within the transmembrane domain of NS2, three possible CRAC motifs and a group of aa were selected, which might be important for PAC cholesterol crosslinking, and their aa are substituted with alanine. The localization of three selected features is shown in the figure 3.6B.

After transfection of Lunet T7 cells with these plasmids, cells were subjected to PAC cholesterol binding assay (Fig. 3.8). The result of the assay revealed significant reduction in PAC cholesterol crosslinking efficiency for NS2 W51A, Y91A, L92A, L93A and R94A, where four of them belong to the CRAC motif indicating the importance of NS2 CRAC motif within aa86-aa94/ aa87-aa94 for PAC cholesterol crosslinking (Fig. 3.8).

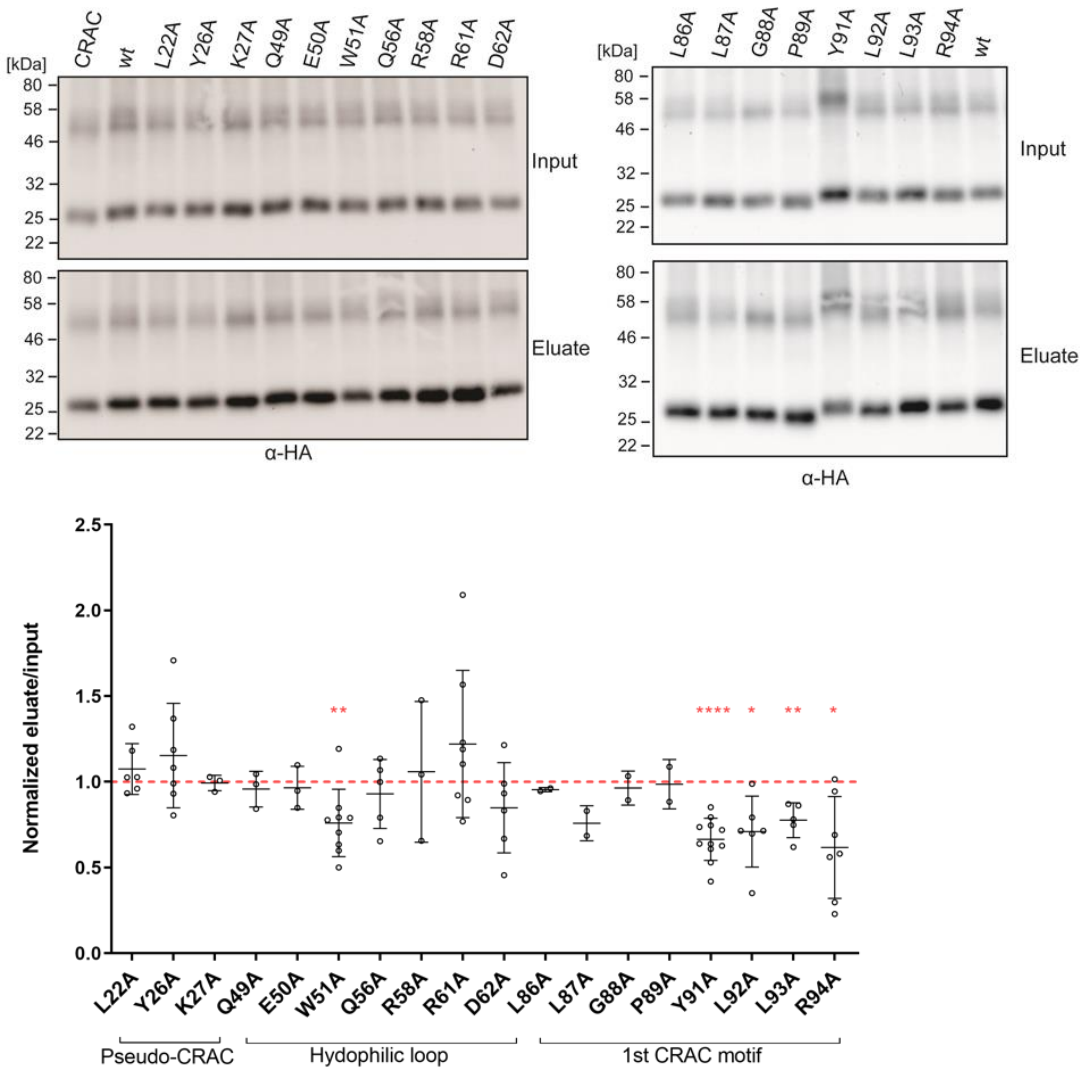

Figure 3.8. Screening for region(s) within NS2 transmembrane domain important for PAC cholesterol crosslinking. Huh7/Lunet T7 cells were transfected with expression vector pTM containing T7 promoter encoding JFH1 HAF-NS2 wt and indicated NS2 mutants. After 24 h, PAC Cholesterol binding assay was done as described previously in the figure 2B. N=2-10.

To prove, whether this CRAC motif indeed is important in context of full-length virus, CD81H cells were electroporated with RNA encoding JFH1 ad. HAF-NS2 wt and alanine substitutions of amino acid residues within the CRAC motif. 72 h after electroporation, cells were subjected to PAC cholesterol binding assay. Significant reduction of PAC cholesterol crosslinking efficiency was only observed for NS2 Y91A (50% reduction) (Fig. 3.9A). Additionally, L86A and L87A also showed reduced eluate/input values by 22% and 25%, respectively (Fig. 3.9A). The level of NS2 R94A in the input was low and barely detectable indicating that this alanine substitution might affect protein stability. Therefore, NS2 R94A was excluded from calculating eluate/input ratio to estimate PAC cholesterol crosslinking efficiency. Interestingly,

amino acid residues L87, Y91A and R94, but not L86, faced to the same direction in the helical wheel model (Fig. 3.9B) and in the 3D Model either based on the published NMR structure [81] or based on the prediction from Alphafold (Fig. 3.9C). This suggests that L87, Y91A and R94, as components of the CRAC motif, are involved in cholesterol interaction. To maximize the extent of reduced PAC cholesterol crosslinking efficiency, NS2 (L86A) L87A and Y91A were combined to double- and triple alanine substitutions (Fig. 3.9D). These combinations strongly decreased the NS2 expression level, although detection of other viral proteins such as core and NS3 were not affected. This data indicated that double- and triple alanine substitutions might affect NS2 stability. Therefor for further studies for characterizing NS2 cholesterol interaction, these NS2 mutants with combined alanine substitutions were excluded.

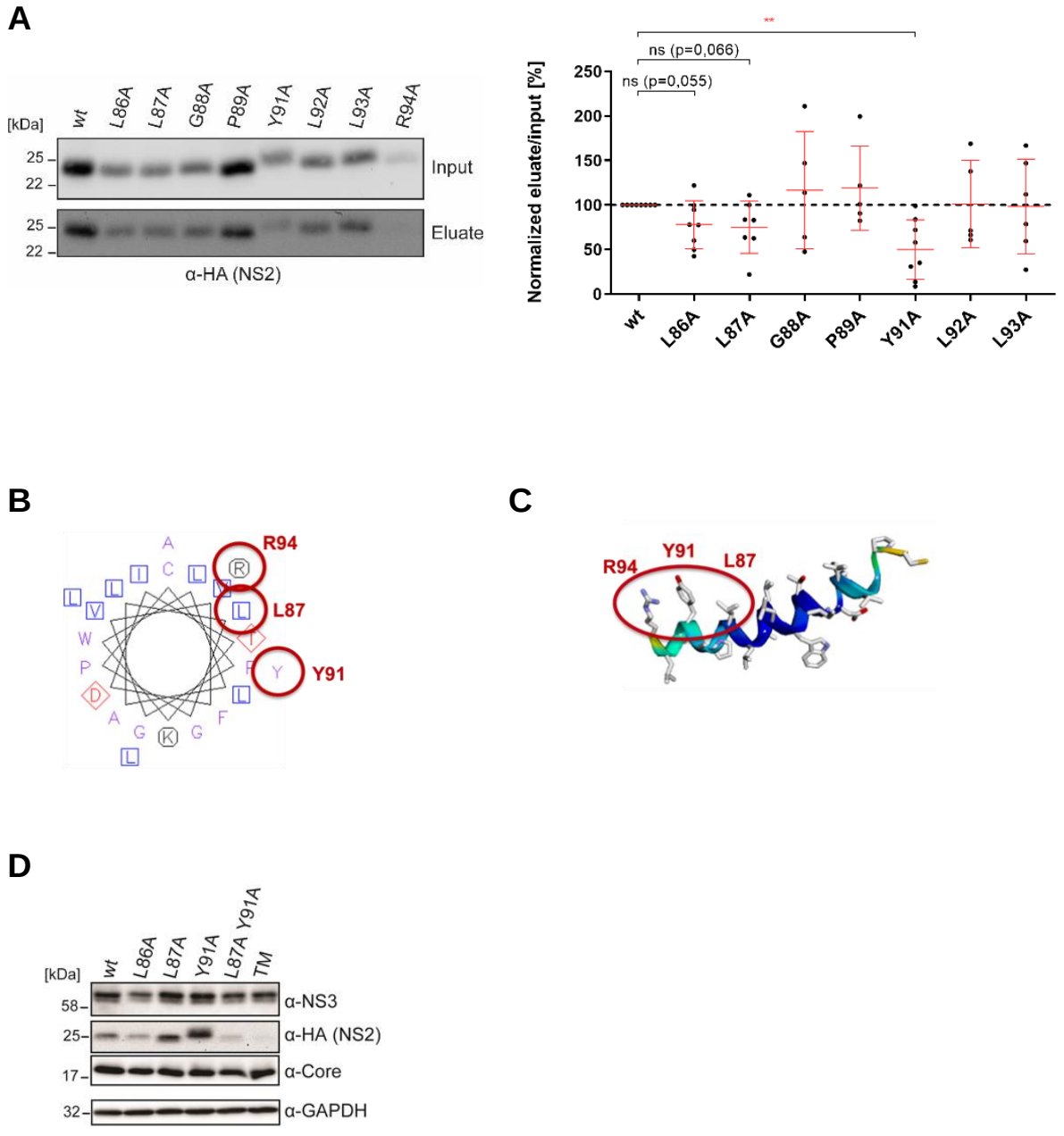

Figure 3.9. Cholesterol Recognition Amino acid Consensus (CRAC) motif might be responsible for NS2 cross-linking with PAC cholesterol. A and D. Huh7/Lunet CD81H cells were electroporated with RNA encoding JFH1 ad. HAF-NS2 wt and NS2 mutants containing alanine substitutions in the possible CRAC motif (aa 86-94) as indicated in the figure. Then, PAC cholesterol binding assay was done 72 h after electroporation as described in figure 3.2B. N=5-8. **B.** Amino acid residues from the third TMS of NS2 were plotted in the helical wheel model by using pepwheel. The CRAC motif amino acid residues L87, Y91 and R94 are marked in red. **C.** 3D model of the third TMS of NS2. The CRAC motif amino acid residues L87, Y91 and R94 are marked in red. The image was generated by using Alphafold. **D.** 72 h after electroporation, cells were lysed and the expression of HCV core, NS2 and NS3 were analyzed by performing SDS-PAGE and WB.

3.1.3. Characterization of HCV expressing NS2 CRAC mutants

3.1.3.1. Subcellular localization of NS2 wt and CRAC mutants

After showing evidence for NS2-cholesterol interaction via the CRAC motif of NS2 (aa 87-94), the subcellular localization of NS2 CRAC mutants was characterized by performing IF (Fig. 3.10). CD81H cells were electroporated with RNA encoding full length JFH1 ad. HAF-NS2 wt, CRAC mutants L87A and Y91A as well as non-CRAC mutant L86A. 72 h after electroporation, cells were fixed and stained for HA (NS2). NS2 wt as well as NS2 L86A and L87A were distributed in cells with predominant membranous structures, whereas NS2 Y91A signals were accumulated in forms of dots next to minor membranous structures (Fig. 3.10). Co-staining with late endosomal marker LAMP1 revealed that these accumulations of NS2 Y91A associate with late endosomes (Fig. 3.10).

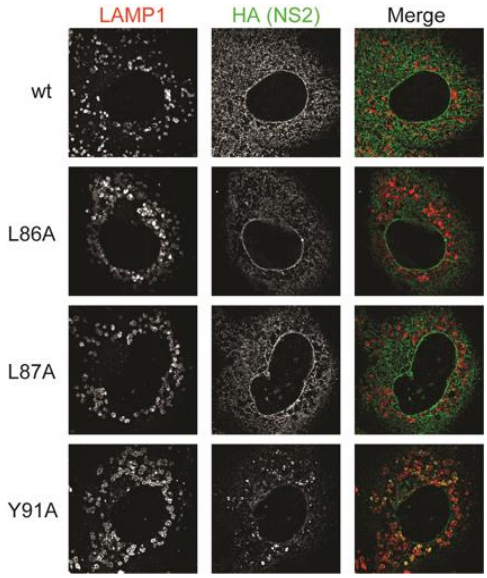

Figure 3.10. Subcellular localization of NS2 wt and CRAC mutants. Huh7/Lunet CD81H cells were electroporated with RNA encoding JFH1 ad. HAF-NS2 wt and NS2 L86A, L87A and Y91A and plated on cover slips. After 72 h cells were fixed with 4% PFA. After permeabilization with 0,5% triton x100, samples were incubated with primary and secondary (LAMP1-Alexa488 and HA-Alexa647) antibodies. Images were taken with confocal spinning disc.

Core and E2 localization on endosomes upon expression of NS2 Y91A

Post-golgi transport to endosomes mediated by clathrin-AP1 complexes is essential for release of infectious HCV particles. There, NS2 is the viral factor exploiting clathrin-mediated transport by interacting with AP1 interaction [90]. This led to the assumption, that NS2 might assist virus particles from golgi to endosomes for their proper release. Since NS2 Y91A is highly associated with LAMP1 positive late endosomes compared to wt NS2, virions might be accumulating in late endosomes with NS2 Y91A. To prove

this hypothesis, late endosomal localization of virus capsid core and envelop E2 was investigated by performing IF experiments using CD81H cells electroporated with RNA encoding JFH1 ad. HAF-NS2 wt and Y91A (Fig. 3.11). However, preliminary quantitative analysis of core- and E2 colocalization with LAMP1-positive late endosomes showed that there is no significant accumulation of core and E2 in the endosomes (Fig. 3.11).

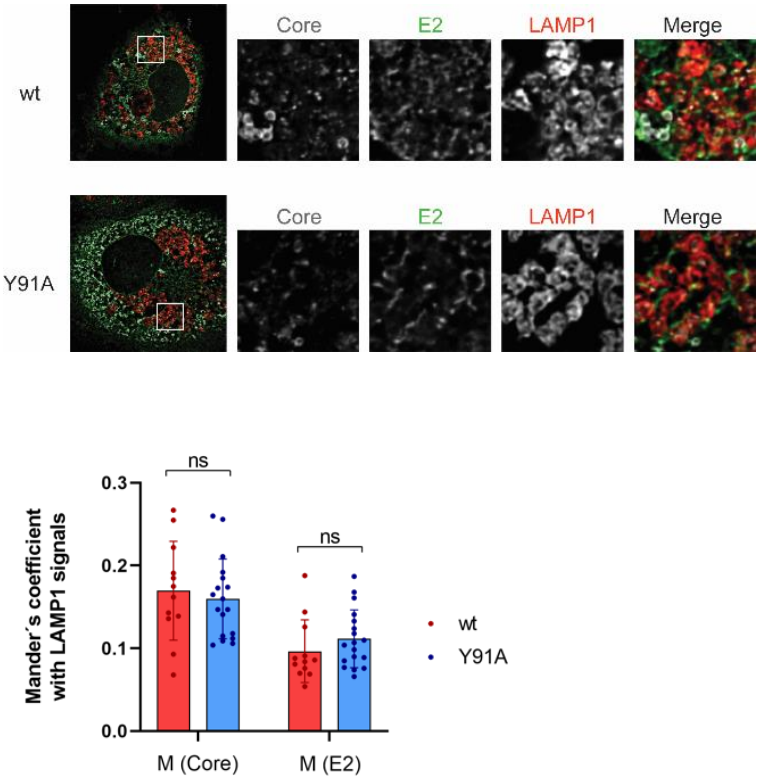

Figure 3.11. Endosomal localization of core and E2. Huh7/Lunet CD81H cells were electroporated with RNA encoding JFH1 ad. HAF-NS2 wt and NS2 L86A, L87A and Y91A and plated on cover slips. After 72 h cells were fixed with 4% PFA. After permeabilization with 0,5% triton x100, samples were incubated with primary and secondary (E2-Alexa488, Core-Alexa568 and LAMP1-Alexa647) antibodies. Images were taken with confocal spinning disc. Images were deconvoluted (Autoquant) and segmented (Ilastik). Then, Mander´s coefficient was calculated (Coloc2 in FIJI). N=1.

Correlation between NS2 cholesterol interaction and NS2 LAMP1 colocalization

Considering that NS2 Y91A was the only mutant showing significant reduction in PAC cholesterol crosslinking (Fig. 3.9A), the observed late endosomal accumulation of NS2 Y91A might be related to reduced NS2 cholesterol interaction. This assumption led us to try to rescue the altered subcellular localization of NS2 Y91A by increasing subcellular cholesterol concentration, so that NS2 might come in contact with cholesterol more frequently in its close proximity. Colocalization of NS2 wt and Y91A

with LAMP1 was assessed by performing IF after treating CD81H cells with ± 50 µg/ml LDL for 3 h (Fig. 3.12). After acquiring images, segmentation of each signal was performed by using Ilastik and Mander's coefficient showed no significant difference between + and - LDL conditions in terms of NS2 Y91A LAMP1 colocalization (Fig 3.12). This result indicated that the late endosomal NS2 Y91A accumulation might not be affected by the increased frequency of being close to cholesterol. Interestingly, NS2 wt seemed to colocalize with LAMP1 more frequently after addition of LDL. However, the Mander's coefficient was still lower than that of NS2 Y91A (Fig 3.12).

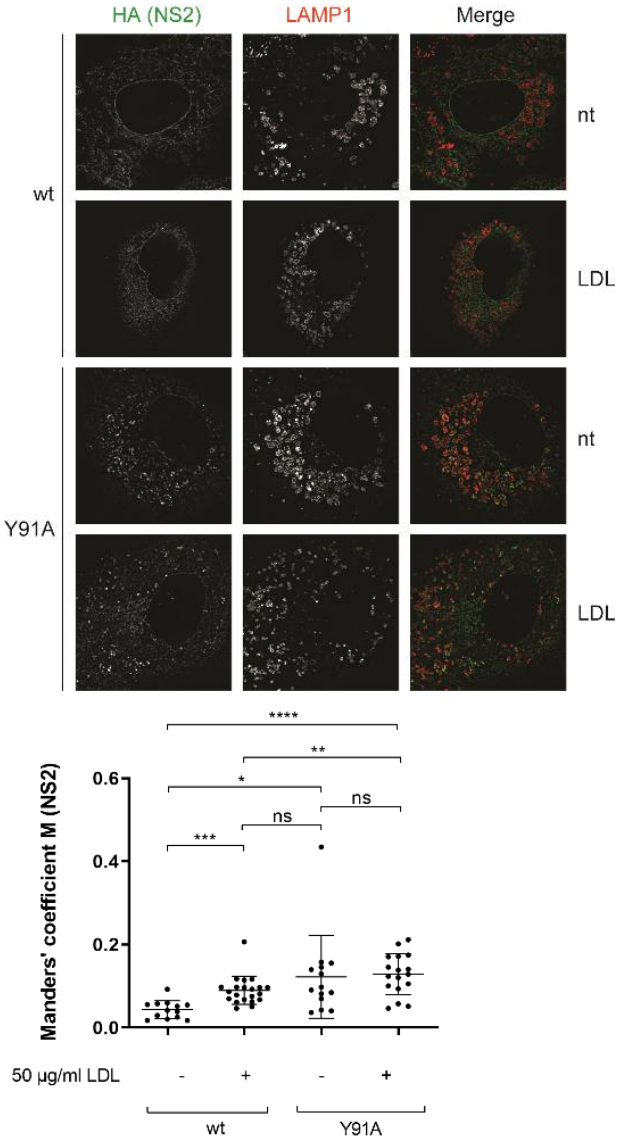

Figure 3.12. Possible role of LDL in endosomal localization of NS2. Huh7/Lunet CD81H cells were electroporated with RNA encoding JFH1 ad. HAF-NS2 wt and Y91A and plated on cover slips. After 72 h cells were incubated either with or without 50 µg/ml LDL for 3 h. Afterwards, cells were fixed with 4% PFA, permeabilized with 0,5% triton x100 and incubated with primary and secondary (LAMP1-Alexa488 and HA-Alexa647) antibodies. Images were taken with confocal spinning disc,

deconvoluted (Autoquant) and segmented (Ilastik). Then, Mander´s coefficient was calculated (Coloc2 in FIJI). N=1.

According to the previous data, a possible increase of subcellular cholesterol concentration by addition of LDL cannot rescue the late endosomal accumulation of NS2 Y91A, because it might just increase the frequency of cholesterol in close proximity to NS2 without affecting the ability of NS2 to interact with cholesterol. However, lowering subcellular cholesterol concentration level might generate a condition where less NS2 can interact with cholesterol. Based on this assumption, NS2 LAMP1 colocalization was assessed after treating cells with methyl-β-cyclodextrin (MβCD), a cholesterol extracting compound (Fig. 3.13). Control, cells were incubated 1) in complete DMEM and 2) in DMEM with delipidated FCS (Fig 3.13). First, lowered cholesterol levels after treating cells with MβCD was confirmed from the cell lysate (Fig. 3.13A). Interestingly, incubating cells with DMEM with delipidated FCS increased cholesterol levels compared to complete DMEM. Then, by performing IF and subsequent segmentation of signals and calculating Mander's coefficient, a significant increase of NS2 LAMP1 colocalization was observed after MβCD treatment (Fig. 3.13B), while there was no significant difference between conditions with complete DMEM and with DMEM with delipidated FCS (Fig. 3.13B). Noticeably, wt NS2 colocalizing with LAMP1 after extraction of cholesterol in the presence of MβCD seemed to be membranous rather than showing dot-like structures as NS2 Y91A mutant did (Fig. 3.10).

A

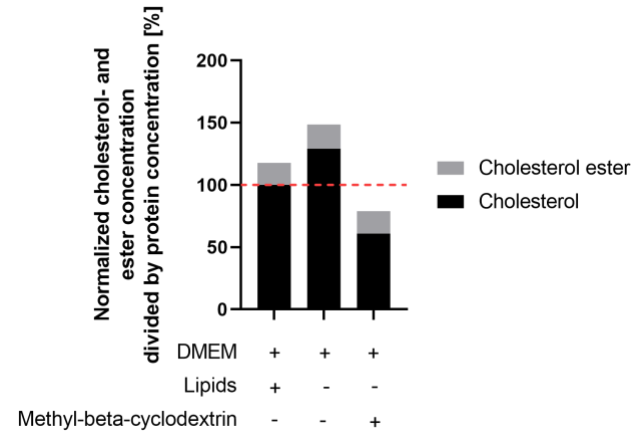

B

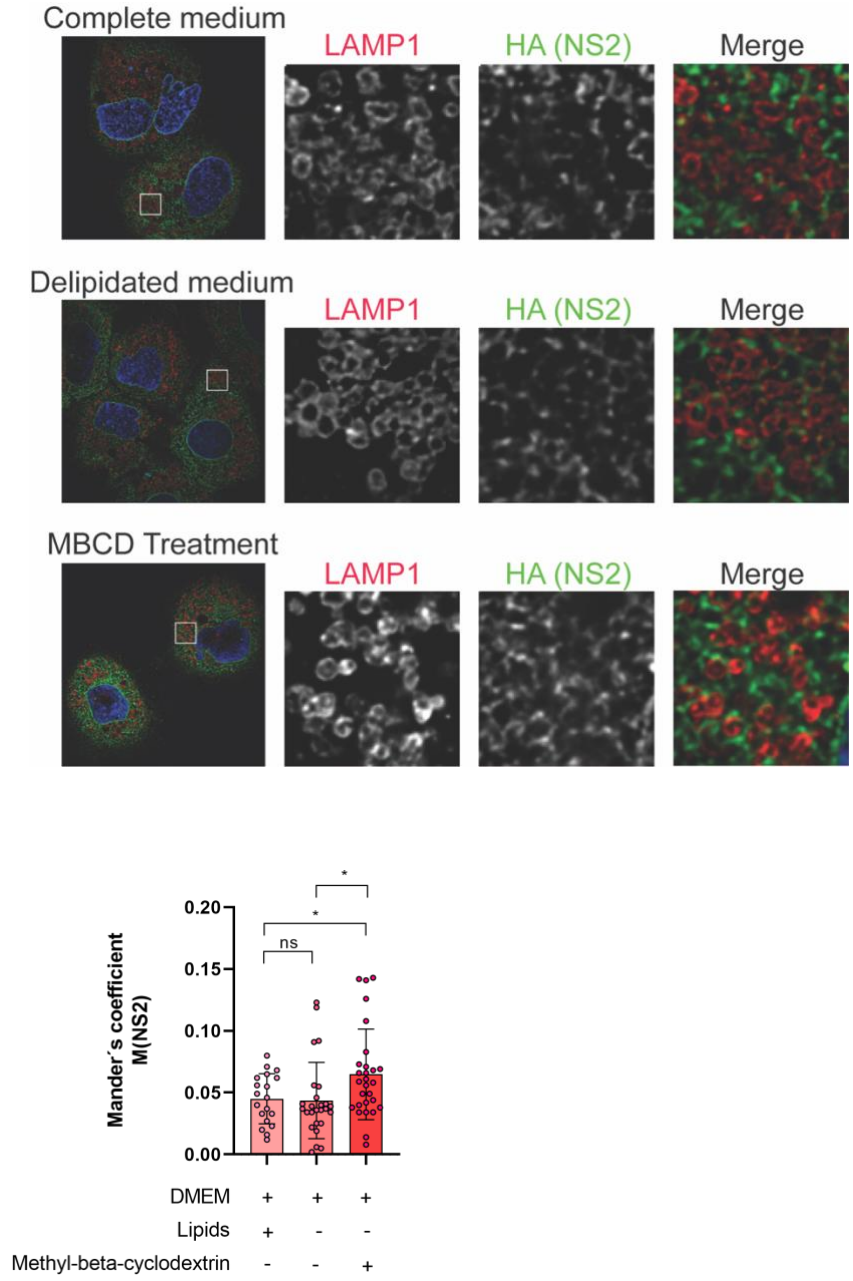

Figure 3.13. Endosomal localization of NS2 might be regulated by NS2 cholesterol interaction. Huh7/Lunet CD81H cells were electroporated with RNA encoding JFH1 ad. HAF-NS2 wt and plated on cover slips. After 72 h cells were incubated 1) in completed DMEM, 2) in DMEM with delipidated FCS and 3) in DMEM with delipidated FCS and 1% MβCD for 6 h. Afterwards, cells were fixed with 4% PFA, permeabilized with 0,5% triton x100 and incubated with primary and secondary (LAMP1-Alexa488 and HA-Alexa647) antibodies as well as DAPI. Images were taken with confocal spinning disc, deconvoluted (Autoquant) and segmented (Ilastik). Then, Mander´s coefficient was calculated (Coloc2 in FIJI). N=1.

3.1.3.2. Involvement of NS2-cholesterol interaction in the HCV replication cycle

NS2 is an essential viral factor for virus assembly [83] and virus release [90]. Therefore, possible defects from reduced NS2-cholesterol interaction might occur in virus assembly and/or virus release. To check possible defects in virus release upon expression of NS2 CRAC mutants, (L86A), L87A and Y91A, intracellular and extracellular core concentrations were measured, which might indicate viral protein translation and virus release, respectively. CD81H cells were electroporated with RNA encoding JFH1 ad. HAF-NS2 wt and three mutants. 72 h after electroporation, intracellular and extracellular core was collected from cell lysates and supernatant, respectively, and their concentration was analyzed by performing core ELISA experiments (Fig. 3.14A and 3.14B). The result showed that the intracellular and extracellular core concentration of virus encoding NS2 CRAC mutants were reduced by less than four- and two-fold, respectively, compared to that of wt virus (Fig. 3.14A). To test, whether NS2 CRAC mutants affect assembly of infectious virus particles, CD81H cells were electroporated with RNA encoding JFH1 ad. HAF-NS2 wt and three NS2 CRAC mutants. 72 h after electroporation, intracellular and extracellular virus were collected from cell lysates generated by freezing-thawing cycles and from supernatant, respectively, which were used for serial infection of Huh7,5 cells. By detecting infected cells by colorimetric staining of NS5A, TCID50 values were calculated indicative for viral titer (Fig. 3.14C). The TCID50 values of intracellular virus did not differ among wt, L86A and Y91A conditions. Only, the TCID50 values of intracellular virus expressing L87A was reduced by three-fold. However, TCID50 values of extracellular virus encoding NS2 L87A and Y91A were 5-fold and >10-fold lower than that of wt virus, respectively, whereas the extracellular TCID50 values of virus encoding NS2 L86A was comparable to that of wt (Fig. 3.14C). These data from TCID50 and core ELISA indicated that in case of virus encoding NS2 L87A and Y91A, infectious virus production might be less efficient than that of wt virus and release of infectious virus might be negatively affected as well. By calculating percentage of intracellular and extracellular TCID50 from the total TCID50, possible defect in infectious virus release became clearer, since the percentage of intracellular TCID50 from viruses encoding L87A and Y91A were approximately 4-fold and 7-fold higher than that of wt virus and virus encoding L86A (Fig. 3.14D).

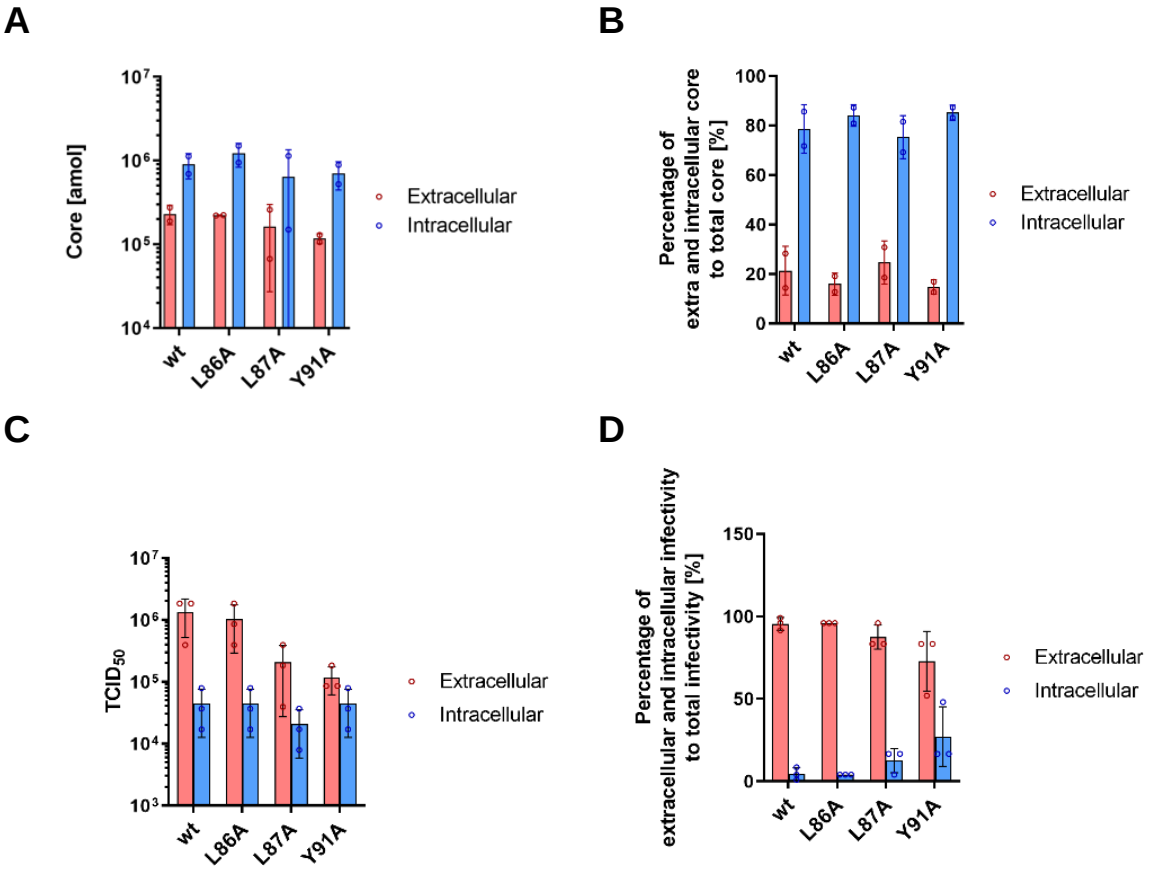

Figure 3.14. HCV expressing NS2 L87A and Y91A has defects in infectious virus production and release. A-D. Influence of expressing NS2 CRAC mutants on core release and virus infectivity. Huh7/Lunet CD81H cells were electroporated with RNA encoding JFH1 ad. HAF-NS2 wt and NS2 L86A, L87A and Y91A. After 72 h cells were harvested in appropriate ways for each experiment: **A.** Released extracellular and intracellular capsid core was collected from supernatant and cell lysate and analyzed by performing core-ELISA. N=2. **B.** Extra- and intracellular core amounts were divided by total core amount. **C.** Released extracellular and intracellular virus particles were collected from supernatant and cell lysate by freezing-thawing cycles, respectively, and were used to infect Huh7.5 cells with serial dilutions. 72 h after infection, infected cells were detected by staining HCV nonstructural protein NS5A and TCID50 values were calculated. N=3. **D.** Extra- and intracellular infectivity was divided by total infectivity.

After showing reduced infectious virus production and virus release of NS2 Y91A mutant virus, I next determined, whether the observed phenotypes are correlated to reduced cholesterol interaction of NS2 Y91A. Therefore, cells were treated with 100 µg/ml LDL to increase subcellular cholesterol levels to increase the frequency that NS2 comes into contact with cholesterol. In this way, reduced cholesterol interaction of NS2 Y91A might be compensated and defects in infectious virus production and release might be rescued. First, the effect of addition of LDL for wt virus was assessed. 72 h after electroporation with RNA encoding JFH1 ad. HAF-NS2, CD81H cells were incubated in OptiMEM ± 100 µg/ml LDL for 3 h. The addition of LDL increased core release by two-fold (Fig. 3.15A) and extracellular virus titer by 4.6-fold (Fig. 3.15B), while the intracellular virus titer decreased by 4.6-fold (Fig. 3.15B), although the

intracellular core level did not change (Fig. 3.15A). This data showed evidence that treatment with LDL supports infectious viral particle release, but it did not affect infectious virus production. Then, the effect of LDL treatment for virus expressing NS2 Y91A was assessed. 72 h after electroporation with RNA encoding JFH1 ad. HAF-NS2 Y91A, CD81H cells were incubated in OptiMEM ± 100 µg/ml LDL for 3 h. As it was the case for wt virus, LDL treatment increased core release by two-fold (Fig. 3.15A). However, compared to wt virus, the increase rate of extracellular titer after addition of LDL was two-fold lower, while the intracellular titer did not change (Fig. 3.15B). This data indicated that the effect of LDL might be limited to core/assembled viral particle release. Since both viruses wt NS2 and Y91A mutant showed comparable increase of core release upon LDL treatment, NS2 Y91A mutant seemed to cause rather defects in infectious virus assembly than release of virus.

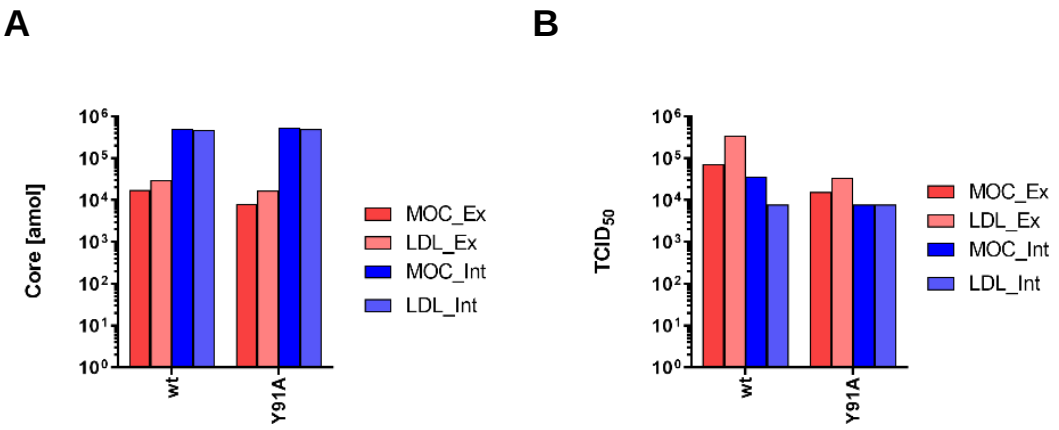

Figure 3.15. Possible role of LDL in rescuing virus phenotype containing NS2 Y91A. Huh7/Lunet CD81H cells were electroporated with RNA encoding JFH1 ad. HAF-NS2 wt and Y91A and plated on cover slips. After 72 h cells were incubated either with or without 50 µg/ml LDL for 3 h. **A.** Released extracellular and intracellular capsid core was collected from supernatant and cell lysate and analyzed by performing core-ELISA. N=1. **B.** Released extracellular and intracellular virus particles were collected from supernatant and cell lysate by freezing-thawing cycles, respectively and were used to infect Huh7.5 cells with serial dilutions. 72 h after infection, infected cells were detected by staining HCV nonstructural protein NS5A and TCID50 values were calculated. N=1.

NS2-cholesterol interaction effect in recruiting viral proteins to virus assembly sites

The assembly of HCV particles is assumed to occur on ER membranes in close proximity to LDs [142]. These ER derived membranes have a specific lipid composition. They are enriched with cholesterol and sphingolipids [85, 182]. This characteristic lipid composition generates tightly packed and ordered membrane microdomain

distinguishable from surrounding ER membranes. This microdomain is called a lipid raft and analysis of lipid rafts as well as its associating proteins have been performed by using its detergent resistant property [13, 15, 186]. Previously, Shanmugam et al. studied lipid raft localization of HCV proteins by isolating detergent resistant membranes (DRMs). They showed that NS2 localizes on DRMs and this localization can be abolished by cholesterol extraction [85]. Moreover, depletion of NS2 results in impaired E2-DRM localization [85]. Considering that NS2 might recruit other viral proteins such as E1, E2, P7 (virus assembly module) and NS3 (viral RNA replication module) to the virus assembly site for efficient virus production [81], we hypothesized NS2-cholesterol interaction might be important for NS2 lipid raft localization and for infectious virus production by recruiting E2 to lipid rafts. To prove the hypothesis, colocalization of NS2 and E2 with ER lipid raft marker Erlin2 was assessed with IF experiments upon virus replication containing either wt NS2 or NS2 Y91A mutation. CD81H cells were electroporated with JFH1 ad. HAF-NS2 wt and Y91A. 72 h after electroporation, cells were fixed and stained for HA (NS2), E2 and Erlin2. Confocal microscopy images were subjected to segmentation and to Mander's coefficient calculations. In case of NS2 Y91A virus the Mander's coefficients calculated from 1) NS2 Erlin2- and 2) E2 Erlin2 signals and they were reduced by 50% and 20-40%, respectively, compared to that from wt virus (Fig. 3.16). This data indicated that reduced NS2 cholesterol interaction might impair lipid raft localization of NS2 and E2. Moreover, NS2 Y91A and E2 colocalization was found to be 40% less efficient than wt NS2 and E2 colocalization (Fig. 3.16) suggesting that NS2 cholesterol interaction might be important for interaction with E2 as well as for E2 lipid raft localization.

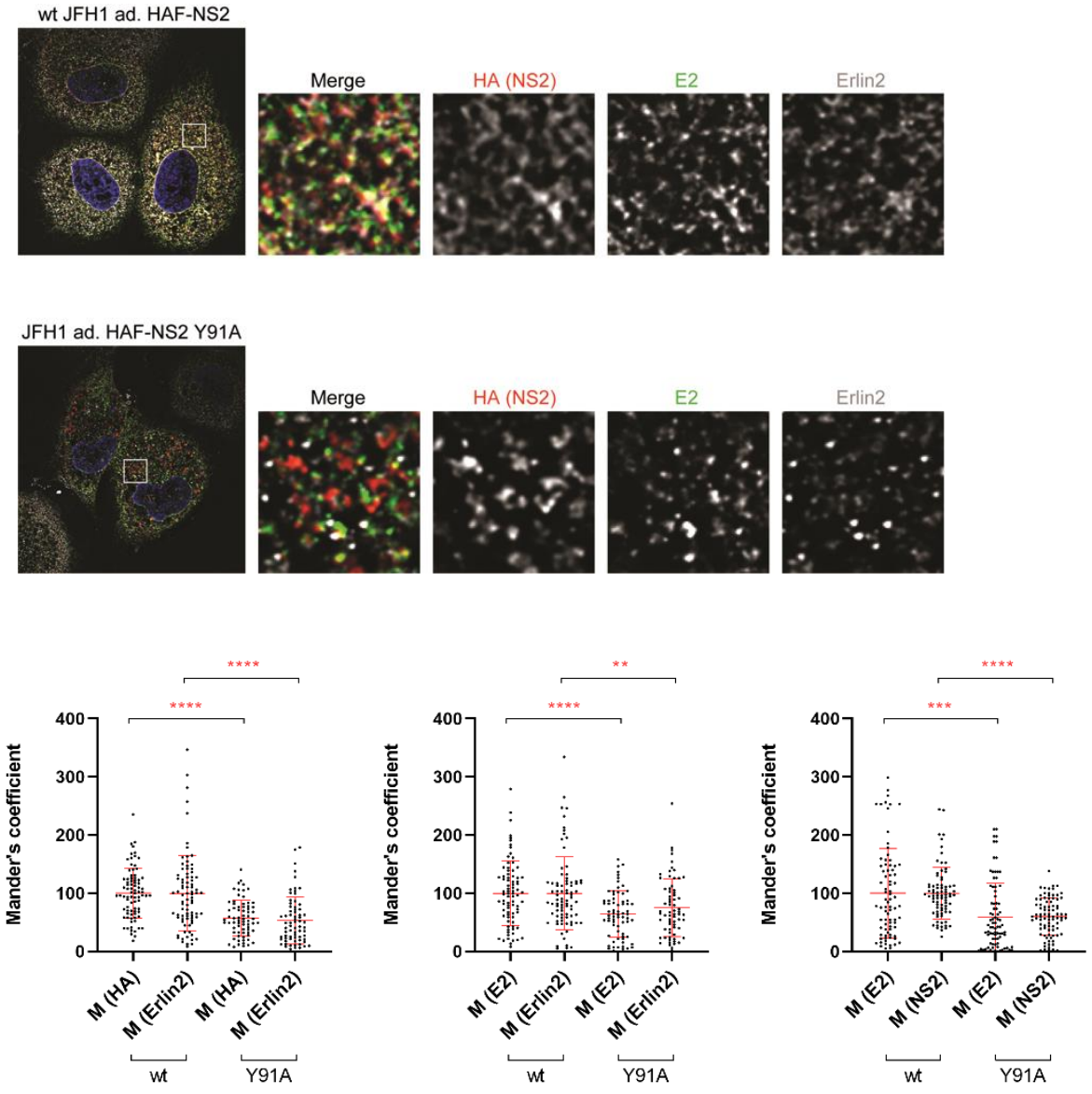

Figure 3.16. DRM localization of NS2 and E2. Huh7/Lunet CD81H cells were electroporated with RNA encoding JFH1 ad. HAF-NS2 wt and Y91A and plated on cover slips. After 72 h cells were fixed with 4% PFA. After permeabilization with 0,5% triton x100, samples were incubated with primary and secondary (E2-Alexa488, Erlin2-Alexa568 and HA-Alexa647) antibodies. Images were taken with confocal spinning disc, deconvoluted (Autoquant) and segmented (Ilastik). Then, Mander´s coefficient was calculated (Coloc2 in FIJI). N=2.

After detecting a correlation between NS2 cholesterol interaction and NS2 E2 colocalization, the role of NS2 cholesterol interaction for NS2 E2 interaction was addressed biochemically by performing IP experiments. CD81H cells were electroporated with RNA encoding JFH1 ad. HAF-NS2 wt, L86A, L87A and Y91A. 72 h after electroporation, cells were lysed and subjected to IP against HA-tagged NS2. Input and eluate were analyzed for NS2 and E2, which was shown to be coprecipitated with NS2 previously [81]. Then NS2 and E2 signals from eluates were quantified and

the E2/NS2 ratio from three NS2 mutants were normalized to that of NS2 wt. NS2 L87A and Y91A showed a reduced E2/NS2 ratio compared to that of wt NS2 by 7.9% and 19.4%, respectively, but not NS2 L86A mutant (Fig 3.17). These data gave the first evidence that reduced cholesterol interaction of NS2 CRAC mutants might have defects in E2 interaction.

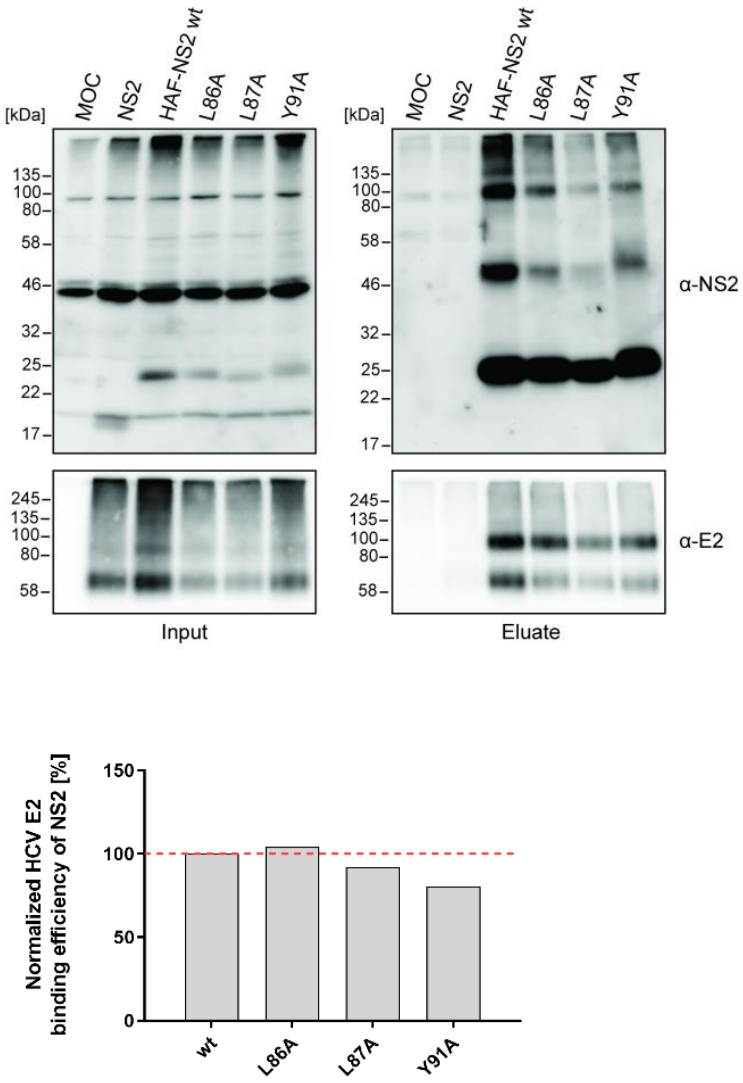

Figure 3.17. Immunoprecipitation with HA-tagged NS2 wt and CRAC mutants of NS2. Huh7/Lunet CD81H cells were electroporated with RNA encoding JFH1 ad. HAF-NS2 wt, L86A (non-CRAC mutant), L87A and Y91A. As negative controls, cells either were electroporated with water (MOC) or with JFH1 ad. without HA-tag (NS2). After 72 h cells were lysed in lysis buffer containing 100 mM NaCl, 20 mM Tris (pH 7.5), 0.5% DDM and protease inhibitor (Input). Then, cell lysates were subjected to affinity chromatography with anti-HA agarose resins. Proteins were eluted in laemli buffer at 95 °C for 5 min. Eluates and inputs were quantitatively analyzed by performing SDS-PAGE and WB. N=1.

Based on previous data (Fig. 3.16 and 3.17), NS2 cholesterol interaction might be important not only for NS2 lipid raft localization, but also for E2 lipid raft localization,

which might be mediated by NS2 E2 interaction, where NS2 cholesterol interaction is necessary. Previously, Shanmugam et al could isolate lipid rafts in forms of DRM and showed localization of, among others, core, E2 and NS2 on DRM by performing floatation assay [85], I decided to perform the same assay to confirm the role of NS2 cholesterol interaction in recruiting E2 to lipid rafts. In this assay, cells are lysed mechanically by passing through needles. In the presence of detergent triton X100 at 4 °C, only DRMs stay unbroken in cell lysate, whereas other membranes are solubilized. Then, cell lysate gets placed to the bottom of Optiprep gradient with increasing Optiprep concentration from the top to bottom. Subsequent ultracentrifugation separates floating DRMs from unfloating solubilized membrane (Fig 3.18A). CD81H cells were electroporated with RNA encoding full length JFH1 ad. HAF-NS2 wt. 48 h after electroporation, cells were subjected to mechanical lysis and incubated with 1% triton X100 at 4 °C for 30 min. As controls, cell lysates were incubated without detergent, where all membranes stay intact or cell lysates were incubated at 37 °C with 1% triton X100, where DRMs become solubilized. After ultracentrifugation of cell lysates, ten fractions from the top were collected and analyzed for membrane associating proteins by performing WB (Fig. 3.18B). As expected in the condition without detergent, not only lipid raft marker Flotilin1 and Caveolin1, but also non-lipid raft protein Calnexin, as well as all tested viral protein core, E2 and NS2 were present in the third fraction indicative for floating intact membranes (Fig. 3.18B, left). However, all tested proteins were only present in the last two to three fractions after incubation with triton X100 independent of the incubation temperature (Fig. 3.18B, middle and right). This result showed that 1% triton X100 might be able to solubilize even DRMs at 4 °C in our experimental set up. Therefore, it was necessary to find the ideal concentration of triton X100 in order to separate DRMs from non-DRMs. To this end, fractionation assay was performed instead of floatation assay due to its faster process. The only difference between these two assays is the DRM separation step: mechanically generated cell lysate in the presence of triton X100 is directly subjected to centrifugation in the fractionation assay for pelleting DRMs (insoluble fraction; I), while solubilized membranes remain in the supernatant (soluble fraction; S) (Fig. 3.18C). In these experiments, cell lysates were generated with four different triton X100 concentrations (1%, 0.5%, 0.1% and 0.05%) either at 4°C or 37 °C. As control, cell lysate was incubated without triton X100. After centrifugation, the condition with 0.05% triton X100 at 4 °C showed that DRM markers

Erlin2 and caveolin1 were present in the insoluble fraction clearly, while the marker for non-DRM, calnexin, was present in the soluble fraction predominantly (Fig. 3.18D). Another marker for DRM, flotilin1, was in both fractions. However, this comparable distribution in both fractions was observed previously too indicating that floilin1 might not only exist on lipid raft [85]. Since treatment with 0.05% TritonX100 led to a clear separation of DRM- and non-DRM markers, I proceeded with this concentration for further experiments. Then, the presence of NS2, core and E2 on DRM was assessed. As shown in the figure 3.18D, core showed signals from both soluble and insoluble fractions, whereas NS2 and E2 remained only in the soluble fraction. This data indicated that this experimental set up cannot be used to assess importance cholesterol interaction in NS2 and E2 lipid raft localization.

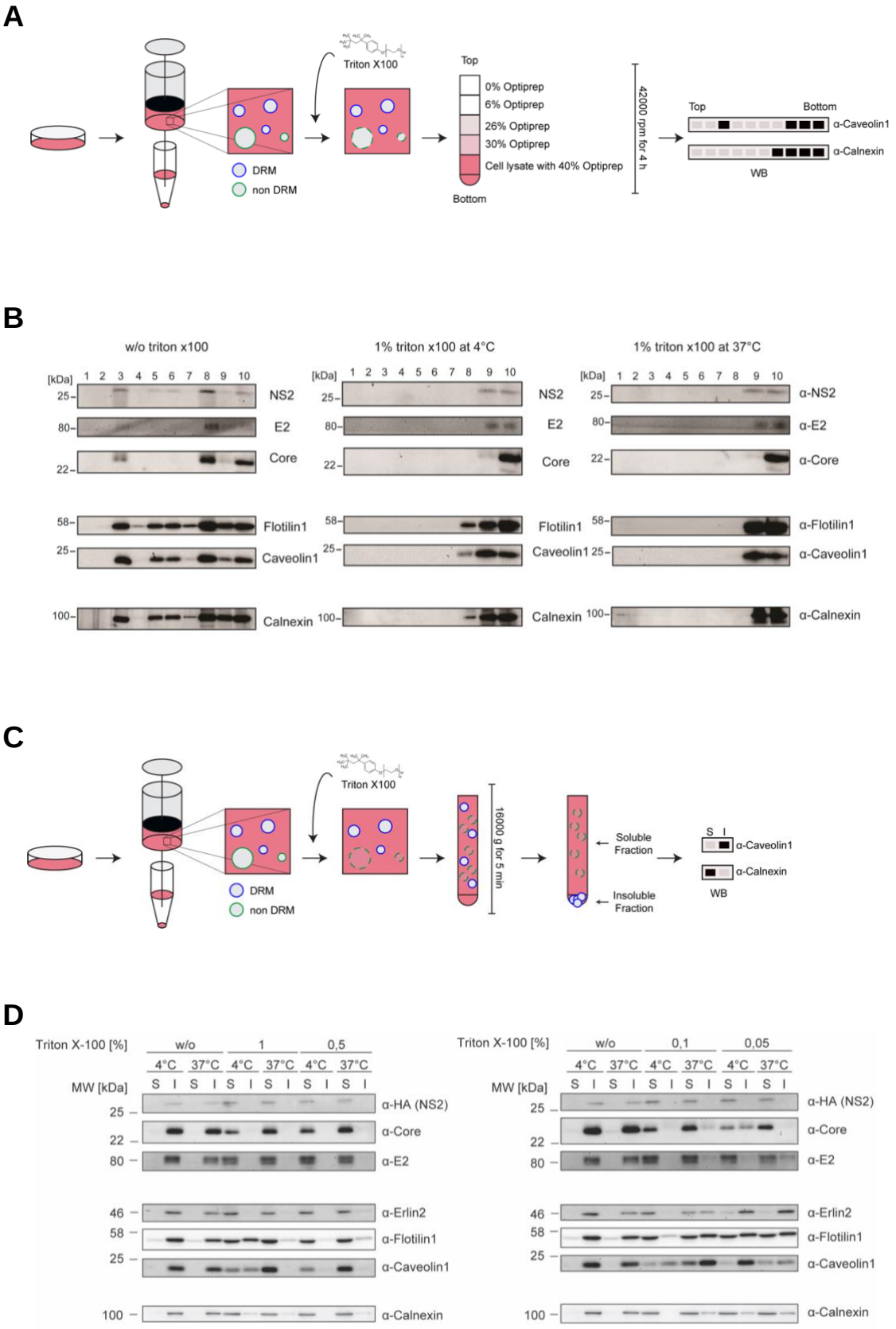

Figure 3.18. Isolation of DRMs. A. Principle of floatation assay. Cells are lysed by passing through 22-gauge needles ten times. By adding 1% triton X100, only DRMs stay intact, whereas other membrane structures are solubilized. By Optiprep gradient ultracentrifugation, DRMs can be separated from solubilized membranes. **B. Flotation assay for addressing the reproducibility.**

Huh7/Lunet CD81H cells were electroporated with RNA encoding JFH1 ad. HAF-NS2 wt. 48 h after electroporation, cells were subjected to mechanical lysis. Then, cell lysate was 1) incubated without detergent (left), 2) with 1% triton X100 at 4 °C (middle) or 3) with 1% triton X100 at 37 °C (right) for 30 min. Subsequently, cell lysate was set to bottom in an Optiprep gradient with increasing concentration from the top. After subsequent ultracentrifugation at 42000 rpm at 4 °C for 4 h, ten fractions were collected, which were analyzed for membrane proteins as well as viral proteins. N=2. **C. Principle of fractionation assay.** Cells are lysed by passing through 22-gauge needles ten times. By adding 1% triton X100, only DRMs stay intact, whereas other membrane structures are solubilized. Subsequent centrifugation pellets DRMs and solubilized membranes are in the supernatant. **D. Fractionation assay to find the ideal triton X100 concentration.** Huh7/Lunet CD81H cells were electroporated with RNA encoding JFH1 ad. HAF-NS2 wt. 48 h after electroporation, cells were harvested either in the absence or in the presence of triton X100 with given concentration in the figure (1%, 0.5%, 0.1% and 0.05%) and subjected to mechanical lysis. Then, cell lysate was incubated at 4 °C or 3 at 37 °C for 30 min. Subsequently, cell lysate was centrifuged at 16000 g for 5 min at 4 °C. Pellets containing DRMs and supernatant containing non-DRMs were analyzed for membrane proteins as well as viral proteins. N=4.

3.2. Role of HCV NS2 in regulation of host cholesterol metabolism

We confirmed the interaction between NS2 and cholesterol through PAC cholesterol assays. PAC cholesterol crosslinking of NS2 was as efficient as that of caveolin1, a well-known cholesterol interacting protein. Next, we decided to focus on a possible role of NS2 cholesterol interaction in terms of host virus interaction. For this purpose, I had closer look on existing unpublished proteomics data of NS2 interacting proteins generated by Dr. Jirasko.

3.2.1. Identification of host factors interacting with NS2

3.2.1.1. Set up and performance of NS2 proteomics

Prior to my PhD project, Dr. Jirasko did proteomics studies of NS2 interacting proteins. First, HCV JFH1 ad. HAF-NS2 was generated and RNA encoding this full-length virus was used for electroporation of Huh7,5 cells to perform tandem affinity chromatography against HA- and FLAG-tag (Fig. 3.19A). As a negative control, JFH1 ad. NS2 without tag was used. After showing the specificity of experimental set up by SDS-PAGE and following coomassie staining (Fig. 3.19B), eluates were analyzed by mass spectrometry (MS) (Fig. 3.19C). Hits are only considered as significant, if the p-value is smaller than that of E2 (p-value < 0,2). Subsequent gene ontology analysis of hits from MS showed that three NS2 interacting proteins are involved in regulation of cholesterol biosynthesis process (Fig. 3.19D). These are fatty acid synthase (FASN), 7-Dehydrocholesterol reductase (DHCR7) and Erlin2. To validate these hits, co-IP experiments were performed. CD81H cells were electroporated with RNA encoding JFH1 ad. HAF-NS2. As controls, no RNA (MOC) or RNA encoding JFH1 ad. with untagged NS2 were used for electroporation. 72 h after electroporation, cells were subjected to co-IP. The result showed that Erlin2 could be detected in the eluate fraction specifically for HAF-tagged NS2 confirming the proteomic studies (Fig. 3.19E).

3.2.2. Characterization of roles of NS2 Erlin2 interaction for host cholesterol metabolism regulated by SREBP2 pathway

Erlin2, ER Lipid raft-associated protein 2 [187], is shown to be component of SREBP-mediated regulation of subcellular lipid concentration [188]. In case of cholesterol deficiency, SREBP1 and SREBP2 is transported to golgi and cleaved by S1P and S2P,

so it can be transported to the nucleus to activate expression of genes involved in cholesterol biosynthesis [189]. In case of cholesterol sufficiency, SCAP and Insig interact with SREBPs inhibiting transport to golgi and cleavage of SREBP1 and SREBP2 [190]. Here, Erlin2 plays a role: Erlin2 interacts with SCAP and Insig possibly stabilizing SREBP-SCAP-Insig complexes in ER inhibiting SREBP2 cleavage. Moreover, depletion of Erlin2 leads to canonical activation of SREBPs [188].

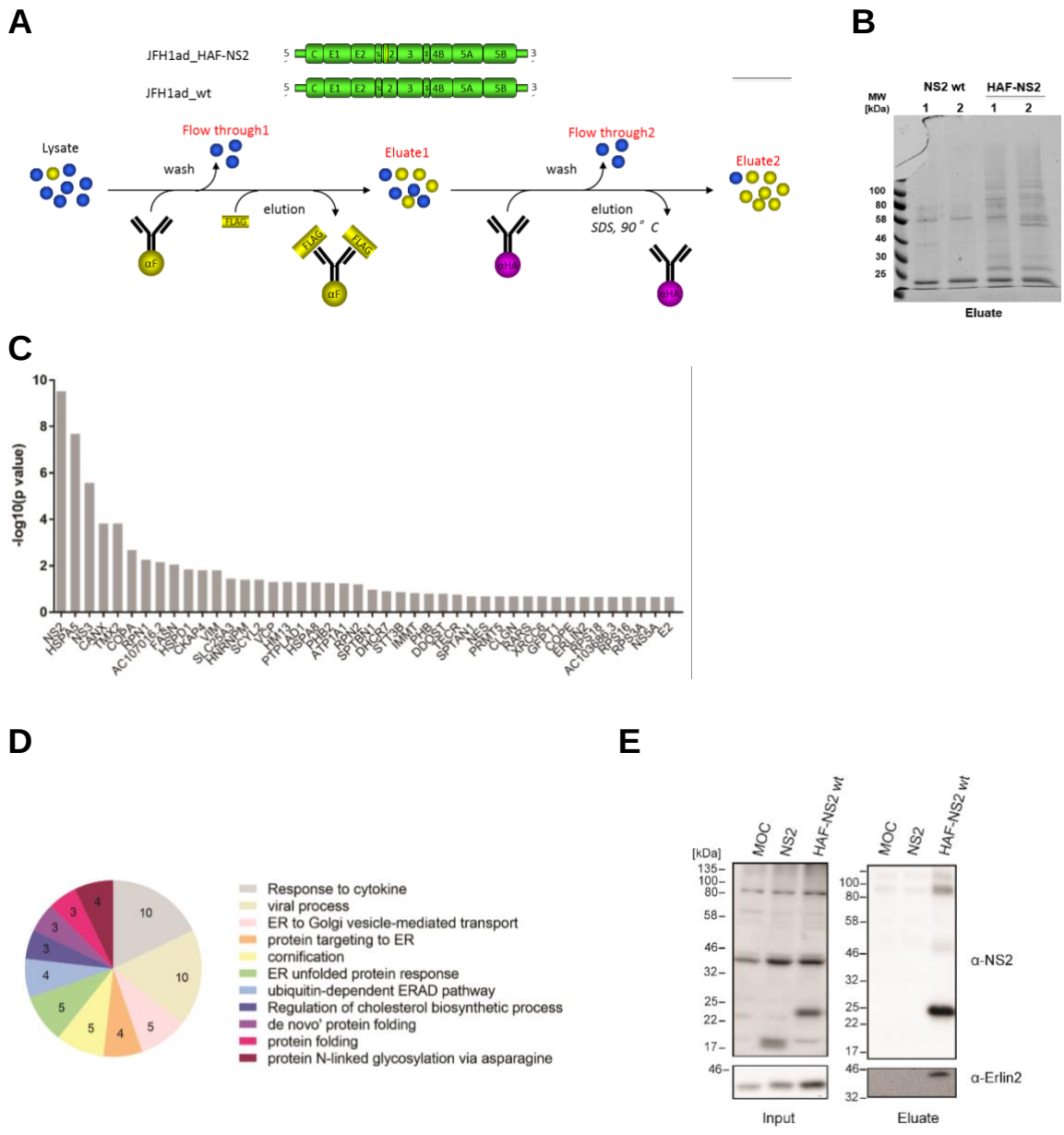

Figure 3.19. Identification of host factors interacting with NS2. A-D. Procedure of FLAG- and HA-tandem affinity chromatography. Huh7,5 cells were electroporated with RNA encoding JFH1 ad. HAF-NS2 and JFH1 ad. without HA- and FLAG tag at the N-terminus of NS2 as negative control. After 72 h, cells were lysed in 100 mM NaCl, 20 mM Tris pH 7,5, 0,5% n-Dodecyl ß-D-maltoside (DDM) and protease inhibitor. Cell lysates were subjected to tandem affinity chromatography using anti-FLAG and anti-HA agarose resins. Proteins were eluted in laemli buffer at 95 °C for 5 min. **B.** Eluates were separated by SDS-PAGE and **C.** analyzed by MS. P values of top hits are shown in –log10. **D.** Gene ontology analysis according to biological process. N=3, done by Dr. Jirasko Vlastimil.

E. Immunoprecipitation with HA-tagged NS2 wt. Huh7/Lunet CD81H cells were electroporated with RNA encoding JFH1 ad. HAF-NS2 wt, L86A, L87A and Y91A. As negative controls, cells either were electroporated with water (MOC) or with JFH1 ad. without HA-tag (NS2). After 72 h cells were lysed in lysis buffer containing 100 mM NaCl, 20 mM Tris (pH 7.5), 0.5% DDM and protease inhibitor (Input). Then, cell lysates were subjected to affinity chromatography with anti-HA agarose resins. Proteins were eluted in laemli buffer at 95 °C for 5 min. Eluates and inputs were quantitatively analyzed by performing SDS-PAGE and WB.

3.2.2.1. NS2 CRAC motif and its role in cholesterol level regulation mediated by SREBP2 pathway

After confirming NS2 Erlin2 interaction through IP experiments, we hypothesized that NS2 Erlin2 interaction might regulate cellular cholesterol levels via SREBP-pathways by manipulating Erlin2 SREBP complex interaction. To prove this hypothesis, possible changes of SREBP activation in forms of SREBP cleavage were assessed upon virus replication. Since SREBP1 is responsible for not only cholesterol- but also fatty acid biosynthesis [189], SREBP2 only was taken into account. On WB, SREBP2 shows a band close to 135 kDa and another band close to 58 kDa representing the uncleaved and cleaved forms of SREBP2, respectively. Therefore, the intensity of the smaller band was considered as the extent of SREBP2 activation. First, lysates from CD81H cells electroporated with 1) no RNA, 2) RNA encoding full length JFH1 ad. HAF-NS2 and 3) RNA encoding full length JFH1 ad. ΔNS2 were analyzed for their SREBP2 cleavage on WB. In contrast to our hypothesis, there was no clear difference according to the signal intensity of cleaved SREBP2 between the three conditions (Fig. 3.21A) indicating that cells in the three different conditions behave comparable to each other in terms of SREBP2 activation in cholesterol sufficiency. Next, SREBP2 activation within cells in the three conditions was checked upon cholesterol deficiency. Beforehand, a condition had to be established, where cells recognize cholesterol deficiency and react in terms of SREBP2 activation. For this purpose, CD81H cells were incubated in DMEM with delipidated FCS (DL-FCS) for 30 min, 1 h and 3h. As control cells were incubated in complete DMEM (FCS). After 3 h incubation in lipid starvation condition, the signal of the cleaved form increased clearly compared to the condition with complete DMEM (Fig. 3.20). This data showed incubation in DMEM + DL-FCS for 3 h is sufficient for activating SREBP2 cleavage.

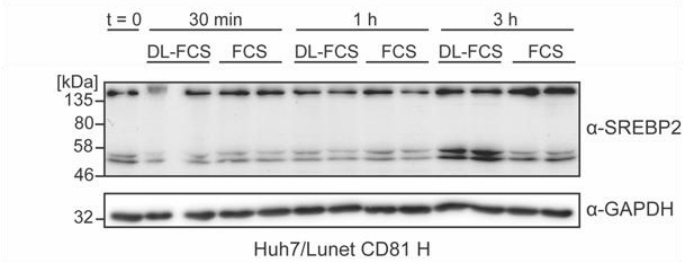

Figure 3.20. SREBP2 cleavage upon starvation. CD81H cells were plated on 6-well plate 1 day prior to the experiment. Cells were incubated with either complete DMEM (FCS) or DMEM with delipidated FCS (DL-FCS) for 30 min, 1 h and 3 h. Then, cells were lysed with 2x LDS buffer, which was analyzed by performing SDS-PAGE and WB for SREBP2. Each condition in duplicate.

After determining SREBP2 activation conditions, the influence of replicating virus on SREBP2 activation was tested. CD81H cells were electroporated with RNA encoding JFH1. Ad. HAF-NS2 wt and NS2 deletion mutant (ΔNS2). As a control, cells were electroporated without any RNA (MOC). 48 h and 72 h after electroporation cells were incubated in DMEM with delipidated FCS (Fig. 3.21B). Afterwards, cells were lysed and subsequently were analyzed for the SREBP levels on WB. Levels of cleaved SREBP2 was reduced upon wt virus replication after incubation in DMEM with delipidated FCS compared to the MOC condition (Fig. 3.21B). Moreover, upon ΔNS2 mutant virus replication, SREBP2 activation was reduced compared to wt virus replication (Fig. 3.21B). These data indicated that SREBP2 activation might be inhibited by virus replication and that NS2 might antagonize this inhibition possibly by suppressing viral RNA replication and viral protein translation [97]. Next, to check, whether NS2 CRAC motif plays a role in virus-mediated inhibition of SREBP2 activation upon lipid deficiency, SREBP2 levels were analyzed on WB after electroporation of CD81H cells with RNA encoding JFH1 ad. HAF-NS2 wt, L86A, L87A and Y91A (Fig. 3.21C). Quantification of the band intensities of cleaved SREBP2 revealed that in case of NS2 L87A and Y91A, the expression level of the cleaved form of SREBP2 was higher compared to NS2 wt and L86A. Interestingly, the level of other viral proteins such as core and NS3 from L87A and Y91A was comparable to the wt indicating functional viral RNA replication and viral protein translation (Fig. 3.21 C). This data suggests, that NS2 L87 and Y91, which belong to CRAC motif of NS2, might contribute to SREBP2 activation in a different manner, not by suppressing viral replication. Along the same line, cholesterol level of cells with replicating viruses expressing NS2 L87A and Y91A were 22% and 19% higher than viruses expressing NS2 wt, respectively. These measurements were performed by using Red Amplex Cholesterol Assay Kit. (Fig. 3.21D).

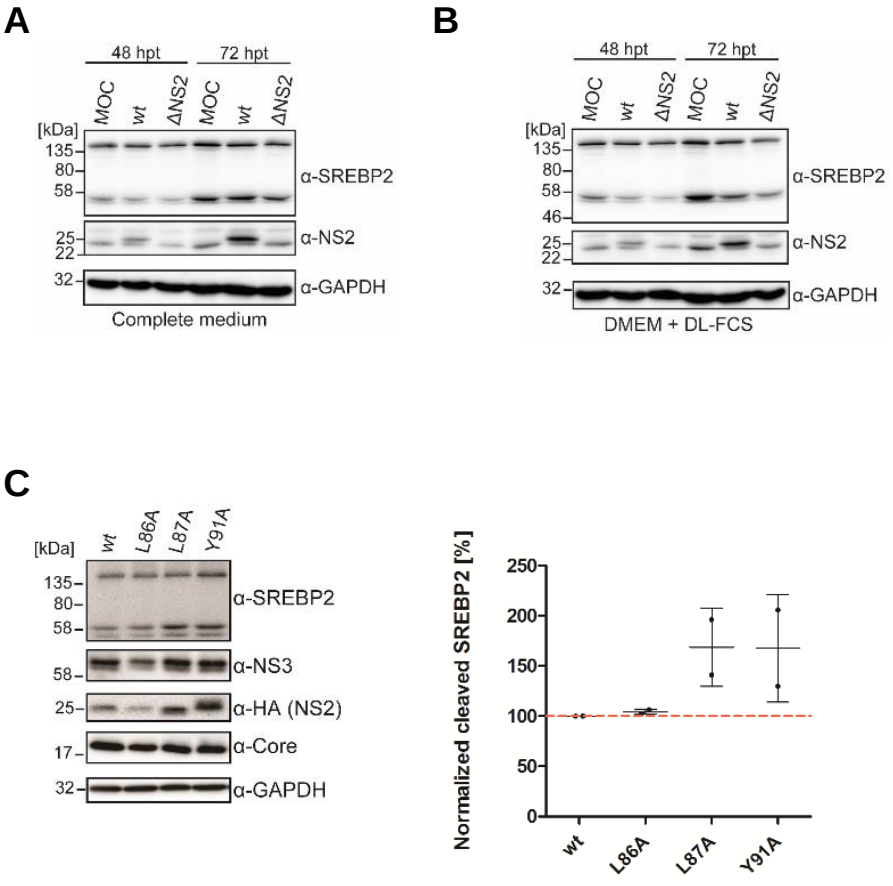

Figure 3.21. Possible role of NS2 in cholesterol metabolism. A and B. Possible role of NS2 in SREBP2 activation. Huh7/Lunet CD81H cells were electroporated with RNA encoding JFH1 ad. HAF-NS2 wt and NS2 deletion mutant (ΔNS2). As MOC, cells were electroporated with water. After 48 h and 72 h, cells were either incubated in DMEM with lipidated FCS (Fig. A) or in DMEM with delipidated FCS (Fig. B) for 3 h and lysed. Cell lysates were analyzed by performing SDS-PAGE and WB. N=1. **C. Possible role of NS2 CRAC motif in SREBP2 activation.** Huh7/Lunet CD81H cells were electroporated with RNA encoding JFH1 ad. HAF-NS2 wt, L86A, L87A and Y91A. After 72 h, cells were incubated in OptiMEM for 3 h and lysed. Cell lysates were quantitatively analyzed by performing SDS-PAGE and WB. N=2. **D. Possible role of NS2 in cellular cholesterol level regulation.** Huh7/Lunet CD81H cells were electroporated with RNA encoding JFH1 ad. HAF-NS2 wt, L86A, L87A and Y91A. After 72 h, cells were lysed and subjected to cholesterol measurement by using Amplex Red Cholesterol Assay Kit according to manufacturer's instruction. Shortly, cholesterol oxidase and cholesterol ester esterase were added to cell lysate resulting in H_2O_2 production. Subsequent addition of Amplex Red will react with H_2O_2 with the final product resorufin, which has absorption and emission wavelength of 571 nm and 585 nm, respectively. The emission was measured with fluorescent plate reader. N=4.

3.2.2.2. Dependence of NS2-erlin2 interaction on NS2 CRAC motif

Regulators of SREBP's activation, SCAP, Insig and Erlin2, are assumed to recognize cholesterol sufficiency by interacting with cholesterol, which leads to their conformational changes [188, 191, 192]. Considering the efficient PAC cholesterol crosslinking of NS2, indicative for efficient NS2 cholesterol interaction, and proteomics of NS2 co-precipitated proteins, it might be possible that NS2 affect SREBP2 pathway by interacting with Erlin2. Depending on cholesterol interaction, NS2 might interact with Erlin2 with different efficiency. To prove this hypothesis, Erlin2 co-precipitation efficiencies of NS2 wt, L86A, L87A and Y91A were assessed by performing co-IP experiments. CD81H cells were electroporated with JFH1 ad. HAF-NS2 wt, L86A, L87A and Y91A. As controls, no RNA (MOC) or RNA encoding JFH1 ad. with untagged NS2 (NS2) were used for electroporation. 72 h after electroporation, cells were subjected to co-IP (Fig. 3.22). Quantification of NS2 and Erlin2 bands in eluate fraction on WB and subsequent calculation of erlin2/NS2 ratios indicated that NS2 L86A, L87A and Y91A showed reduction in Erlin2 interaction efficiency by 17%, 69% and 25% compared to that of NS2 wt, respectively (Fig. 3.22). NS2 Y91A mutant was the only one showing significant reduction in PAC cholesterol crosslinking efficiency. However, according to this result, NS2 Y91A binding to Erlin2 was as efficient as L86A mutant, which does not belong to CRAC mutant, and less efficient than L87A mutant. Therefore, it was not coherent with the hypothesis, that NS2 Erlin2 interaction might be depending on extent of NS2 cholesterol interaction efficiency reflected by PAC cholesterol crosslinking.

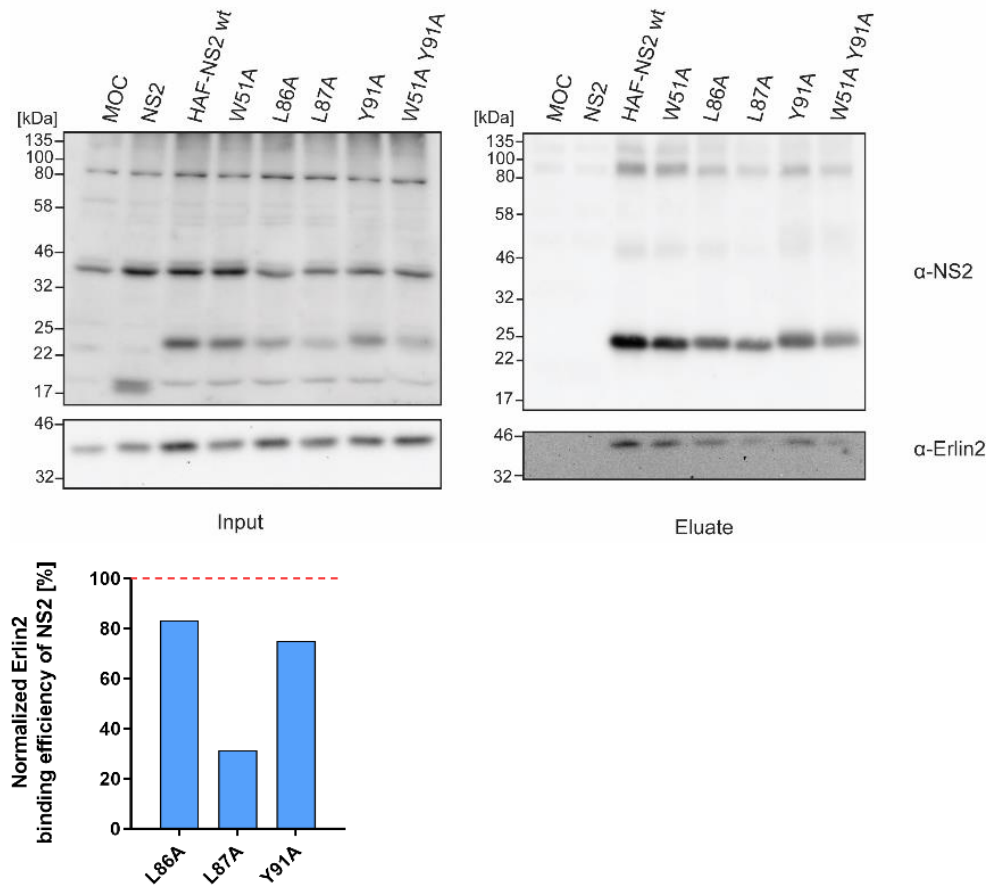

Figure 3.22. Possible importance of CRAC motif for NS2 Erlin2 interaction. Huh7/Lunet CD81H cells were electroporated with RNA encoding JFH1 ad. HAF-NS2 wt, L86A, L87A and Y91A (as well as W51A and W51A Y91A). As negative controls, cells either were electroporated with water (MOC) or with JFH1 ad. without HA-tag (NS2). After 72 h cells were lysed in lysis buffer containing 100 mM NaCl, 20 mM Tris (pH 7.5), 0.5% DDM and protease inhibitor (Input). Then, cell lysates were subjected to affinity chromatography with anti-HA agarose resins. Proteins were eluted in laemli buffer at 95 °C for 5 min. Eluates and inputs were quantitatively analyzed by performing SDS-PAGE and WB.

3.3. Role of Rab18 in ER wrapping of LDs and its importance for HCV replication cycle

HCV assembly is assumed to occur at ER membranes which are closely localized to LDs [69]. Evidence for the importance of the close association between ER and LDs for virus assembly was recently revealed. It has been shown that HCV envelop E2, which is ubiquitously distributed within cells in early time point of virus propagation, relocalizes to NS5A-positive LDs in a later stages of viral life cycle and this relocalization depends on functional viral RNA replication and virus assembly [142]. Ultrastructural data showed that this E2-NS5A positive LDs were specifically surrounded by ER membranes and DMVs, RNA replication organelles for HCV [142]. Since Rab18, a small GTPase, is known to bring ER membranes to LDs [179] and since Rab18 is also involved in HCV replication cycle by interacting with components of viral replicase complex such as NS5A [180], it might be possible, that Rab18 mediates ER-LD association establishing possible link between viral RNA replication and virus assembly, where HCV structural proteins such as E2 and viral replicase complex are recruited. To prove this hypothesis, *RAB18* was knocked out and its phenotypes according to viral RNA replication, virus production and ER-LD association were elucidated.

3.3.1. Knockout of *RAB18*

CRISPR/Cas9 system was used to generate CD81H *RAB18* KO cell lines with three different guide RNAs (gRNA1, 2 and 4) by performing lentiviral transduction. As a control, a CD81H-based cell line stably expressing cas9 and non-targeting gRNA were generated (Fig. 3.23A). The expression levels of Rab18 and viral RNA replication as well as virus production with the KO cell lines were investigated. For the cell line generated with gRNA1, Rab18 was not detectable on WB. However, in case of KO cell lines using gRNA2 and 4, there were still Rab18 detected, although the expression level decreased compared to the control cell line (Fig. 3.23A). To confirm previous reports from Salloum et al. showing the importance of Rab18 for HCV replication cycle [180], these three KO cell lines and the control cell line were subjected to electroporation with RNA encoding full length HCV chimera JcR2a containing a reporter, renila luciferase. Viral RNA replication levels were assessed by measuring reporter activity from cell lysates 4 h, 24 h, 48 h and 72 h after electroporation. For

assessing virus production/release, supernatant was collected 24 h, 48 h and 72 h after electroporation and used for infecting Huh7,5 cells, which were lysed 72 h after infection for measuring reporter activity (reinfection). In contrast to previous publication from Salloum et al. [180], viral RNA replication (Fig. 3.23B) and virus production estimated by calculating reinfection/replication ratio (Fig. 3.23C) did not show a reduction compared to the control cell line. Interestingly, KO cell lines with gRNA2 and 4, which contained detectable Rab18 in their cell lysates, showed higher viral RNA replication and virus production than that of the control cell line and KO cell line with gRNA1. This data indicated that Rab18 might be dispensable for HCV replication cycle. However, the possibility, that the KO cell lines still contained cells expressing Rab18, could not be excluded.

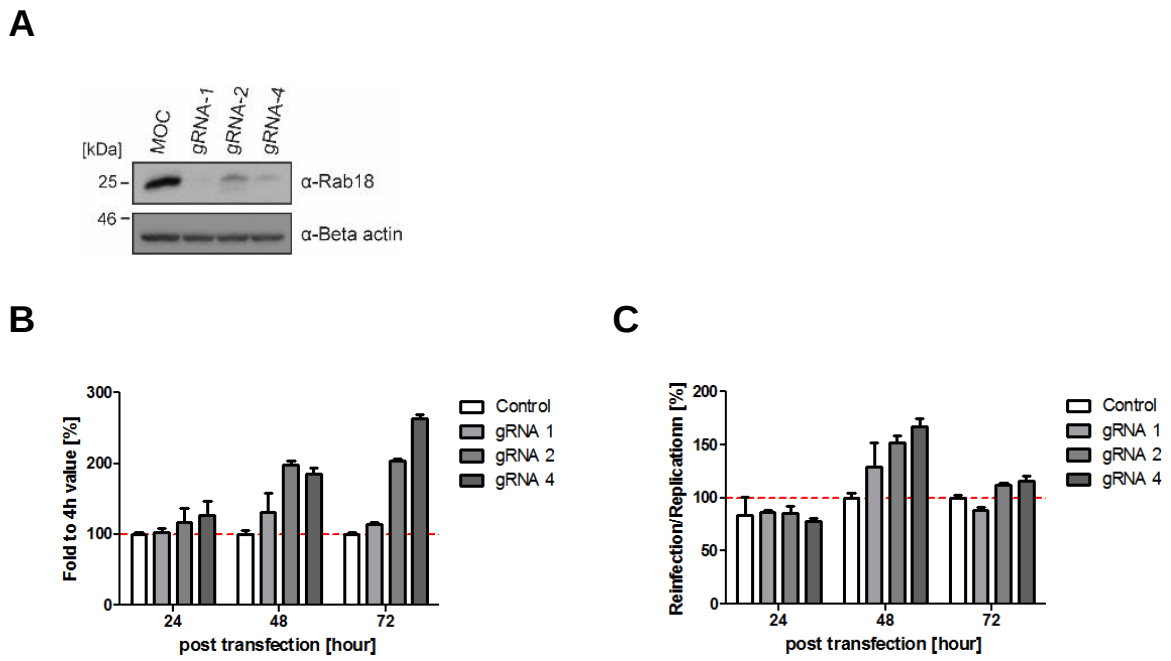

Figure 3.23. *RAB18* knockout and virus phenotypes. A-C. HCV JcR2a RNA replication and virus production. Huh7/Lunet CD81H cells stably expressing Cas9 and non-targeting gRNA (Control) and three different gRNAs targeting *RAB18* (gRNA 1-2 and 4) were electroporated with RNA encoding renila luciferase and JcR2a. **A.** 72 h after electroporation, cells were lysed and analyzed by performing SDS-PAGE and WB. Done by Katharina Lindner. **B.** 4 h, 24 h, 48 h and 72 h after electroporation, cells were lysed and viral RNA replication was assessed by measuring renila luciferase activity from the cell lysate. The kinetics of luciferase activity, which were calculated by normalizing values from 24 h, 48 and 72 h to 4 h values, was normalized to that of control. Done by Katharina Lindner. **C.** Assessing the extent of virus production, supernatants were collected at given time points and used for infecting Huh7,5 cells. 72 h after infection, cells were lysed and renila luciferase activity was measured. Luciferase activity values from infection (reinfection) were divided by that from electroporation (replication) and these values are normalized to that of control. Done by Katharina Lindner.

3.3.1.1. Generating single cell clones from a *RAB18* knockout cell line

Previous results showing that *RAB18* KO cell lines did not have defects in viral RNA replication and virus production (Fig. 3.2.3). However, this finding might reflect interclonal heterogeneity and presence of cells with incomplete *RAB18* ablation. Therefore, single cell-derived KO clones were generated to analyze exact loss-of-function mutations and to assign them to certain virus phenotypes. Since *RAB18* KO cell lines generated with gRNA2 and 4 still contained cells expressing Rab18 (Fig. 3.23A), which indicated inefficient KO, only gRNA1-mediated KO cell line was used for generating ten single cell clones. These ten clones showed no detectable Rab18 expression on WB (Fig. 3.24A). Then, to test possible defects in viral RNA replication independent of virus assembly, cell clones were electroporated with RNA encoding JFH1 subgenomic replicon containing a reporter, firefly luciferase. As controls, cells stably expressing cas9 and non-targeting gRNA (nt) and KO cell line (pool) were electroporated with the same viral subgenomic RNA. 4 h, 24 h, 48 h and 72 h after electroporation, RNA replication was assessed by measuring luciferase activity from cell lysates (Fig. 3.24B). The kinetics of RNA replication in the cell clones, which were calculated by normalizing values to the 4 h values (Fig. 3.24C), showed the interclonal heterogeneity: clone 3 and 6 showed increased RNA replication compared to controls; clone 5 and 9 showed almost no replication of viral RNA; clone 1, 2, 4, 7, 8 and 10 showed intermediate RNA replication (Fig. 3.24C).

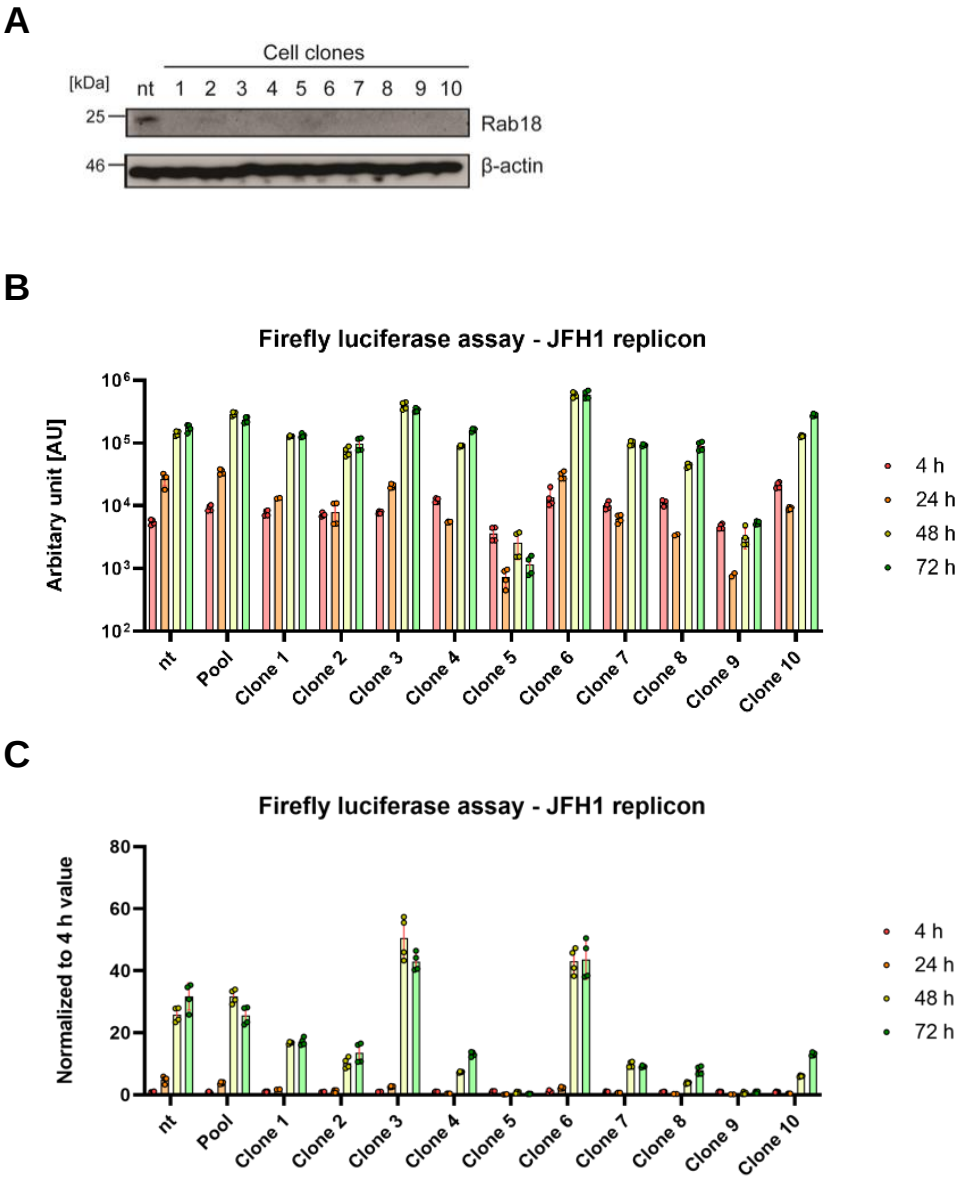

Figure 3.24. Generation of *RAB18* KO cell clones. A. Expression of Rab18. From Huh7/Lunet CD81H cells stably expressing Cas9 and gRNA1 targeting *RAB18*, ten single cell clones were generated and their cell lysate were analyzed by SDS-PAGE and WB. As a control, lysate from Huh7/Lunet CD81H cells stably expressing Cas9 and non-targeting gRNA (nt) was used. **B and C. HCV JFH1 subgenomic RNA replication upon *RAB18* KO.** Huh7/Lunet CD81H cells stably expressing Cas9 and non-targeting gRNA (Control), gRNA1 targeting *RAB18* (pool) and ten *RAB18* KO cell clones were electroporated with RNA encoding firefly luciferase and JFH1 regenomic RNA. **B.** 4 h, 24 h, 48 h and 72 h after electroporation, cells were lysed and viral RNA replication was assessed by measuring firefly luciferase activity from the cell lysate. N=4. **C.** Values of luciferase activity were normalized to 4 h values.

Characterization of *RAB18* knockout cell clones: subgenomic JFH1

All three *RAB18* KO cell lines, which were generated prior to this study, showed no virus phenotypes (Fig. 3.23). Moreover, two of ten single cell clones from the *RAB18* KO cell line generated with gRNA1, which showed no Rab18 expression on WB, did

not show KO phenotypes for viral RNA replication (Fig. 3.24). This indicated that Rab18 might be dispensable for HCV replication cycle. However, whether establishing ER-wrapping of NS5A-positive LDs is important for HCV replication cycle, which might be mediated by Rab18 still remains unclear. To address the question, clone 3 representative for KO cell clones without virus phenotypes and clone 1 representative for KO cell clones showing virus phenotypes were characterized further. Before proceeding with ER-LD association upon HCV replication cycle I further characterized the KO cell line clones. Genotype analysis revealed that clone 1 and 3 contained an insertion- and a deletion (3 aa deletion) mutation, respectively (Fig. 3.25A). These mutations did not seem to affect cell viability measured by celltiterglo (Fig. 3.25B). Since subgenomic RNAs of HCV are sufficient to induce NS5A-positive LDs surrounded by ER membranes [142], subgenomic JFH1 with mCherry tagged NS5A was used to study the frequency of ER wrapping of NS5A-positive LDs in clone 1 and 3 compared to control cells. First, RNA replication of this subgenomic JFH1 was assessed by electroporation of the control cell line (nt), single cell clone 1 and 3 with subgenomic viral RNA encoding a reporter, renila luciferase gene. After 4 h, 24 h, 48 h and 72 h, RNA luciferase activity was measured. Clone 1 and 3 showed intermediate and no phenotype according to viral RNA replication, repectively (Fig. 3.25C). After characterizing the sugenomic RNA replication in the KO cell clones, the subgenomic RNA was further used for ultrastructural studies of NS5A-positive LDs. 48 h after electroporation, nt, clone 1 and 3 were firstly subjected to IF to detect NS5A and LD signals (Fig. 3.25D) and subsequently to EM to visualize ultrastructures of the NS5A-positive LD signals (Fig. 3.25E and 3.25F). The analysis of IF images showed that NS5A and LDs colocalized less in *RAB18* KO cell clone compared to nt (Fig. 3.25D) confirming the result reported by Salloum et al [180]. The ultrastructural analysis of NS5A-positive LDs revealed the tendency that KO cell clones contained less ER-wrapped NS5A-positive LDs (Fig. 3.25F). This data indicated that ER-wrapping of NS5A-positive LDs might be mediated by Rab18. However, considering that the clone 3 did not have defects in viral RNA replication, the ER-wrapping of NS5A-positive LDs might not be essential for subgenomic RNA replication.

A

	Mutation	Details
Clone 1	Insertion mutation	Two different insertions: from 28321 bp and from 28389 bp
Clone 3	Deletion mutation	Deletion of 28388 bp - 28396 bp: Ala-Gln-Gly (81-83 aa)

B

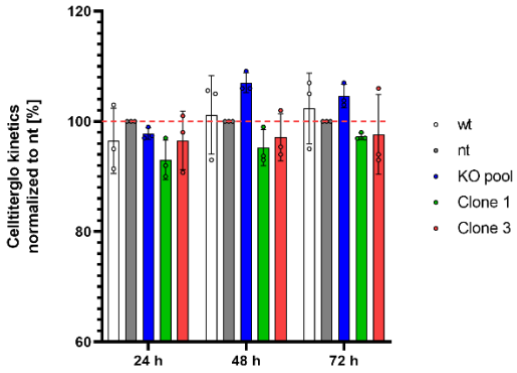

C

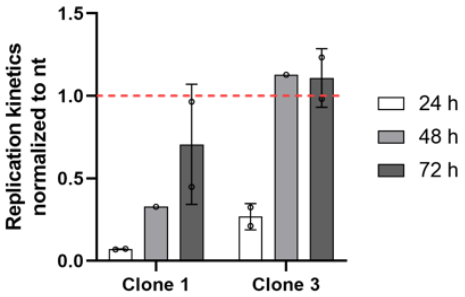

D

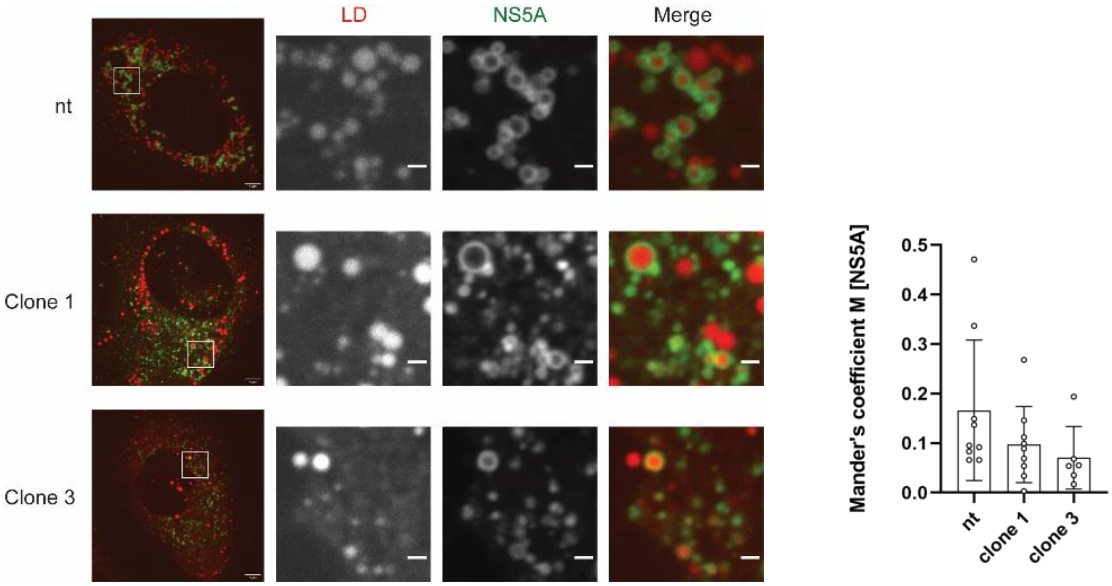

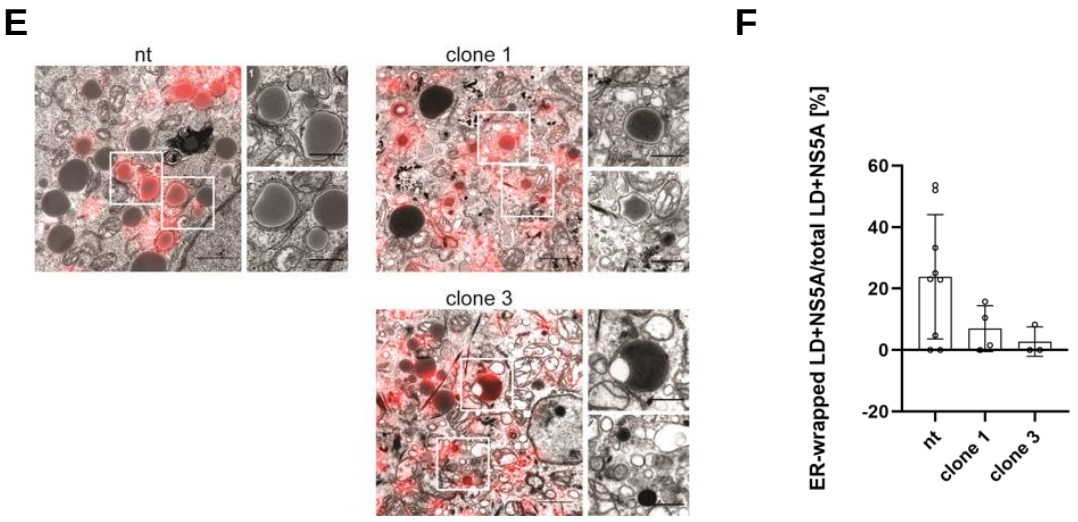

Figure 3.25. Characterization of *RAB18* KO cell clones. A. Schematic illustration of RAB18 and genetic modifications occurred *RAB18* KO cell clone 1 and 3. gRNA (red) targets the forth exon (28334 bp – 28406 bp). **B. Cytotoxicity of *RAB18* KO.** Huh7/Lunet CD81H naïve cells (wt), those stably expressing Cas9 and non-targeting gRNA (nt), gRNA1 targeting *RAB18* (KO Pool) as well as KO cell clone 1 and 3 were plated on 96-well plate and after 4 h, 24 h, 48 h and 72 h, cells were subjected to celltiterglo measurement which assesses the cellular ATP concentration as an indication of cell viability. N=3. **C-G. Impact of *RAB18* KO for ER wrapping of lipid droplets with NS5A signals.** Huh7/Lunet CD81H cells stably expressing Cas9 and non-targeting gRNA (nt) and *RAB18* KO cell clone 1 and 3 were electroporated with RNA encoding JFH1 subgenomic RNA containing mCherry-tagged NS5A. **C.** 4 h, 24 h, 48 h and 72 h after electroporation, cells were lysed and viral RNA replication was assessed by measuring renila luciferase activity from the cell lysate. The kinetics of luciferase activity, which were calculated by normalizing values from 24 h, 48 and 72 h to 4 h values, was normalized to that of control. N=2. **D-F.** 48 h after electroporation, cells were fixed with 4% of PFA and 0,2% glutaraldehyde and treated with 150 mM glycine. Staining of lipid droplets was done by addition of LipidTox (far red) shortly before acquiring images. N=1. Images were deconvoluted (Autoquant) and each signal was segmented (Ilastik). By performing Coloc2 in FIJI, Mander's coefficient between NS5A and lipid droplets signals was measured. **E.** After acquiring IF images, cells were fixed again for grid preparation for electron microscopy (EM) in EM fixatives containing 2.5% GA, 50 mM KCl, 2.6 mM $MgCl_2$, 2.6 mM $CaCl_2$, 2% sucrose, 50 mM Caco. Overlapping of IF and EM images were done by assigning IF lipid droplets signals to lipid droplets on EM images. Scale bar in the bigger panels 1 µm and in the smaller panels 500 nm. **F.** Lipid droplets with NS5A signals were counted and investigated for presence of surrounding ER membranes. Percentages of NS5A positive lipid droplets with surrounding ER membranes from total NS5A positive lipid droplets were calculated for each cell.

Characterization of *RAB18* knockout cell clones: full length JcR2a and Rab18 reconstitution

To assess KO phenotypes in the context of full-length HCV, a control (ct), clone 1 and 3 were electroporated with RNA encoding full length HCV JcR2a containing a reporter gene, firefly luciferase. 4 h, 24 h, 48 h and 72 h after electroporation, cells were lysed and the lysates were subjected to measuring luciferase activity indicative for JcR2a RNA replication. For estimating virus production/release, 24 h, 48 h and 72 h after electroporation, supernatants were collected to infect Huh7,5 cells, which were lysed

72 h after infection for measuring luciferase activity (reinfection). The full-length viral RNA replication was decreased for clone 1 and 3 compared to control (Fig. 3.26C). The reinfection/replication ratio indicative for virus production/release were both under the value of that from control cells (Fig. 3.26D). These data suggested that Rab18 depletion might affect viral RNA replication and virus production/release in the full length JcR2a system. Rab18 reconstitution in the clone 1 and 3 (Fig. 3.26A) increased viral RNA replication to the level of control cells from 48 h after electroporation (Fig. 3.26C). In the subgenomic JFH1 system, Rab18 reconstitution also increased the viral RNA replication in clone 1, whereas there were no changes for clone 3, which did not show KO phenotypes (Fig. 3.26B). These data indicated possible involvement of Rab18 in viral RNA replication. However according to the reinfection/replication ratio, Rab18 reconstitution did not increase the values from clone 1 and 3 (Fig. 3.26D) suggesting that these clones might have off target effects affecting virus production. Consequently, the presence of off target effects would evaluate these cell clones as inappropriate for further studies.

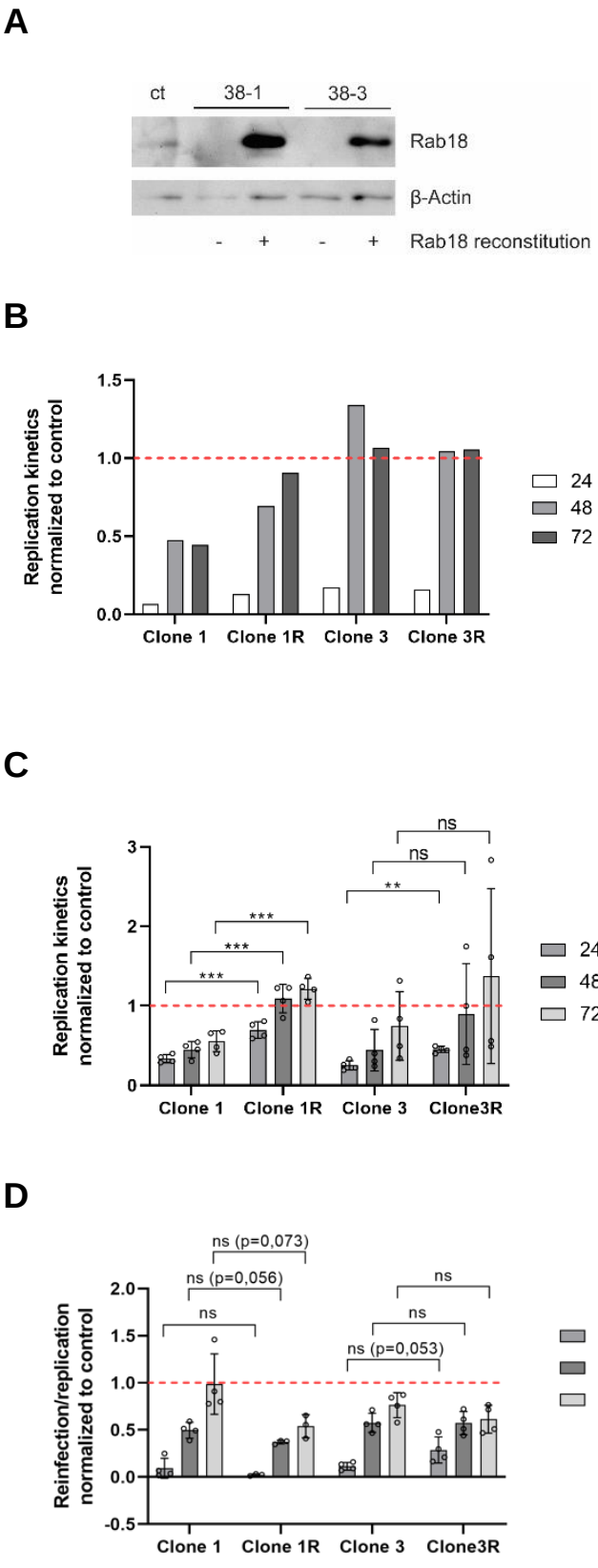

Figure 3.26. Rab18 reconstitution and its impact on observed KO phenotypes. A. Expression of reconstituted Rab18. Rab18 reconstitution in KO cell clone 1 (38-1) and 3 (38-3) were done by lentiviral transfection. Rab18 expression level of Huh7/Lunet CD81H stably expressing Cas9 and non-

targeting gRNA was tested as well as control (ct). **B. Replication of JFH1 subgenomic RNA upon Rab18 reconstitution.** *RAB18* KO cell clone 1 and 3 with their respective Rab18 reconstituted cells, Clone 1R and Clone 3R, respectively as well as control cells (nt), were electroporated with RNA encoding firefly luciferase and JFH1 subgenomic RNA. 4 h, 24 h, 48 h and 72 h after electroporation, cells were lysed and viral RNA replication was assessed by measuring firefly luciferase activity from the cell lysate. The kinetics of luciferase activity, which were calculated by normalizing values from 24 h, 48 and 72 h to 4 h values, was normalized to that of control. N=1. **C-D. Replication and virus production of JcR2a upon Rab18 reconstitution.** Huh7/Lunet CD81H cells stably expressing Cas9 and non-targeting gRNA (Control) and Clone 1, 1R, 3 and 3R were electroporated with RNA encoding renila luciferase and JcR2a. **C.** 4 h, 24 h, 48 h and 72 h after electroporation, cells were lysed and viral RNA replication was assessed by measuring renila luciferase activity from the cell lysate. The kinetics of luciferase activity, which were calculated by normalizing values from 24 h, 48 and 72 h to 4 h values, was normalized to that of control. **D.** Assessing the extent of virus production, supernatants were collected at given time points and used for infecting Huh7,5 cells. 72 h after infection, cells were lysed and renila luciferase activity was measured. Luciferase activity values from infection (reinfection) were divided by that from electroporation (replication) and these values are normalized to that of control.

3.3.2. Complications of knockout and reconstitution with lenti viral transduction

To assess possible complications from KO and reconstitution by lenti viral transduction, CD81H cells without previous lenti viral transduction were electroporated with RNA encoding subgenomic JFH1 with a reporter, firefly luciferase. 4 h, 24 h, 48 h and 72 h after electroporation the luciferase activity was compared with that from CD81 cells stably expressing Cas9 and non-targeting gRNA and/or blasticidin resistance gene and/or Rab18 via lenti viral transduction (Fig. 3.27). The result showed that expression of Cas9, non-targeting gRNA and blasticidin resistance gene affected luciferase activity negatively indicating, that lenti transduction might cause complications affecting viral RNA replication. Rab18 expression did not decrease the luciferase activity further compared to CD81H cells stably expressing Cas9 and BlaR (Fig. 3.27). This data demonstrated that the previously generated *RAB18* KO cell lines using lenti virus transduction might have complications with high probability and might therefore be inappropriate for studying the role of Rab18 in HCV replication cycle.

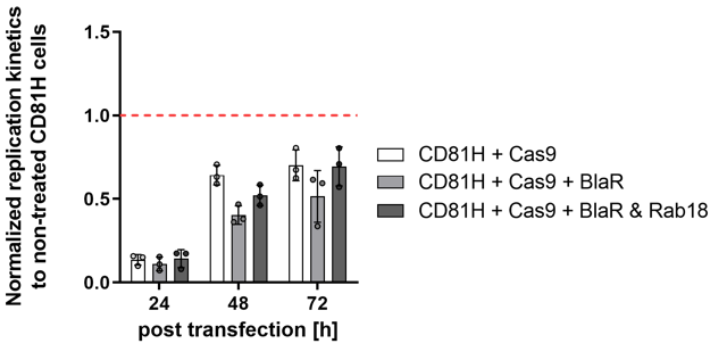

Figure 3.27. Impact of lenti viral transfection for Knockout and Rab18 reconstitution procedures. 1) Huh7/Lunet CD81H (CD81H), 2) CD81H cells stably expressing Cas9 (CD81H + Cas9), 3) CD81H + Cas9 cells stably expressing and blasticidin resistance gene (CD81H + Cas9 + BlaR) and 4) CD81H + Cas9 + BlaR cells stably expressing reconstituted Rab18 (CD81H + Cas9 + BlaR & Rab18) were electroporated with RNA encoding firefly luciferase and JFH1 sugenomic RNA. 4 h, 24 h, 48 h and 72 h after electroporation, cells were lysed and viral RNA replication was assessed by measuring firefly luciferase activity from the cell lysate. The kinetics of luciferase activity, which were calculated by normalizing values from 24 h, 48 and 72 h to 4 h values, was normalized to that of CD81H.

4. Discussion

4.1. PAC cholesterol as a useful tool for studying cholesterol protein interaction

In this study, PAC cholesterol has been the main tool to investigate the direct interaction between HCV proteins and cholesterol (Fig. 3.5). By using PAC cholesterol, I provided strong evidence that HCV NS2 might interact with cholesterol via its CRAC motif (Fig. 3.8 and Fig. 3.9).

For studying the direct interactions between proteins and cholesterol, the crosslinking ability of PAC cholesterol based on its diazirine group is essential (Fig. 3.2A). Crosslinking between PAC cholesterol and proteins occurs with UV-irradiation, which activates diazirine group of PAC cholesterol and generates a reactive intermediate carbene (Fig. 3.2B and Fig. 1.5B). Radicals of carbenes undergo covalent bonds to any side chains of amino acid or to any peptide backbones. Possible crosslinking distances by using diazirine group is depending on the spacer arm length. In case of PAC cholesterol the carbene intermediate localizes in the fused-ring which restricts crosslinking distances (≤3Å) compared to carbene i.e. localized at the end of long aliphatic chains [43]. This ensures the specificity of PAC cholesterol crosslinking to direct interacting proteins.

The relevance of PAC cholesterol protein crosslinking for physiological cholesterol protein interactions was demonstrated by Hulce et al. previously: proteins discovered by PAC cholesterol binding assay were mostly integral membrane proteins, among others, known cholesterol binding proteins, which were sensitive to cholesterol competition and selective for stereospecific PAC cholesterol (trans- over epi- or cis-PAC cholesterol) [43]. Along the same lines, PAC cholesterol crosslinking to Caveolin1, a cholesterol binding protein, could be reproduced in this study as well (Fig. 3.6).

Considering that most HCV proteins are localized on lipid rafts, ordered membrane microdomains with high concentration of cholesterol [85, 99, 133], it is expected that HCV proteins as crosslinked to PAC cholesterol should be detectable. Indeed, E2, NS2 and NS4B were identified for the first time as crosslinked to PAC cholesterol (Fig. 3.5). Interestingly, other tested viral proteins such as core, NS3 and NS5A were not crosslinked to PAC cholesterol. However, cholesterol was shown to be important not only for their localization on lipid rafts, but also for the functions of core, NS3 and NS5A [85, 133, 182]. This discrepancy might be due to the fact, that core, NS3 and NS5A

are peripheral membrane proteins. Therefore, they cannot reach the diazirine group of PAC cholesterol for crosslinking which is embedded in the hydrophobic part of lipid bilayers. This demonstrates a limitation of PAC cholesterol to study cholesterol interaction of peripheral membrane proteins.
Apart from that, PAC cholesterol might have another limitation due to its extended flexible hydrocarbon chain for the linkage of alkyne group to PAC cholesterol via an ester bond (Fig. 3.2A). With the longer flexible hydrocarbon chain which provides an extra due to ester bond, PAC cholesterol might have different affinity towards the surrounding lipids as well as membrane proteins compared to physiological cholesterol [13]. This might be the reason, why PAC cholesterol was not crosslinked to Erlin2 (Fig. 3.3) and ASGR2 (Fig. 3.6), which are known for their localization on membranes, where cholesterol levels are higher such as ER specific lipid rafts and plasma membrane, respectively [187, 193].

For evaluating the physiological relevance of the established PAC cholesterol binding assay, subcellular distribution of PAC cholesterol was compared to that of physiological cholesterol by performing IF after treating cells as for the binding assay.
In case of cholesterol deficiency, cholesterol is either provided by cells via biosynthesis or by uptake of LDL from extracellular space. In the latter case, LDL binds to LDL receptors at cell surface and the clathrine-mediated endocytosis of LDL occurs. Endocytosed LDL is subsequently transported to the early endosomes. Along the endosomal maturation pathway, cholesterol is released from LDL in late endosomes/lysosomes, where it is distributed to other subcellular organelles [194]. Similar to LDL, PAC cholesterol, which might be incorporated into FCS in cell culture medium, might be endocytosed into cells in complex with FCS [195]. Then, endocytosed PAC cholesterol in complex with FCS might move along the endosomal maturation pathway to late endosomes and lysosomes, where free PAC cholesterol might be released from FCS. From late endosomes/lysosomes PAC cholesterol might be distributed to other subcellular organelles such as to ER and to Golgi [196].
In the IF data the PAC cholesterol distribution to ER, Golgi and late endosomes were different compared to that of physiological cholesterol (Fig. 3.4). The most noticeable difference was that PAC cholesterol showed predominant dot-like structures, while physiological cholesterol was distributed in cells in forms of fine membranous structures. Interestingly, physiological cholesterol also displayed dot-like structures

which colocalized with late endosomal signals, whereas dot-like structures of PAC cholesterol could not be assigned to late endosomes. This indicated that dot-like structures of PAC cholesterol might reflect endocytosed PAC cholesterol, which did not follow the maturation process to late endosomes. Along these lines, cells might need longer time for maturation of PAC cholesterol containing endosomes for distributing PAC cholesterol to other subcellular organelles.

However, the data also showed that the PAC cholesterol distribution to ER, Golgi and late endosomes worked in the given condition which should ensure detecting cholesterol interacting proteins in these subcellular organelles.

4.2. NS2 cholesterol interaction

In this study, HCV NS2 showed the most efficient PAC cholesterol crosslinking among tested viral proteins, which was an indication for an efficient NS2 cholesterol interaction (Fig. 3.5). Indeed, NS2 from the genotype JFH1 contains a Cholesterol Recognition Amino acid Consensus, CRAC motif (L/I-X_5-Y-X_5-K/R; X_5 are1-5 random amino acid residues) at the C-terminal end of its third TMS (aa 87-94 (**L**GPA**Y**LL**R**)) (Fig. 3.7). The presence of CRAC motif supported the possibility of NS2 cholesterol direct interaction [35]. According to the definition, there were two possible compositions for the CRAC motif: either 1) L86, Y91 and R94 or 2) L87, Y91 and R94. Performing PAC cholesterol binding assay could not determine which composition is the right one for the CRAC motif, since both NS2 L86A and L87A mutants showed the same extent of PAC cholesterol crosslinking reduction (Fig. 3.9). Only after modeling of helical wheel and 3D structure of the third TMS of NS2, it became clear that L87, Y91A and R94, but not L86 fulfill the additional requirement of CRAC motif, that all three amino acid residues face to the same direction [28] (Fig. 3.9). The discrepancy between the results from PAC cholesterol binding assay and modeling in terms of defining amino acid residues of the NS2 CRAC motif might come from the fact that the extended aliphatic chain of PAC cholesterol is structurally distorted because of alkyne group addition via an ester bond. This distorted chain might be able to interact with the L86 and therefore the alanine substitution of L86 might reduce PAC cholesterol crosslinking of NS2. This demonstrates another limitation of PAC cholesterol for studying protein cholesterol interaction.

Although the CRAC motif of NS2 consists of three amino acid residues, the alanine substitution of them reduced the crosslinking of NS2 in a different extent (Fig. 3.8 and

Fig. 3.9). Since the alanine substitution of R94 might affect not only its cholesterol interaction (Fig. 3.9), but also its stability, I investigated L87A and Y91A mutations further. L87A of NS2 showed a non-significant reduction in PAC cholesterol crosslinking by 25%, whereas Y91A mutant showed a significant reduction by 50%. This indicated that Y91 might be the key amino acid residue of the CRAC motif mediating NS2 cholesterol interaction. This unequal contribution of CRAC amino acid residues to cholesterol interaction has been already observed by others previously: Single mutation at Tyr 152 within the CRAC motif of the Peripheral type Benzodiazepine Receptor (PBR), which transports cholesterol into mitochondria, abolished cholesterol binding completely indicating that PBR cholesterol interaction might be mediated mainly by Tyr 152 [32]. However, in some cases Tyr is not important for protein cholesterol interaction as it was shown by molecular modeling of the human nicotinic acetylcholine receptor, thereby demonstrating the flexibility of CRAC motif definition [197].

Apart from the identified CRAC motif at the C-terminal end of TMS3, there was no other linear amino acid sequences reflecting CRAC or CARC motifs. The presence of non-linear cholesterol binding motif, CCM, was not predictable due to the lack of 3D structure of NS2 transmembrane domain. Interestingly, there is evidence that NS2 palmitoylation at C113 on its cytosolic cysteine protease is important for NS2 lipid raft localization [86]. This indicates that palmitoylation of NS2 might contribute to NS2 cholesterol interaction. Supporting that indication, the role of palmitoylation of proteins for stabilizing protein cholesterol interaction has been reported previously [198, 199]. Therefore, the role of C113 in NS2 cholesterol interaction remains to be elucidated.

4.2.1. NS2 cholesterol interaction for late endosomal motility

After demonstrating the major role of Tyr 91 within the NS2 CRAC motif in cholesterol binding, the role of NS2 cholesterol interaction during HCV replication cycle was assessed by characterizing alanine substitution of CRAC amino acid residues.

Investigation of subcellular localization of NS2 wt, L87A and Y91A as well as L86A as non-CRAC control, revealed that NS2 Y91A was the only mutant being accumulated in late endosomal compartments, whereas the other NS2 showed predominant membranous structures (Fig. 3.10). Endosomes are involved in HCV replication cycle,

such as in virus entry [200], viral RNA replication [136] and virus release [201]. Since NS2 is not incorporated in virus [69] and dispensable for viral RNA replication [70], observed NS2 Y91A accumulation in late endosomes (LEs) might display a possible defect in virus release from impaired NS2 cholesterol interaction.

HCV exploits, among others, endosomal traffic for its release: viral particles are transported from early endosomes (EEs) to LEs and from LEs they might be released to extracellular space possibly by fusion with plasma membrane [201]. Interestingly, NS2 contains two dileucine motifs in its cytosolic domain, which are recognized as cargo by adaptor proteins AP1 and AP4 for intracellular trafficking, among others, from TGN to endosomes [202, 203]. Mutations of these motifs displayed defects in infectious virus release indicating an essential role of NS2 in assisting viral particles along the endosomal trafficking [90].

For late endosomal motility cholesterol is an important factor. LEs can move either from the microtubule-organizing center (MTOC) towards cell periphery (plus-end transport) or the other way around (minus-end transport). This bidirectionality is controlled by small GTPase, Rab7 on LEs. Depending on its interaction with two different effectors, RILP and FYCO1, Rab7 recruits different motor proteins Dynactin, part of dynein motor complex, and Kinesin1 for the minus-end and for the plus-end transport, respectively [204]. This LEs motility towards a certain direction can be reversed by negative regulators such as the oxysterol-binding protein ORP1L. ORP1L interacts with Rab7-RILP complex and affects RILP-mediated dynein recruitment depending on the cholesterol level of LEs [205, 206]. By recognizing cholesterol on LEs, ORP1L takes a closed conformation favorable for dynein recruitment. However, in the case of cholesterol deficiency on LEs ORP1L displays an open conformation leading to its interaction with VAP-A on ER thereby generating LE-ER contact sites. This LE-ER contact generation disrupts LEs movement towards minus-end and the direction of LEs motility can be changed to plus-end [206]. As another example for the importance of late endosomal cholesterol level for the motility of LEs, cholesterol accumulation in LEs induced by U18666A treatment [207] inhibits release of the virions indicated by the core accumulation in LEs. This observation suggests the inhibitory effect of high cholesterol level in LEs for fusion with plasma membrane [201, 208].

Cholesterol levels can be sensed due to conformational changes of cholesterol sensing proteins after cholesterol interaction [189, 191, 207]. NS2 might compete for cholesterol with host cholesterol binding proteins on LEs, thereby manipulating their cholesterol sensing. Along these lines, NS2 might support fusion of LEs and PM and consequently the release of virions by reducing the cholesterol content of the late endosomal membranes available for host protein cholesterol interaction. In case of NS2 Y91A, NS2 might not be able to capture cholesterol efficiently, which then can be sensed by host factors leading to reduced fusion of LEs and PM and impairs virion release and accumulation of NS2 in LEs. Coherently, HCV JFH1 expressing NS2 Y91A showed reduced extracellular- and increased intracellular viral titers compared to that of wt indicating defects in virion release (Fig. 3.14D). However, the alanine substitution of Y91 did not inhibit virus release completely. Possibly, other viral proteins such as E2 and NS4B, which were shown to be crosslinked to PAC cholesterol (Fig. 3.5A), might also compete for cholesterol with host factors on LEs to support LE PM fusion. Apart from that, the mild phenotype in virus release of HCV expressing NS2 Y91A might indicate the existence of other virus release pathways.

Along the same lines, addition of LDL, which was expected to increase the subcellular cholesterol levels, indeed increased the frequency of wt NS2 dot-like structures and its colocalization with LEs significantly, whereas it did not affect late endosomal localization of NS2 Y91A (Fig. 3.12). This data supported the hypothesis that NS2 LE colocalization is depending on cholesterol level. Interestingly, cholesterol extraction by using MβCD for lowering subcellular cholesterol level increased colocalization of wt NS2 and LEs (Fig. 3.13). However, colocalizing areas are similar to those seen in membrane contact sites to LEs reflecting ER-LE contact sites upon cholesterol deficiency. In the future, possible changes of NS2 Y91A subcellular localization upon cholesterol extraction should be assessed.

Defects in virus release and late endosomal accumulation of NS2 Y91A suggested that virus might be accumulating in the late endosomes with NS2. However, the frequency of the late endosomal localization of core and E2 in the condition with virus expressing NS2 Y91A was not significantly different compared to that with the wt virus (Fig. 3.11). It might be that the extent of impaired virus release due to reduction in NS2 cholesterol interaction was not sufficient to be displayed in forms of core and E2 accumulation in LEs.

Taken together, this study provided first evidence for the role of NS2 cholesterol interaction in regulating endosomal motility and in virus release.

4.2.2. NS2 cholesterol interaction for virus assembly

NS2 is dispensable for viral RNA replication [70], but essential for virus assembly and release indicating possible role of NS2 cholesterol interaction in these steps during the viral replication cycle [81, 90]. To assess whether this hypothesis is correct, core ELISA and TCID50 were performed with wt virus and viruses expressing NS2 CRAC mutants L87A and Y91A (Fig. 3.14). These experiments gave the first evidence for the importance of NS2 cholesterol interaction for infectious viral particle assembly: while the core release of NS2 L87A and Y91A mutant viruses were reduced by less than two-fold compared to that of wt virus, these alanine substitutions of NS2 caused five- and ten-fold reduction in extracellular virus titers, respectively, without showing altered intracellular virus titer. Moreover, the extent of extracellular virus titer reduction of L87A and Y91A mutants were correlated to the extent of reduction in PAC cholesterol crosslinking efficiency (25% and 50%, respectively) (Fig. 3.9A) indicating that the observed assembly phenotype might be due to impaired NS2 cholesterol interaction. Apart from that, calculating the percentage of intra- and extracellular virus titer from the sum of them indicated defects in virus release (Fig. 3.14D). However as discussed in the previous section, defects in virus release after mutating CRAC motif seemed to result in minor phenotypes.

Next, possible impact of subcellular cholesterol level on virus assembly was assessed by incubating virus producing cells in OptiMEM ± LDL (Fig. 3.15). OptiMEM, minimal essential medium, was used to investigate the effect of LDL addition independent of other cell culture medium factors and it should be mentioned that this condition is different than the other condition used for studying the impact of cholesterol level for late endosomal localization of NS2 (Fig. 3.12).

For wt virus and NS2 Y91A expressing virus, addition of LDL supported core release and it reduced intracellular core level indicating for activated virus release (Fig. 3.15A). However, the addition of LDL did not increase the extracellular virus titer of the NS2 Y91A mutant virus, whereas it showed enhanced extracellular virus titer for wt virus (Fig. 3.15B). This data indicated that possible defects in virus release might be reversed by adjusting the subcellular cholesterol level by addition of LDL, however the

virus assembly defect cannot. This leads to the assumption that the virus assembly might be affected by cholesterol interaction-dependent conformational changes of NS2, but not by the subcellular cholesterol level as observed for the virus release.

NS2 interacts with viral components of virus assembly such as E1, E2 and P7 as well as with the viral component of RNA replicase NS3 [81]. Therefore, NS2 is assumed to recruit these viral proteins together, thereby establishing virus assembly platform. The site of HCV assembly is considered to be on ER lipid rafts closely localized to LDs [85, 142]. The localization of viral proteins on lipid rafts was demonstrated by isolating detergent-resistant membranes (DRMs) and analyzing DRM-associating proteins. Interestingly, DRM-localization of viral proteins belonging to virus assembly module such as core, E2 and NS2 was depending on cholesterol. Moreover, E2 DRM association was depending on the presence of NS2 [85]. Based on this data, I hypothesized that NS2 cholesterol interaction might be responsible for NS2 lipid raft localization and E2 recruitment to lipid raft. By performing IF experiments with wt virus and virus expressing NS2 Y91A mutant, this hypothesis was confirmed (Fig. 3.16). Furthermore, the data from IP suggested that E2 recruitment to lipid raft might be mediated by NS2 E2 interaction which is depending on NS2 cholesterol interaction (Fig. 3. 17). Finally, I tried to demonstrate lipid raft localization of NS2 and E2 depending on NS2 cholesterol interaction by isolating DRMs (Fig. 3.18). However, in the given condition with CD81H cells and JFH1 ad. HAF-NS2, no viral protein except core could be isolated with DRMs (Supplementary figure 1). Different genotypes and strains of HCV regulate host lipid metabolism uniquely [209, 210]. Moreover, different Huh7-derived cell lines show variable HCV permissiveness [118]. Previously, a different HCV genotype/strain and a different cell line were used for showing viral protein localization on lipid rafts: a full length HCV chimera consisting of H77S gene encoding core to NS2 and JFH1 gene encoding NS3 to NS5B and FT3-7 cells, which are Huh7-derived cell clones after clearing self-replicating subgenomic RNA [85]. This difference according to the used HCV genotype/strain and cell line might be the reason for the different result in terms of isolating DRM and DRM associating viral proteins.

Taken together, data produced in this study indicated for the importance of NS2 cholesterol interaction in virus assembly and in NS2 E2 interaction, which might be

essential for recruiting E2 to virus assembly platform. Consequences of impaired NS2 E2 interaction remained to be elucidated in the future.

4.2.3. NS2 cholesterol interaction for regulating host cholesterol biosynthesis

The first indication for a possible role of NS2 in regulating cholesterol biosynthesis came from the unpublished NS2 proteomics data, which revealed several host proteins as NS2 interacting partners which are involved in cholesterol metabolism, such as FASN, DHCR7 and Erlin2 (Fig. 3.19).

The necessity of cholesterol biosynthesis is sensed in the ER by SREBP2. In case of cholesterol deficiency, SREBP2 and SCAP take a certain conformation favorable for COPII mediated transport to Golgi, where SREBP2 is cleaved. The cleaved soluble SREBP2 subsequently enters nucleus where it acts as a transcription factor activating transcriptions of genes involved in cholesterol biosynthesis and cholesterol uptake in forms of LDL endocytosis [189]. In case of cholesterol sufficiency, SREBP2-SCAP complex goes under a conformational change and block COPII docking. Moreover, this is further stabilized by interaction with Insig and Erlin, thereby inhibiting the transport SREBP2 to Golgi for the cleavage [188, 190, 192]. Therefore, the level of cleaved SREBP2 can be interpreted as the extent of SREBP2-meidated cholesterol biosynthesis activation.

In this study, a possible impact of full-length HCV genotype 2a JFH1 replication on SREBP2 activation was investigated (Fig. 3.21). In case of lipid sufficiency, the cleaved SREBP2 levels upon virus replication were not different compared to mock cells (Fig. 3.21A). However, upon lipid deficiency, while mock cells activated SREBP2 cleavage (Fig. 3.20), wt virus replication inhibited the cleavage of SREBP2 (Fig. 3.21B). Possibly, subcellular cholesterol levels might be decreased as consequence. This observed inhibitory effect of JFH1 replication according to SREBP2 cleavage might be coherent to the previous data showing the difficulty of lipid raft isolation in forms of DRM. DRM isolation was possible only after diluting detergent concentration by factor of 20 compared to the protocols suggested previously [85] (Fig. 3.18D). Since DRM isolation is depending on cholesterol levels (Supplementary figure 2), this observation might suggest that in the given condition, the level of subcellular cholesterol is low. This result showing inhibitory effect of virus in SREBP2 activation was contrary to previous

findings, where the supporting role of HCV genotype 1b in activation of SREBP2 cleavage via core and NS4B was suggested [137, 211]. For these contradictory observations, the different HCV genotype and cell lines used might be responsible. Moreover, HCV JFH1 might use another cellular pathway such as Peroxisome Proliferator-Activated Receptor (PPAR) pathways to fulfil the need of cholesterol instead of activating SREBP2 pathway [212].

Interestingly, deletion of NS2 resulted in more pronounced inhibition of SREBP2 cleavage upon lipid deficiency (Fig. 3.21B). NS2 impairs the RdRp activity of NS5B leading to reduced viral RNA replication [213]. Therefore, deletion of NS2 might increase the viral RNA replication rate and this might result in further inhibition of SREBP2 cleavage.

Considering NS2 cholesterol interaction as a possible way to sense subcellular cholesterol level and to manipulate cholesterol sensing of other host factors, it was plausible to hypothesize that NS2 might regulate subcellular cholesterol levels by its cholesterol interaction. Indeed, upon lipid starvation virus expressing NS2 CRAC mutants L87A and Y91A increased the level of cleaved SREBP2 and subcellular cholesterol level compared to wt virus (Fig. 3.21C and D). This data indicated that NS2 cholesterol interaction might support the inhibitory role of HCV JFH1 in SREBP2 activation.

While trying to elucidate the mechanism of the inhibitory role of NS2 cholesterol interaction in SREBP2 activation, unpublished NS2 proteomics data provided a hint that the mediator between NS2 and SREBP2 might be Erlin2, which stabilizes SREBP2-SCAP-Insig complex in cholesterol sufficiency, thereby inhibiting SREBP2 activation [188]. Although, wt NS2 Erlin2 interaction could be reproduced by performing IP in this study (Fig. 3.19E), I could not determine the correlation between NS2 Erlin2 interaction and NS2 cholesterol interaction (Fig. 3.22).

Taken together, data from this study provides the first evidence for an inhibitory role of HCV JFH1 replication in SREBP2 pathway at least partially via NS2 cholesterol interaction. How NS2 cholesterol interaction might affect SREBP2 pathway remains to be elucidated.

4.3. Review of trials to investigate roles of Rab18 in HCV replication cycle

In the late time points of HCV replication, ubiquitously distributed envelop protein E2 relocalizes to NS5A-positive LDs and this E2 NS5A colocalization on LDs depends on functional virus assembly. Interestingly, LDs positive for E2 and NS5A are surrounded by ER membranes reflecting previous definition of virus assembly sites [142]. During the investigation of mechanism for establishing ER-surrounded LDs positive for E2 and NS5A, Rab18 caught our attention.

Rab18 is a small GTPase known for its role in bringing ER and LDs to close proximity [179]. Moreover, Rab18 is involved in the viral RNA replication as well as in the virus assembly [180, 214]. However, *RAB18* KO by lentiviral transduction of stable expression of Cas9 and a specific guide RNA in CD81H cells did not show any defects in JcR2a viral RNA replication (Fig. 3.23B) and virus production (Fig. 3.23C) in contrast to previous reports. These contradictory results might be due to using different cell lines and HCV strains in our study compared to previously published studies. Apart from the differences in used materials, this data might indicate possible redundancy of the Rab18 functions in bringing ER and LD close to each other: there are other host factors known for mediating ER-LD contact sites such as Seipin, DGAT2, FATP1, NRZ, Syntaxin18, USE1, BNIP1 and Ice2, which might compensate the loss of Rab18 function upon KO [146]. The analysis of cell lysate from KO cell pool for Rab18 expression revealed that there were cells still expressing Rab18 (Fig. 3.23A). However, the level of Rab18 in this KO cell lysates was clearly lower than that of mock cells indicating that this might not affect the result in a decisive way.

Considering the heterogeneity of cells in the KO cell pools according to their response to viral replication, KO cell lines derived from KO single cell clones were generated hoping that there are several single cell clone-derived cell lines showing a consistant phenotype (Fig. 3.24). Subsequently two representative KO cell lines were characterized for their genotypes, cytotoxicity and previously reported virus phenotypes by using JFH1-derived subgenomic replicon (Fig. 3.25 and 26B). Initial data supported success of Rab18 KO at least according to their genotypes (Fig. 3.25A), according to LD localization of NS5A (Fig. 3.25D) and according to establishing ER-LD contacts (Fig. 3. 25E and F). Interestingly, viral subgenomic RNA replication in one KO cell line was downregulated, whereas in the other cell line, it was not (Fig. 3.25C

and 26B). This result therefore led to the conclusion, that Rab18 might be dispensable for viral RNA replication.

Next, these two cell lines were subjected to evaluation for full-length HCV JcR2a RNA replication (Fig. 3.26C) and virus production (Fig. 3.26D). In contrast to data generated with JFH1-derived subgenomic replicon, JcR2a RNA replication was decreased in both KO cell lines. This difference according to RNA replication of subgenomic JFH1 and full-length JcR2a might come from the efficient RNA replication of JFH1 [119], which might be additionally supported by the absence of core to NS2 suppressing viral RNA replication [213]. Apart from that, they showed reduced virus production compared to cells stably expressing Cas9 and non-targeting guide RNA. Reconstitution of Rab18 in these KO cell lines (Fig. 3.26A), however, could not rescue observed virus phenotypes (Fig. 3.26C and D) indicating that cells might be affected by off target effects. Indeed, control cells showed reduced JFH1-derived subgenomic RNA replication already after lentiviral transduction for stable expression of Cas9 and non-targeting guide RNA with selection marker (Fig. 3.27). This observation of off target effects even in control cells demonstrated that in this system, no conclusive statement can be made. These analyses indicate that other loss of function approaches or different strategies to reduce off target effects of CRISPR/Cas9 system might be convenient to achieve abolishing the Rab18 function.

5. Outlook

In this study, PAC cholesterol binding assay has been established for studying cholesterol viral protein interaction. Initial screening for PAC cholesterol crosslinking of viral proteins indicated that not only NS2 but also E2 and NS4B can directly interact with cholesterol. Therefore, it is interesting to characterize possible cholesterol interaction of E2 and NS4B and its importance for HCV replication cycle. Furthermore, PAC cholesterol can be used to elucidate importance of cholesterol for other plus stranded RNA viruses, such as dengue or SARS-COV-2, where cholesterol is an important host factor for viral replication cycle [215, 216].

Next, a CRAC (Cholesterol Recognition Amino acid Consensus) motif in the third TMS of NS2 (aa 87-94) was identified which seemed to be responsible for NS2 cholesterol interaction. Further characterization of NS2 CRAC mutants indicated the importance of NS2 cholesterol interaction for NS2 E2 interaction, which might be necessary for recruitment of viral envelops to the virus assembly sites. To demonstrate possible role of NS2 cholesterol interaction in recruiting E2 to lipid rafts, which are assumed to be virus assembly sites, I tried to isolate lipid rafts in forms of DRMs. However, in the given conditions most of viral proteins did not localize on DRMs, although other cellular marker for lipid rafts were present. Another way to prove the hypothesis might be performing IP against FLAG-tagged E2 from supernatant in wt- and mutant virus conditions. Subsequent analysis of core level in the supernatant and in the eluate might reveal the efficiency of E2 incorporation into viral particles. After assessing the role of NS2 cholesterol interaction for recruitment of E2 to virus assembly platform and possibly for incorporation of E2 into viral particles, the level of ApoE present in viral particles should be investigated by performing IP against FLAG-tagged E2. E2 directly interacts with ApoE, which is important for the viral infectivity and this E2 ApoE interaction possibly results in incorporation of ApoE into virus [217, 218].

Lastly, characterization of Rab18 KO cell lines indicated that Rab18 might be involved in establishing E2/NS5A double positive LDs surrounded by ER, potential HCV assembly sites. However, due to off target effects of applied CRISPR/Cas9 KO system, the KO phenotypes according to viral replication cycle could not be assessed. Beside the fact, that another Rab18 depletion methods are necessary, other host factors involved in bringing ER membranes close to LDs such as Seipin, DGAT2, FATP1, NRZ,

Syntaxin18, USE1, BNIP1 and Ice2 can be checked for their possible role in HCV replication cycle [146].

6. Supplement

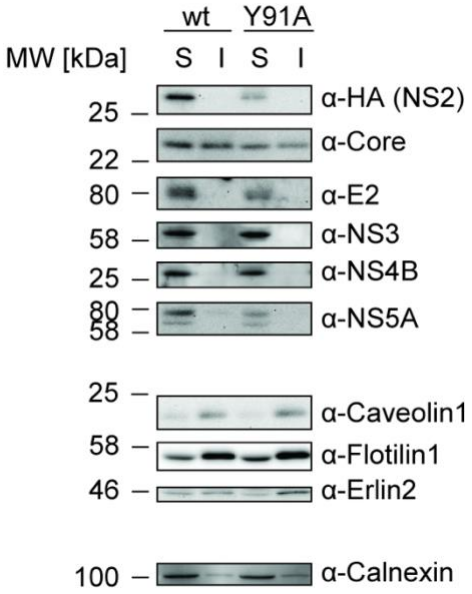

Supplementary figure 1. Assessment of lipid raft localization of HCV proteins. Huh7/Lunet CD81H cells were electroporated with RNA encoding JFH1 ad. HAF-NS2 wt and Y91A. 48 h after electroporation, cells were harvested in the presence of 0.05% triton X100 and subjected to mechanical lysis. Then, cell lysate was incubated at 4 °C for 30 min. Subsequently, cell lysate was centrifuged at 16000 g for 5 min at 4 °C. Pellets containing DRMs and supernatant containing non-DRMs were analyzed for membrane proteins as well as viral proteins. N=2.

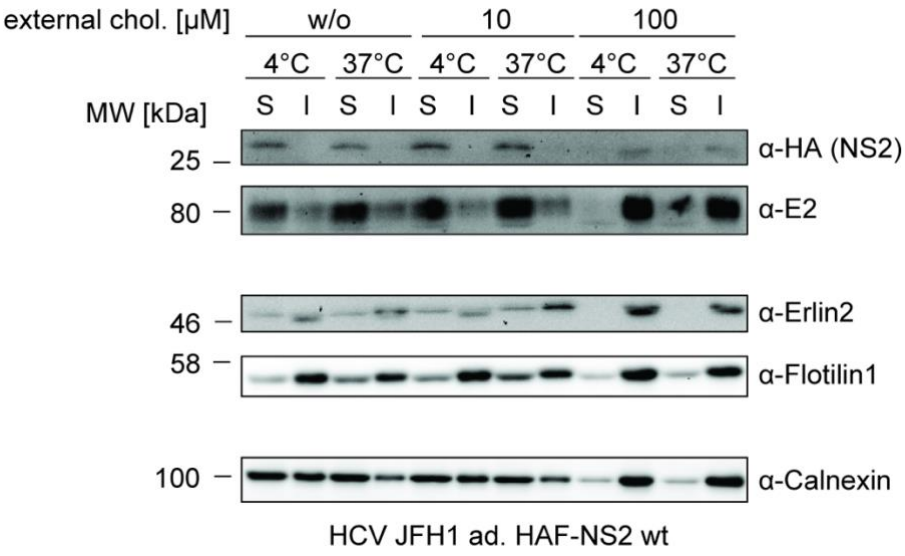

Supplementary figure 2. DRM localization of membrane proteins is depending on cholesterol level. Huh7/Lunet CD81H cells were electroporated with RNA encoding JFH1 ad. HAF-NS2 wt. 48 h after electroporation, cells were harvested in the presence of 0.05% triton X100. Cells were subjected to mechanical lysis either with no (w/o), 10µM or 100 µM additional cholesterol. Then, cell lysate was incubated either at 4 °C or at 37 °C for 30 min. Subsequently, cell lysate was centrifuged at 16000 g for 5 min at 4 °C. Pellets containing DRMs and supernatant containing non-DRMs were analyzed for membrane proteins as well as viral proteins. N=1.

7. References

1. Watson, H., *Biological membranes.* Essays Biochem, 2015. **59**: p. 43-69.
2. Jeremy M. Berg, J.L.T., Gregory J. Gatto jr. Lubert Stryer, *Stryer Biochemistry*. 2018: Springer Spektrum.
3. Jacobson, K., A. Ishihara, and R. Inman, *Lateral diffusion of proteins in membranes.* Annu Rev Physiol, 1987. **49**: p. 163-75.
4. Sanyal, S. and A.K. Menon, *Flipping lipids: why an' what's the reason for?* ACS Chem Biol, 2009. **4**(11): p. 895-909.
5. Ballweg, S., et al., *Regulation of lipid saturation without sensing membrane fluidity.* Nat Commun, 2020. **11**(1): p. 756.
6. Forte, S.N., A.A. Ferrero, and T.S. Alonso, *Content and composition of phosphoglycerols and neutral lipids at different developmental stages of the eggs of the codling moth, Cydia pomonella (Lepidoptera: Tortricidae).* Arch Insect Biochem Physiol, 2002. **50**(3): p. 121-30.
7. Bieberich, E., *Sphingolipids and lipid rafts: Novel concepts and methods of analysis.* Chem Phys Lipids, 2018. **216**: p. 114-131.
8. Marlow, B., et al., *Structural determinants of cholesterol recognition in helical integral membrane proteins.* Biophys J, 2021. **120**(9): p. 1592-1604.
9. Yang, S.T., et al., *The role of cholesterol in membrane fusion.* Chem Phys Lipids, 2016. **199**: p. 136-143.
10. Sankaram, M.B. and T.E. Thompson, *Modulation of phospholipid acyl chain order by cholesterol. A solid-state 2H nuclear magnetic resonance study.* Biochemistry, 1990. **29**(47): p. 10676-84.
11. Chen, Z. and R.P. Rand, *The influence of cholesterol on phospholipid membrane curvature and bending elasticity.* Biophys J, 1997. **73**(1): p. 267-76.
12. Feigenson, G.W., *Phase behavior of lipid mixtures.* Nat Chem Biol, 2006. **2**(11): p. 560-3.
13. Lingwood, D. and K. Simons, *Lipid rafts as a membrane-organizing principle.* Science, 2010. **327**(5961): p. 46-50.
14. Shaikh, S.R. and M.A. Edidin, *Membranes are not just rafts.* Chem Phys Lipids, 2006. **144**(1): p. 1-3.
15. Brown, D.A. and E. London, *Structure and origin of ordered lipid domains in biological membranes.* J Membr Biol, 1998. **164**(2): p. 103-14.
16. Pan, J., et al., *Cholesterol perturbs lipid bilayers nonuniversally.* Phys Rev Lett, 2008. **100**(19): p. 198103.
17. Baumgart, T., S.T. Hess, and W.W. Webb, *Imaging coexisting fluid domains in biomembrane models coupling curvature and line tension.* Nature, 2003. **425**(6960): p. 821-4.
18. García-Sáez, A.J., S. Chiantia, and P. Schwille, *Effect of line tension on the lateral organization of lipid membranes.* J Biol Chem, 2007. **282**(46): p. 33537-33544.
19. Mercker, M. and A. Marciniak-Czochra, *Bud-neck scaffolding as a possible driving force in ESCRT-induced membrane budding.* Biophys J, 2015. **108**(4): p. 833-843.
20. Chorlay, A. and A.R. Thiam, *An Asymmetry in Monolayer Tension Regulates Lipid Droplet Budding Direction.* Biophys J, 2018. **114**(3): p. 631-640.
21. Vind-Kezunovic, D., et al., *Line tension at lipid phase boundaries regulates formation of membrane vesicles in living cells.* Biochim Biophys Acta, 2008. **1778**(11): p. 2480-6.
22. Yang, S.T., V. Kiessling, and L.K. Tamm, *Line tension at lipid phase boundaries as driving force for HIV fusion peptide-mediated fusion.* Nat Commun, 2016. **7**: p. 11401.

23. Falck, E., et al., *Impact of cholesterol on voids in phospholipid membranes.* J Chem Phys, 2004. **121**(24): p. 12676-89.
24. Niu, S.L., D.C. Mitchell, and B.J. Litman, *Manipulation of cholesterol levels in rod disk membranes by methyl-beta-cyclodextrin: effects on receptor activation.* J Biol Chem, 2002. **277**(23): p. 20139-45.
25. Soubias, O. and K. Gawrisch, *The role of the lipid matrix for structure and function of the GPCR rhodopsin.* Biochim Biophys Acta, 2012. **1818**(2): p. 234-40.
26. Ekanayake, E.V., R. Fu, and T.A. Cross, *Structural Influences: Cholesterol, Drug, and Proton Binding to Full-Length Influenza A M2 Protein.* Biophys J, 2016. **110**(6): p. 1391-9.
27. Rossman, J.S., et al., *Influenza virus M2 protein mediates ESCRT-independent membrane scission.* Cell, 2010. **142**(6): p. 902-13.
28. Fantini, J., R.M. Epand, and F.J. Barrantes, *Cholesterol-Recognition Motifs in Membrane Proteins.* Adv Exp Med Biol, 2019. **1135**: p. 3-25.
29. Fantini, J., et al., *Molecular mechanisms of protein-cholesterol interactions in plasma membranes: Functional distinction between topological (tilted) and consensus (CARC/CRAC) domains.* Chem Phys Lipids, 2016. **199**: p. 52-60.
30. Lee, A.G., *Lipid-protein interactions in biological membranes: a structural perspective.* Biochim Biophys Acta, 2003. **1612**(1): p. 1-40.
31. Li, H., et al., *Cholesterol binding at the cholesterol recognition/ interaction amino acid consensus (CRAC) of the peripheral-type benzodiazepine receptor and inhibition of steroidogenesis by an HIV TAT-CRAC peptide.* Proc Natl Acad Sci U S A, 2001. **98**(3): p. 1267-72.
32. Jamin, N., et al., *Characterization of the cholesterol recognition amino acid consensus sequence of the peripheral-type benzodiazepine receptor.* Mol Endocrinol, 2005. **19**(3): p. 588-94.
33. Pydi, S.P., et al., *Cholesterol modulates bitter taste receptor function.* Biochim Biophys Acta, 2016. **1858**(9): p. 2081-2087.
34. Sharpe, L.J., et al., *Cholesterol sensing by the ABCG1 lipid transporter: Requirement of a CRAC motif in the final transmembrane domain.* Biochim Biophys Acta, 2015. **1851**(7): p. 956-64.
35. Fantini, J. and F.J. Barrantes, *How cholesterol interacts with membrane proteins: an exploration of cholesterol-binding sites including CRAC, CARC, and tilted domains.* Front Physiol, 2013. **4**: p. 31.
36. Hanson, M.A., et al., *A specific cholesterol binding site is established by the 2.8 A structure of the human beta2-adrenergic receptor.* Structure, 2008. **16**(6): p. 897-905.
37. de Vries, M., A. Herrmann, and M. Veit, *A cholesterol consensus motif is required for efficient intracellular transport and raft association of a group 2 HA from influenza virus.* Biochem J, 2015. **465**(2): p. 305-14.
38. Kermani, A.A., *A guide to membrane protein X-ray crystallography.* Febs j, 2020.
39. Elkins, M.R., I.V. Sergeyev, and M. Hong, *Determining Cholesterol Binding to Membrane Proteins by Cholesterol (13)C Labeling in Yeast and Dynamic Nuclear Polarization NMR.* J Am Chem Soc, 2018. **140**(45): p. 15437-15449.
40. Chakrabarti, P. and G. Khorana, *A new approach to the study of phospholipid-protein interactions in biological membranes. Synthesis of fatty acids and phospholipids containing photosensitive groups.* Biochemistry, 1975. **14**(23): p. 5021-33.
41. Thiele, C., et al., *Cholesterol binds to synaptophysin and is required for biogenesis of synaptic vesicles.* Nat Cell Biol, 2000. **2**(1): p. 42-9.

42. Lepage, M.L., et al., *A broadly applicable cross-linker for aliphatic polymers containing C-H bonds.* Science, 2019. **366**(6467): p. 875-878.
43. Hulce, J.J., et al., *Proteome-wide mapping of cholesterol-interacting proteins in mammalian cells.* Nat Methods, 2013. **10**(3): p. 259-64.
44. Worrell, B.T., J.A. Malik, and V.V. Fokin, *Direct evidence of a dinuclear copper intermediate in Cu(I)-catalyzed azide-alkyne cycloadditions.* Science, 2013. **340**(6131): p. 457-60.
45. WHO, *Hepatitis*. 2019.
46. Feinstone, S.M., et al., *Transfusion-associated hepatitis not due to viral hepatitis type A or B.* N Engl J Med, 1975. **292**(15): p. 767-70.
47. Choo, Q.L., et al., *Isolation of a cDNA clone derived from a blood-borne non-A, non-B viral hepatitis genome.* Science, 1989. **244**(4902): p. 359-62.
48. Simmonds, P., et al., *ICTV Virus Taxonomy Profile: Flaviviridae.* J Gen Virol, 2017. **98**(1): p. 2-3.
49. Bukh, J., R.H. Miller, and R.H. Purcell, *Genetic heterogeneity of hepatitis C virus: quasispecies and genotypes.* Semin Liver Dis, 1995. **15**(1): p. 41-63.
50. Simmonds, P., *Genetic diversity and evolution of hepatitis C virus--15 years on.* J Gen Virol, 2004. **85**(Pt 11): p. 3173-3188.
51. Wyles, D.L. and A.F. Luetkemeyer, *Understanding Hepatitis C Virus Drug Resistance: Clinical Implications for Current and Future Regimens.* Top Antivir Med, 2017. **25**(3): p. 103-109.
52. Hadziyannis, S.J., et al., *Peginterferon-alpha2a and ribavirin combination therapy in chronic hepatitis C: a randomized study of treatment duration and ribavirin dose.* Ann Intern Med, 2004. **140**(5): p. 346-55.
53. WHO, *Hepatitis C*. 2021.
54. Messina, J.P., et al., *Global distribution and prevalence of hepatitis C virus genotypes.* Hepatology, 2015. **61**(1): p. 77-87.
55. Petruzziello, A., et al., *Global epidemiology of hepatitis C virus infection: An up-date of the distribution and circulation of hepatitis C virus genotypes.* World J Gastroenterol, 2016. **22**(34): p. 7824-40.
56. Moon, A.M., et al., *High mortality rates for SARS-CoV-2 infection in patients with pre-existing chronic liver disease and cirrhosis: Preliminary results from an international registry.* J Hepatol, 2020. **73**(3): p. 705-708.
57. Manns, M.P., H. Wedemeyer, and M. Cornberg, *Treating viral hepatitis C: efficacy, side effects, and complications.* Gut, 2006. **55**(9): p. 1350-9.
58. *EASL Recommendations on Treatment of Hepatitis C 2018.* J Hepatol, 2018. **69**(2): p. 461-511.
59. Bhattacharjee, C., et al., *Current therapeutics against HCV.* Virusdisease, 2021. **32**(2): p. 1-16.
60. Rajender Reddy, K., M.W. Modi, and S. Pedder, *Use of peginterferon alfa-2a (40 KD) (Pegasys) for the treatment of hepatitis C.* Adv Drug Deliv Rev, 2002. **54**(4): p. 571-86.
61. Kyuregyan, K.K., et al., *Factors Influencing the Prevalence of Resistance-Associated Substitutions in NS5A Protein in Treatment-Naive Patients with Chronic Hepatitis C.* Biomedicines, 2020. **8**(4).
62. Sarrazin, C., *Treatment failure with DAA therapy: Importance of resistance.* J Hepatol, 2021. **74**(6): p. 1472-1482.
63. Duncan, J.D., et al., *Hepatitis C Virus Vaccine: Challenges and Prospects.* Vaccines (Basel), 2020. **8**(1).

64. Takamizawa, A., et al., *Structure and organization of the hepatitis C virus genome isolated from human carriers.* J Virol, 1991. **65**(3): p. 1105-13.
65. Grakoui, A., et al., *Expression and identification of hepatitis C virus polyprotein cleavage products.* J Virol, 1993. **67**(3): p. 1385-95.
66. Tabata, K., C.J. Neufeldt, and R. Bartenschlager, *Hepatitis C Virus Replication.* Cold Spring Harb Perspect Med, 2020. **10**(3).
67. Tsukiyama-Kohara, K., et al., *Internal ribosome entry site within hepatitis C virus RNA.* J Virol, 1992. **66**(3): p. 1476-83.
68. Bartenschlager, R., V. Lohmann, and F. Penin, *The molecular and structural basis of advanced antiviral therapy for hepatitis C virus infection.* Nat Rev Microbiol, 2013. **11**(7): p. 482-96.
69. Bartenschlager, R., et al., *Assembly of infectious hepatitis C virus particles.* Trends Microbiol, 2011. **19**(2): p. 95-103.
70. Lohmann, V., et al., *Replication of subgenomic hepatitis C virus RNAs in a hepatoma cell line.* Science, 1999. **285**(5424): p. 110-3.
71. Murray, C.L., C.T. Jones, and C.M. Rice, *Architects of assembly: roles of Flaviviridae non-structural proteins in virion morphogenesis.* Nat Rev Microbiol, 2008. **6**(9): p. 699-708.
72. Santolini, E., G. Migliaccio, and N. La Monica, *Biosynthesis and biochemical properties of the hepatitis C virus core protein.* J Virol, 1994. **68**(6): p. 3631-41.
73. McLauchlan, J., et al., *Intramembrane proteolysis promotes trafficking of hepatitis C virus core protein to lipid droplets.* Embo j, 2002. **21**(15): p. 3980-8.
74. Cristofari, G., et al., *The hepatitis C virus Core protein is a potent nucleic acid chaperone that directs dimerization of the viral (+) strand RNA in vitro.* Nucleic Acids Res, 2004. **32**(8): p. 2623-31.
75. Moradpour, D. and F. Penin, *Hepatitis C virus proteins: from structure to function.* Curr Top Microbiol Immunol, 2013. **369**: p. 113-42.
76. Boulant, S., et al., *Hepatitis C virus core protein is a dimeric alpha-helical protein exhibiting membrane protein features.* J Virol, 2005. **79**(17): p. 11353-65.
77. Nakai, K., et al., *Oligomerization of hepatitis C virus core protein is crucial for interaction with the cytoplasmic domain of E1 envelope protein.* J Virol, 2006. **80**(22): p. 11265-73.
78. Boulant, S., et al., *Structural determinants that target the hepatitis C virus core protein to lipid droplets.* J Biol Chem, 2006. **281**(31): p. 22236-22247.
79. Carrère-Kremer, S., et al., *Subcellular localization and topology of the p7 polypeptide of hepatitis C virus.* J Virol, 2002. **76**(8): p. 3720-30.
80. Madan, V. and R. Bartenschlager, *Structural and Functional Properties of the Hepatitis C Virus p7 Viroporin.* Viruses, 2015. **7**(8): p. 4461-81.
81. Jirasko, V., et al., *Structural and functional studies of nonstructural protein 2 of the hepatitis C virus reveal its key role as organizer of virion assembly.* PLoS Pathog, 2010. **6**(12): p. e1001233.
82. Lorenz, I.C., et al., *Structure of the catalytic domain of the hepatitis C virus NS2-3 protease.* Nature, 2006. **442**(7104): p. 831-5.
83. Jones, C.T., et al., *Hepatitis C virus p7 and NS2 proteins are essential for production of infectious virus.* J Virol, 2007. **81**(16): p. 8374-83.
84. Jirasko, V., et al., *Structural and functional characterization of nonstructural protein 2 for its role in hepatitis C virus assembly.* J Biol Chem, 2008. **283**(42): p. 28546-62.

85. Shanmugam, S., D. Saravanabalaji, and M. Yi, *Detergent-resistant membrane association of NS2 and E2 during hepatitis C virus replication.* J Virol, 2015. **89**(8): p. 4562-74.
86. Wu, M.J., et al., *Palmitoylation of Hepatitis C Virus NS2 Regulates Its Subcellular Localization and NS2-NS3 Autocleavage.* J Virol, 2019. **94**(1).
87. Barouch-Bentov, R., et al., *Hepatitis C Virus Proteins Interact with the Endosomal Sorting Complex Required for Transport (ESCRT) Machinery via Ubiquitination To Facilitate Viral Envelopment.* mBio, 2016. **7**(6).
88. Kumar, S., et al., *MARCH8 Ubiquitinates the Hepatitis C Virus Nonstructural 2 Protein and Mediates Viral Envelopment.* Cell Rep, 2019. **26**(7): p. 1800-1814.e5.
89. Franck, N., et al., *Hepatitis C virus NS2 protein is phosphorylated by the protein kinase CK2 and targeted for degradation to the proteasome.* J Virol, 2005. **79**(5): p. 2700-8.
90. Xiao, F., et al., *Interactions between the Hepatitis C Virus Nonstructural 2 Protein and Host Adaptor Proteins 1 and 4 Orchestrate Virus Release.* mBio, 2018. **9**(2).
91. Yang, X.J., et al., *HCV NS2 protein inhibits cell proliferation and induces cell cycle arrest in the S-phase in mammalian cells through down-regulation of cyclin A expression.* Virus Res, 2006. **121**(2): p. 134-43.
92. Bittar, C., et al., *Hepatitis C virus NS2 protein inhibits DNA damage pathway by sequestering p53 to the cytoplasm.* PLoS One, 2013. **8**(4): p. e62581.
93. Erdtmann, L., et al., *The hepatitis C virus NS2 protein is an inhibitor of CIDE-B-induced apoptosis.* J Biol Chem, 2003. **278**(20): p. 18256-64.
94. Dumoulin, F.L., et al., *Hepatitis C virus NS2 protein inhibits gene expression from different cellular and viral promoters in hepatic and nonhepatic cell lines.* Virology, 2003. **305**(2): p. 260-6.
95. Kaukinen, P., et al., *Hepatitis C virus NS2 protease inhibits host cell antiviral response by inhibiting IKKε and TBK1 functions.* J Med Virol, 2013. **85**(1): p. 71-82.
96. Zhou, H., et al., *Hepatitis C Virus NS2 Protein Suppresses RNA Interference in Cells.* Virol Sin, 2020. **35**(4): p. 436-444.
97. von dem Bussche, A., et al., *Hepatitis C virus NS2 protein triggers endoplasmic reticulum stress and suppresses its own viral replication.* J Hepatol, 2010. **53**(5): p. 797-804.
98. She, Y., et al., *Hepatitis C virus NS2/3 protease regulates HCV IRES-dependent translation and NS5B RdRp activity.* Arch Virol, 2009. **154**(9): p. 1465-73.
99. Paul, D., V. Madan, and R. Bartenschlager, *Hepatitis C virus RNA replication and assembly: living on the fat of the land.* Cell Host Microbe, 2014. **16**(5): p. 569-79.
100. Kohlway, A., et al., *The linker region of NS3 plays a critical role in the replication and infectivity of hepatitis C virus.* J Virol, 2014. **88**(18): p. 10970-4.
101. Egger, D., et al., *Expression of hepatitis C virus proteins induces distinct membrane alterations including a candidate viral replication complex.* J Virol, 2002. **76**(12): p. 5974-84.
102. Einav, S., et al., *The nucleotide binding motif of hepatitis C virus NS4B can mediate cellular transformation and tumor formation without Ha-ras co-transfection.* Hepatology, 2008. **47**(3): p. 827-35.
103. Einav, S., et al., *A nucleotide binding motif in hepatitis C virus (HCV) NS4B mediates HCV RNA replication.* J Virol, 2004. **78**(20): p. 11288-95.
104. Jones, D.M., et al., *The hepatitis C virus NS4B protein can trans-complement viral RNA replication and modulates production of infectious virus.* J Virol, 2009. **83**(5): p. 2163-77.

105. Tellinghuisen, T.L., et al., *The NS5A protein of hepatitis C virus is a zinc metalloprotein.* J Biol Chem, 2004. **279**(47): p. 48576-87.
106. Huang, L., et al., *Hepatitis C virus nonstructural protein 5A (NS5A) is an RNA-binding protein.* J Biol Chem, 2005. **280**(43): p. 36417-28.
107. Miyanari, Y., et al., *The lipid droplet is an important organelle for hepatitis C virus production.* Nat Cell Biol, 2007. **9**(9): p. 1089-97.
108. Romero-Brey, I., et al., *NS5A Domain 1 and Polyprotein Cleavage Kinetics Are Critical for Induction of Double-Membrane Vesicles Associated with Hepatitis C Virus Replication.* mBio, 2015. **6**(4): p. e00759.
109. Love, R.A., et al., *Crystal structure of a novel dimeric form of NS5A domain I protein from hepatitis C virus.* J Virol, 2009. **83**(9): p. 4395-403.
110. Tellinghuisen, T.L., J. Marcotrigiano, and C.M. Rice, *Structure of the zinc-binding domain of an essential component of the hepatitis C virus replicase.* Nature, 2005. **435**(7040): p. 374-9.
111. Appel, N., et al., *Essential role of domain III of nonstructural protein 5A for hepatitis C virus infectious particle assembly.* PLoS Pathog, 2008. **4**(3): p. e1000035.
112. Masaki, T., et al., *Interaction of hepatitis C virus nonstructural protein 5A with core protein is critical for the production of infectious virus particles.* J Virol, 2008. **82**(16): p. 7964-76.
113. Zayas, M., et al., *Coordination of Hepatitis C Virus Assembly by Distinct Regulatory Regions in Nonstructural Protein 5A.* PLoS Pathog, 2016. **12**(1): p. e1005376.
114. Ross-Thriepland, D. and M. Harris, *Hepatitis C virus NS5A: enigmatic but still promiscuous 10 years on!* J Gen Virol, 2015. **96**(Pt 4): p. 727-738.
115. Behrens, S.E., L. Tomei, and R. De Francesco, *Identification and properties of the RNA-dependent RNA polymerase of hepatitis C virus.* Embo j, 1996. **15**(1): p. 12-22.
116. Bartenschlager, R., *Hepatitis C virus replicons: potential role for drug development.* Nat Rev Drug Discov, 2002. **1**(11): p. 911-6.
117. Lohmann, V., et al., *Viral and cellular determinants of hepatitis C virus RNA replication in cell culture.* J Virol, 2003. **77**(5): p. 3007-19.
118. Blight, K.J., J.A. McKeating, and C.M. Rice, *Highly permissive cell lines for subgenomic and genomic hepatitis C virus RNA replication.* J Virol, 2002. **76**(24): p. 13001-14.
119. Kato, T., et al., *Efficient replication of the genotype 2a hepatitis C virus subgenomic replicon.* Gastroenterology, 2003. **125**(6): p. 1808-17.
120. Kaul, A., et al., *Cell culture adaptation of hepatitis C virus and in vivo viability of an adapted variant.* J Virol, 2007. **81**(23): p. 13168-79.
121. Delgrange, D., et al., *Robust production of infectious viral particles in Huh-7 cells by introducing mutations in hepatitis C virus structural proteins.* J Gen Virol, 2007. **88**(Pt 9): p. 2495-2503.
122. Pietschmann, T., et al., *Construction and characterization of infectious intragenotypic and intergenotypic hepatitis C virus chimeras.* Proc Natl Acad Sci U S A, 2006. **103**(19): p. 7408-13.
123. Reiss, S., et al., *Recruitment and activation of a lipid kinase by hepatitis C virus NS5A is essential for integrity of the membranous replication compartment.* Cell Host Microbe, 2011. **9**(1): p. 32-45.
124. André, P., et al., *Characterization of low- and very-low-density hepatitis C virus RNA-containing particles.* J Virol, 2002. **76**(14): p. 6919-28.
125. Chang, K.S., et al., *Human apolipoprotein e is required for infectivity and production of hepatitis C virus in cell culture.* J Virol, 2007. **81**(24): p. 13783-93.

126. Merz, A., et al., *Biochemical and morphological properties of hepatitis C virus particles and determination of their lipidome.* J Biol Chem, 2011. **286**(4): p. 3018-32.
127. Neufeldt, C.J., et al., *Rewiring cellular networks by members of the Flaviviridae family.* Nat Rev Microbiol, 2018. **16**(3): p. 125-142.
128. Kapadia, S.B., et al., *Initiation of hepatitis C virus infection is dependent on cholesterol and cooperativity between CD81 and scavenger receptor B type I.* J Virol, 2007. **81**(1): p. 374-83.
129. Palor, M., et al., *Cholesterol sensing by CD81 is important for hepatitis C virus entry.* J Biol Chem, 2020. **295**(50): p. 16931-16948.
130. Banse, P., et al., *CD81 Receptor Regions outside the Large Extracellular Loop Determine Hepatitis C Virus Entry into Hepatoma Cells.* Viruses, 2018. **10**(4).
131. Aizaki, H., et al., *Characterization of the hepatitis C virus RNA replication complex associated with lipid rafts.* Virology, 2004. **324**(2): p. 450-61.
132. Mannová, P., et al., *Modification of host lipid raft proteome upon hepatitis C virus replication.* Mol Cell Proteomics, 2006. **5**(12): p. 2319-25.
133. Kim, J.Y., et al., *Hepatitis C Virus Induces the Localization of Lipid Rafts to Autophagosomes for Its RNA Replication.* J Virol, 2017. **91**(20).
134. Paul, D., et al., *Morphological and biochemical characterization of the membranous hepatitis C virus replication compartment.* J Virol, 2013. **87**(19): p. 10612-27.
135. Wang, H., et al., *Oxysterol-binding protein is a phosphatidylinositol 4-kinase effector required for HCV replication membrane integrity and cholesterol trafficking.* Gastroenterology, 2014. **146**(5): p. 1373-85.e1-11.
136. Stoeck, I.K., et al., *Hepatitis C Virus Replication Depends on Endosomal Cholesterol Homeostasis.* J Virol, 2018. **92**(1).
137. Park, C.Y., et al., *Hepatitis C virus nonstructural 4B protein modulates sterol regulatory element-binding protein signaling via the AKT pathway.* J Biol Chem, 2009. **284**(14): p. 9237-46.
138. Tallorin, L., et al., *Hepatitis C virus NS3-4A protease regulates the lipid environment for RNA replication by cleaving host enzyme 24-dehydrocholesterol reductase.* J Biol Chem, 2020. **295**(35): p. 12426-12436.
139. Targett-Adams, P., et al., *Maturation of hepatitis C virus core protein by signal peptide peptidase is required for virus production.* J Biol Chem, 2008. **283**(24): p. 16850-9.
140. Herker, E., et al., *Efficient hepatitis C virus particle formation requires diacylglycerol acyltransferase-1.* Nat Med, 2010. **16**(11): p. 1295-8.
141. Park, E.M., et al., *AAM-B Interacts with Nonstructural 4B and Regulates Hepatitis C Virus Propagation.* PLoS One, 2015. **10**(7): p. e0132839.
142. Lee, J.Y., et al., *Spatiotemporal Coupling of the Hepatitis C Virus Replication Cycle by Creating a Lipid Droplet- Proximal Membranous Replication Compartment.* Cell Rep, 2019. **27**(12): p. 3602-3617.e5.
143. Huang, H., et al., *Hepatitis C virus production by human hepatocytes dependent on assembly and secretion of very low-density lipoproteins.* Proc Natl Acad Sci U S A, 2007. **104**(14): p. 5848-53.
144. Syed, G.H., et al., *Hepatitis C Virus Lipoviroparticles Assemble in the Endoplasmic Reticulum (ER) and Bud off from the ER to the Golgi Compartment in COPII Vesicles.* J Virol, 2017. **91**(15).

145. Mankouri, J., et al., *Release of Infectious Hepatitis C Virus from Huh7 Cells Occurs via a trans-Golgi Network-to-Endosome Pathway Independent of Very-Low-Density Lipoprotein Secretion.* J Virol, 2016. **90**(16): p. 7159-70.
146. Olzmann, J.A. and P. Carvalho, *Dynamics and functions of lipid droplets.* Nat Rev Mol Cell Biol, 2019. **20**(3): p. 137-155.
147. Khandelia, H., et al., *Triglyceride blisters in lipid bilayers: implications for lipid droplet biogenesis and the mobile lipid signal in cancer cell membranes.* PLoS One, 2010. **5**(9): p. e12811.
148. Duelund, L., et al., *Composition, structure and properties of POPC-triolein mixtures. Evidence of triglyceride domains in phospholipid bilayers.* Biochim Biophys Acta, 2013. **1828**(8): p. 1909-17.
149. Krahmer, N., R.V. Farese, Jr., and T.C. Walther, *Balancing the fat: lipid droplets and human disease.* EMBO Mol Med, 2013. **5**(7): p. 973-83.
150. Greenberg, A.S., et al., *The role of lipid droplets in metabolic disease in rodents and humans.* J Clin Invest, 2011. **121**(6): p. 2102-10.
151. Fei, W., et al., *A role for phosphatidic acid in the formation of "supersized" lipid droplets.* PLoS Genet, 2011. **7**(7): p. e1002201.
152. Skinner, J.R., et al., *Diacylglycerol enrichment of endoplasmic reticulum or lipid droplets recruits perilipin 3/TIP47 during lipid storage and mobilization.* J Biol Chem, 2009. **284**(45): p. 30941-8.
153. Adeyo, O., et al., *The yeast lipin orthologue Pah1p is important for biogenesis of lipid droplets.* J Cell Biol, 2011. **192**(6): p. 1043-55.
154. Choudhary, V., et al., *Architecture of Lipid Droplets in Endoplasmic Reticulum Is Determined by Phospholipid Intrinsic Curvature.* Curr Biol, 2018. **28**(6): p. 915-926.e9.
155. Choudhary, V., et al., *A conserved family of proteins facilitates nascent lipid droplet budding from the ER.* J Cell Biol, 2015. **211**(2): p. 261-71.
156. Bulankina, A.V., et al., *TIP47 functions in the biogenesis of lipid droplets.* J Cell Biol, 2009. **185**(4): p. 641-55.
157. Szymanski, K.M., et al., *The lipodystrophy protein seipin is found at endoplasmic reticulum lipid droplet junctions and is important for droplet morphology.* Proc Natl Acad Sci U S A, 2007. **104**(52): p. 20890-5.
158. Ben M'barek, K., et al., *ER Membrane Phospholipids and Surface Tension Control Cellular Lipid Droplet Formation.* Dev Cell, 2017. **41**(6): p. 591-604.e7.
159. Krahmer, N., et al., *Phosphatidylcholine synthesis for lipid droplet expansion is mediated by localized activation of CTP:phosphocholine cytidylyltransferase.* Cell Metab, 2011. **14**(4): p. 504-15.
160. Wilfling, F., et al., *Arf1/COPI machinery acts directly on lipid droplets and enables their connection to the ER for protein targeting.* Elife, 2014. **3**: p. e01607.
161. Thiam, A.R., et al., *COPI buds 60-nm lipid droplets from reconstituted water-phospholipid-triacylglyceride interfaces, suggesting a tension clamp function.* Proc Natl Acad Sci U S A, 2013. **110**(33): p. 13244-9.
162. Bersuker, K., et al., *A Proximity Labeling Strategy Provides Insights into the Composition and Dynamics of Lipid Droplet Proteomes.* Dev Cell, 2018. **44**(1): p. 97-112.e7.
163. Schrul, B. and R.R. Kopito, *Peroxin-dependent targeting of a lipid-droplet-destined membrane protein to ER subdomains.* Nat Cell Biol, 2016. **18**(7): p. 740-51.
164. Wilfling, F., et al., *Triacylglycerol synthesis enzymes mediate lipid droplet growth by relocalizing from the ER to lipid droplets.* Dev Cell, 2013. **24**(4): p. 384-99.

165. Olzmann, J.A., C.M. Richter, and R.R. Kopito, *Spatial regulation of UBXD8 and p97/VCP controls ATGL-mediated lipid droplet turnover.* Proc Natl Acad Sci U S A, 2013. **110**(4): p. 1345-50.
166. Prévost, C., et al., *Mechanism and Determinants of Amphipathic Helix-Containing Protein Targeting to Lipid Droplets.* Dev Cell, 2018. **44**(1): p. 73-86.e4.
167. Bacle, A., et al., *Interdigitation between Triglycerides and Lipids Modulates Surface Properties of Lipid Droplets.* Biophys J, 2017. **112**(7): p. 1417-1430.
168. Valm, A.M., et al., *Applying systems-level spectral imaging and analysis to reveal the organelle interactome.* Nature, 2017. **546**(7656): p. 162-167.
169. Salo, V.T., et al., *Seipin regulates ER-lipid droplet contacts and cargo delivery.* Embo j, 2016. **35**(24): p. 2699-2716.
170. Xu, N., et al., *The FATP1-DGAT2 complex facilitates lipid droplet expansion at the ER-lipid droplet interface.* J Cell Biol, 2012. **198**(5): p. 895-911.
171. Xu, D., et al., *Rab18 promotes lipid droplet (LD) growth by tethering the ER to LDs through SNARE and NRZ interactions.* J Cell Biol, 2018. **217**(3): p. 975-995.
172. Markgraf, D.F., et al., *An ER protein functionally couples neutral lipid metabolism on lipid droplets to membrane lipid synthesis in the ER.* Cell Rep, 2014. **6**(1): p. 44-55.
173. Prinz, W.A., *Bridging the gap: membrane contact sites in signaling, metabolism, and organelle dynamics.* J Cell Biol, 2014. **205**(6): p. 759-69.
174. Shai, N., et al., *Systematic mapping of contact sites reveals tethers and a function for the peroxisome-mitochondria contact.* Nat Commun, 2018. **9**(1): p. 1761.
175. Pereira-Leal, J.B., A.N. Hume, and M.C. Seabra, *Prenylation of Rab GTPases: molecular mechanisms and involvement in genetic disease.* FEBS Lett, 2001. **498**(2-3): p. 197-200.
176. Dejgaard, S.Y. and J.F. Presley, *Rab18: new insights into the function of an essential protein.* Cell Mol Life Sci, 2019. **76**(10): p. 1935-1945.
177. Pulido, M.R., et al., *Rab18 dynamics in adipocytes in relation to lipogenesis, lipolysis and obesity.* PLoS One, 2011. **6**(7): p. e22931.
178. Martin, S., et al., *Regulated localization of Rab18 to lipid droplets: effects of lipolytic stimulation and inhibition of lipid droplet catabolism.* J Biol Chem, 2005. **280**(51): p. 42325-35.
179. Ozeki, S., et al., *Rab18 localizes to lipid droplets and induces their close apposition to the endoplasmic reticulum-derived membrane.* J Cell Sci, 2005. **118**(Pt 12): p. 2601-11.
180. Salloum, S., et al., *Rab18 binds to hepatitis C virus NS5A and promotes interaction between sites of viral replication and lipid droplets.* PLoS Pathog, 2013. **9**(8): p. e1003513.
181. Ruggieri, A., et al., *Dynamic oscillation of translation and stress granule formation mark the cellular response to virus infection.* Cell Host Microbe, 2012. **12**(1): p. 71-85.
182. Matto, M., et al., *Hepatitis C virus core protein associates with detergent-resistant membranes distinct from classical plasma membrane rafts.* J Virol, 2004. **78**(21): p. 12047-53.
183. Yang, G., et al., *Interactions of caveolin-1 scaffolding and intramembrane regions containing a CRAC motif with cholesterol in lipid bilayers.* Biochim Biophys Acta, 2014. **1838**(10): p. 2588-99.
184. Windler, E., et al., *The human asialoglycoprotein receptor is a possible binding site for low-density lipoproteins and chylomicron remnants.* Biochem J, 1991. **276 (Pt 1)**(Pt 1): p. 79-87.

185. DeMattos, R.B., et al., *Purification and characterization of astrocyte-secreted apolipoprotein E and J-containing lipoproteins from wild-type and human apoE transgenic mice.* Neurochem Int, 2001. **39**(5-6): p. 415-25.
186. Schuck, S., et al., *Resistance of cell membranes to different detergents.* Proc Natl Acad Sci U S A, 2003. **100**(10): p. 5795-800.
187. Browman, D.T., et al., *Erlin-1 and erlin-2 are novel members of the prohibitin family of proteins that define lipid-raft-like domains of the ER.* J Cell Sci, 2006. **119**(Pt 15): p. 3149-60.
188. Huber, M.D., et al., *Erlins restrict SREBP activation in the ER and regulate cellular cholesterol homeostasis.* J Cell Biol, 2013. **203**(3): p. 427-36.
189. Brown, M.S. and J.L. Goldstein, *The SREBP pathway: regulation of cholesterol metabolism by proteolysis of a membrane-bound transcription factor.* Cell, 1997. **89**(3): p. 331-40.
190. Yang, T., et al., *Crucial step in cholesterol homeostasis: sterols promote binding of SCAP to INSIG-1, a membrane protein that facilitates retention of SREBPs in ER.* Cell, 2002. **110**(4): p. 489-500.
191. Brown, A.J., et al., *Cholesterol addition to ER membranes alters conformation of SCAP, the SREBP escort protein that regulates cholesterol metabolism.* Mol Cell, 2002. **10**(2): p. 237-45.
192. Adams, C.M., J.L. Goldstein, and M.S. Brown, *Cholesterol-induced conformational change in SCAP enhanced by Insig proteins and mimicked by cationic amphiphiles.* Proc Natl Acad Sci U S A, 2003. **100**(19): p. 10647-52.
193. Spiess, M. and H.F. Lodish, *Sequence of a second human asialoglycoprotein receptor: conservation of two receptor genes during evolution.* Proc Natl Acad Sci U S A, 1985. **82**(19): p. 6465-9.
194. Goldstein, J.L., R.G. Anderson, and M.S. Brown, *Receptor-mediated endocytosis and the cellular uptake of low density lipoprotein.* Ciba Found Symp, 1982(92): p. 77-95.
195. Manwaring, W.W.a.J., *Lipids in Cell Culture Media*, A.-S.T.I.-A. Notes, Editor., Fisher Scientific.
196. Scott, C.C., F. Vacca, and J. Gruenberg, *Endosome maturation, transport and functions.* Semin Cell Dev Biol, 2014. **31**: p. 2-10.
197. Baier, C.J., J. Fantini, and F.J. Barrantes, *Disclosure of cholesterol recognition motifs in transmembrane domains of the human nicotinic acetylcholine receptor.* Sci Rep, 2011. **1**: p. 69.
198. Zheng, H., et al., *Palmitoylation and membrane cholesterol stabilize μ-opioid receptor homodimerization and G protein coupling.* BMC Cell Biol, 2012. **13**: p. 6.
199. Patrone, M., et al., *Palmitoylation Strengthens Cholesterol-dependent Multimerization and Fusion Activity of Human Cytomegalovirus Glycoprotein B (gB).* J Biol Chem, 2016. **291**(9): p. 4711-22.
200. Blanchard, E., et al., *Hepatitis C virus entry depends on clathrin-mediated endocytosis.* J Virol, 2006. **80**(14): p. 6964-72.
201. Lai, C.K., et al., *Hepatitis C virus egress and release depend on endosomal trafficking of core protein.* J Virol, 2010. **84**(21): p. 11590-8.
202. Nakatsu, F. and H. Ohno, *Adaptor protein complexes as the key regulators of protein sorting in the post-Golgi network.* Cell Struct Funct, 2003. **28**(5): p. 419-29.
203. Park, S.Y. and X. Guo, *Adaptor protein complexes and intracellular transport.* Biosci Rep, 2014. **34**(4).

204. Wijdeven, R.H., et al., *ER contact sites direct late endosome transport.* Bioessays, 2015. **37**(12): p. 1298-302.
205. Johansson, M., et al., *Activation of endosomal dynein motors by stepwise assembly of Rab7-RILP-p150Glued, ORP1L, and the receptor betalll spectrin.* J Cell Biol, 2007. **176**(4): p. 459-71.
206. Vihervaara, T., et al., *Sterol binding by OSBP-related protein 1L regulates late endosome motility and function.* Cell Mol Life Sci, 2011. **68**(3): p. 537-51.
207. Rocha, N., et al., *Cholesterol sensor ORP1L contacts the ER protein VAP to control Rab7-RILP-p150 Glued and late endosome positioning.* J Cell Biol, 2009. **185**(7): p. 1209-25.
208. Rituper, B., et al., *Vesicle cholesterol controls exocytotic fusion pore.* Cell Calcium, 2022. **101**: p. 102503.
209. d'Avigdor, W.M.H., et al., *Virus Genotype-Dependent Transcriptional Alterations in Lipid Metabolism and Inflammation Pathways in the Hepatitis C Virus-infected Liver.* Sci Rep, 2019. **9**(1): p. 10596.
210. Galli, A., S. Ramirez, and J. Bukh, *Lipid Droplets Accumulation during Hepatitis C Virus Infection in Cell-Culture Varies among Genotype 1-3 Strains and Does Not Correlate with Virus Replication.* Viruses, 2021. **13**(3).
211. Li, M., et al., *MicroRNA-185-5p mediates regulation of SREBP2 expression by hepatitis C virus core protein.* World J Gastroenterol, 2015. **21**(15): p. 4517-25.
212. Rakic, B., et al., *Peroxisome proliferator-activated receptor alpha antagonism inhibits hepatitis C virus replication.* Chem Biol, 2006. **13**(1): p. 23-30.
213. She, Y., et al., *Hepatitis C virus (HCV) NS2 protein up-regulates HCV IRES-dependent translation and down-regulates NS5B RdRp activity.* Arch Virol, 2008. **153**(11): p. 1991-7.
214. Dansako, H., et al., *Rab18 is required for viral assembly of hepatitis C virus through trafficking of the core protein to lipid droplets.* Virology, 2014. **462-463**: p. 166-74.
215. Theken, K.N., et al., *The roles of lipids in SARS-CoV-2 viral replication and the host immune response.* J Lipid Res, 2021. **62**: p. 100129.
216. Osuna-Ramos, J.F., J.M. Reyes-Ruiz, and R.M. Del Ángel, *The Role of Host Cholesterol During Flavivirus Infection.* Front Cell Infect Microbiol, 2018. **8**: p. 388.
217. Lee, J.Y., et al., *Apolipoprotein E likely contributes to a maturation step of infectious hepatitis C virus particles and interacts with viral envelope glycoproteins.* J Virol, 2014. **88**(21): p. 12422-37.
218. Bankwitz, D., et al., *Maturation of secreted HCV particles by incorporation of secreted ApoE protects from antibodies by enhancing infectivity.* J Hepatol, 2017. **67**(3): p. 480-489.

8. Oral presentations

- 26th International Symposium on Hepatitis C Virus and Related Viruses 2019 (HCV 2019), held at the COEX, Seoul, South Korea, on October 5-8, 2019

  “Photoactivatable and Clickable Cholesterol to Determine Direct Interaction with HCV Proteins”

- 30th Annual Meeting of the Society for Virology, 24-26 March 2021, Digital

  “Photoactivatable and clickable cholesterol to determine direct Interaction between HCV proteins and cholesterol”